INFORMATION TO USERS

This manuscript has been reproduced from the microfilm master. UMI films the text directly from the original or copy submitted. Thus, some thesis and dissertation copies are in typewriter face, while others may be from any type of computer printer.

The quality of this reproduction is dependent upon the quality of the copy submitted. Broken or indistinct print, colored or poor quality illustrations and photographs, print bleedthrough, substandard margins, and improper alignment can adversely affect reproduction.

In the unlikely event that the author did not send UMI a complete manuscript and there are missing pages, these will be noted. Also, if unauthorized copyright material had to be removed, a note will indicate the deletion.

Oversize materials (e.g., maps, drawings, charts) are reproduced by sectioning the original, beginning at the upper left-hand corner and continuing from left to right in equal sections with small overlaps.

ProQuest Information and Learning
300 North Zeeb Road, Ann Arbor, MI 48106-1346 USA
800-521-0600

THE FUNCTIONAL ROLE OF PHE-10 AND THE ANOMALOUS TYR-9 pK_a IN GLUTATHIONE S-TRANSFERASE A1-1

Catherine A. Ibarra

A dissertation submitted in partial fulfillment of the
requirements for the degree of

Doctor of Philosopy

University of Washington

2002

Program Authorized to Offer Degree: Medicinal Chemistry

UMI Number: 3062953

ProQuest Information and Learning Company
300 North Zeeb Road
P.O. Box 1346
Ann Arbor, MI 48106-1346

In presenting this dissertation in partial fulfillment of the requirements for the Doctoral degree at the University of Washington, I agree that the Library shall make its copies freely available for inspection. I further agree that extensive copying of the dissertaton is allowable only for scholarly purposes, consistent with "fair use" as prescribed in the U.S. Copyright Law. Requests for copying or reproduction of this dissertation may be referred to ProQuest Information and Learning, 300 North Zeeb Road, Ann Arbor, MI 48106-1346, to whom the author has granted "the right to reproduce and sell (a) copies of the manuscript in microfilm and/or (b) printed copies of the manuscript made from microform."

Signature: Catherine Stamm

Date: 8/22/02

University of Washington
Graduate School

This is to certify that I have examined this copy of a doctoral dissertation by

Catherine A. Ibarra

and have found that it is complete and satisfactory in all respects,
and that any and all revisions required by the final
examining committee have been made.

Chair of Supervisory Committee:

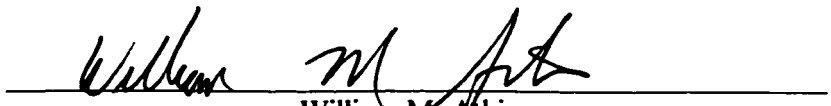

William M. Atkins

Reading Committee:

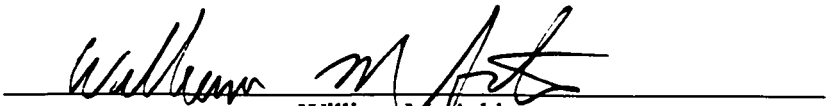

William M. Atkins

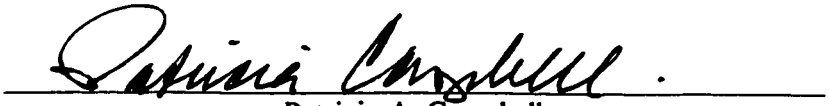

Patricia A. Campbell

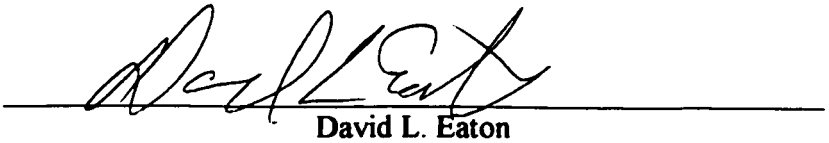

David L. Eaton

Date: 8/22/02

University of Washington

Abstract

THE FUNCTIONAL ROLE OF PHE-10 AND THE ANOMALOUS TYR-9 pK_a IN GLUTATHIONE S-TRANSFERASE A1-1

Catherine A. Ibarra

Chair of the Supervisory Committee:
Associate Professor William M. Atkins
Department of Medicinal Chemistry

As the most abundant isoform of GST in the liver, the GST A1-1 is the major catalyst of detoxification. This isoform is of particular interest because it exhibits an unusually low pK_a (~8.1-8.3) of active site Tyr-9 and a ligand-dependent dynamics of the C-terminus. This dynamics is catalytically important, as product release is rate-limiting for a number of substrates.

A major emphasis of this dissertation is the elucidation of the structural and functional significance of the anomalous pK_a of Tyr-9 in rat GST A1-1. The edge-to-face electrostatic interaction between Phe-10 and Tyr-9 contributes to the ionization properties of the tyrosyl hydroxyl group in the apo-enzyme, consistent with crystal structure observations. Additionally, Phe-10 plays a vital role in ligand binding, as the two steps of the binding reaction are significantly reduced upon removal of aromatic-aromatic interactions. The results presented herein demonstrate the importance of Phe-10 in orchestrating the dynamics of the C-terminus.

Previous data suggest that Tyr-9 ionization is closely coupled to the C-terminal dynamics of GST A1-1. To directly probe this possibility, engineered W21F:F222W and Y9F:W21F:F222W mutants, which contain single Trp at the C-terminus, were used as fluorescent reporters of C-terminal dynamics. Only the W21F:F222W mutant exhibited

pH-dependent change in Trp-222 emission properties consistent with changes in C-terminal solvation. Moreover, the pH-dependent equilibrium binding and stopped-flow studies with product conjugate resulted in decreased equilibrium binding affinity (K_D), concomitant with increased binding and dissociation rates at higher pHs. The recovered pK_as for the change in microscopic rate constants reflect the pK_a of Tyr-9 in the apo-enzyme. In contrast, these pH-dependent changes were not observed in the Y9F:W21F:F222W mutant. These results demonstrate that the ionization status of Tyr-9 controls the C-terminal dynamics, providing parallel pathways for product dissociation.

Finally, the utility of GST-mediated hydrolysis of thiol esters formed from glutathione (GSH) and several carboxylic acid-containing drugs were exploited as a means of delivering drugs to tumors that overexpress GSTs. The competence of several human GSTs was examined, with the Pi-class GST being the most active in hydrolyzing the thiol ester formed from ethacrynic acid (EA) and GSH. Moreover, the P-class GST was inhibited and modified by the released EA. Results also indicate the importance of active site Tyr in the Alpha-, Pi-, and Mu-class GSTs. However, the exact mechanism by which this residue participates in the hydrolysis remains unknown.

TABLE OF CONTENTS

LIST OF FIGURES

LIST OF TABLES

ACKNOWLEDGEMENTS

My sincerest gratitude goes to Dr. Bill Atkins for his unconditional support and guidance throughout my graduate studies at the University of Washington. Your vast knowledge and enthusiasm for research truly make you a great role model. This thesis would not have been completed without the assistance of Michael Dabrowski, Dr. Brenda Nieslanik, Bob Lyon, Doug Lu and Josh Pearson with the graphic and molecular biology, rapid kinetics, synthetic, and mass spectrometry aspects of these studies. Thank you for all of the friendship and support throughout the years. Last but not the least, my heartfelt thanks to my family and friends for their emotional support and encouragement.

DEDICATION

To my parents, Alex and Glenia Ibarra,

and sisters Hilda, Glea, and Maribeth

CHAPTER 1

INTRODUCTION

1.1 Introduction

Living organisms are versatile in that they have adopted many defense mechanisms to respond to changes in their environment, such as the enormous number of toxic substances that an individual organism is continually subjected to. Generally, these toxic substances are electrophiles that arise from xenobiotics or oxidative metabolism. One detoxification system that has evolved to provide protection against toxic compounds is glutathione S-transferase (GST). Since the discovery of this enzyme and its ability to catalyze the addition of glutathione (GSH) to 1,2-dichloro-4-nitrobenzene (Booth, et al., 1961), numerous studies have been performed to gain a better understanding of the enzymology of GSTs, and eventually elucidate the three-dimensional structures of several isoenzymes. The structural information has greatly influenced many ideas on the function of these enzymes. One such idea is the importance of modes of mobility observed in the enzyme on substrate selectivity and turnover. For example, hexokinase exists in 'open' and 'closed' states. Upon ligand binding, the two domains of the enzyme fold toward each other, causing the binding site cleft to close (Bennet, et al., 1978). However, whether or not various conformational states sampled by the enzyme are coupled with the chemical steps of catalysis has not been demonstrated. Another example in which protein flexibility can facilitate access to the active site involves hemoglobin. In this case, binding of oxygen to hemoglobin requires

some structural movement to allow access to the heme (Case, et al., 1979). As will be discussed in Section 1.3, glutathione S-transferases afford an opportunity to study the relationship between the enzymes' ability to access different conformational states and their efficiency at catalysis.

1.2 Glutathione S-transferases

One of the most important families of drug-metabolizing enzyme is glutathione S-transferase (GST) which catalyzes the conjugation of reduced glutathione (γ-glutamyl-cysteinyl-glycine) (GSH) to a wide variety of electrophilic compounds. Essentially, GST renders the drugs or toxicants more water-soluble by forming GSH conjugates that can be directly eliminated or undergo further metabolism. Glutathione conjugates that are further metabolized proceed via cleavage of glutamate and glycine residues, followed by N-acetylation of cysteine to yield a mercapturic acid that is then excreted (Mannervik, et al., 1988; Chasseaud, 1979). An ATP-dependent transport of GSH conjugates out of the cells has also been described (Ishikawa, 1992). However, in some cases, the metabolism of GSH conjugates can lead to toxicity. For example, GSH conjugates of dichloromethane and dibromoethane are metabolized to formaldehyde and episulfonium, respectively, which can covalently bind to macromolecules (van Bladeren, 2000). Nonetheless, GSTs represent an important family of detoxification enzymes, as they are found in virtually all species in multiple forms.

To date, eight mammalian cytosolic classes of GSTs have been identified on the basis of sequence similarity and substrate specificity: Alpha (A), Mu (M), Pi (P), Sigma

(S), Theta (T), Zeta (Z), Kappa (K), and Omega (O) (Mannervik, 1985a; Meyer, et al., 1991; Pemble, et al., 1996; Meyer, et al., 1995; Board, et al., 1997, 2000). These enzymes exist as homodimers or heterodimers with subunit molecular masses in the range of 23-27 kDa. Despite the 30% sequence homology between classes, a catalytic device common to cytosolic GSTs is a conserved hydrogen bond between the hydroxyl group of active site tyrosine (Tyr) or serine (Ser) and the thiol group of GSH. This first-sphere electrostatic interaction, which is a term used in reference to ligands directly coordinated to the sulfur, essentially lowers the pK_a of bound GSH from ~9.3 in solution to about 6.3-7.4 at the active site of various GSTs (Liu, et al., 1992; Ji, et al., 1995; Kolm, et al., 1992; Dietze, et al., 1996a; Kong, et al., 1992; Board, et al., 1997). Although the exact nature of the hydrogen bond in the binary complex [GST•GSH] is still in dispute, the catalytic advantage is obvious, in that a decreased pK_a of GSH results in more reactive thiolate anion GS^-. Apparently, removal of the catalytic hydroxyl group in GSTs results in significant reduction in steady-state turnover rates, indicating its importance in enzyme catalysis (Kong, et al., 1992; Liu, et al., 1992; Wang, et al., 1992).

1.2.1 Biological Significance

A prominent feature of GSTs is their ability to catalyze the conjugation of GSH to a multitude of substrates. These substrates contain electrophilic functional groups, such as aryl and alkyl halides, aryl and alkyl epoxides, α,β-unsaturated carbonyls, thiocyanate, and organic nitrate esters (Figure1.1) (Chasseaud, 1979; Jakoby, et al., 1980; Ketterer, 1988).

Despite the overlapping substrate specificities exhibited by the GST isoenzymes, different classes can be distinguished by their preference for catalyzing a particular reaction. For example, A-class, M-class, and P-class GSTs are characterized by their

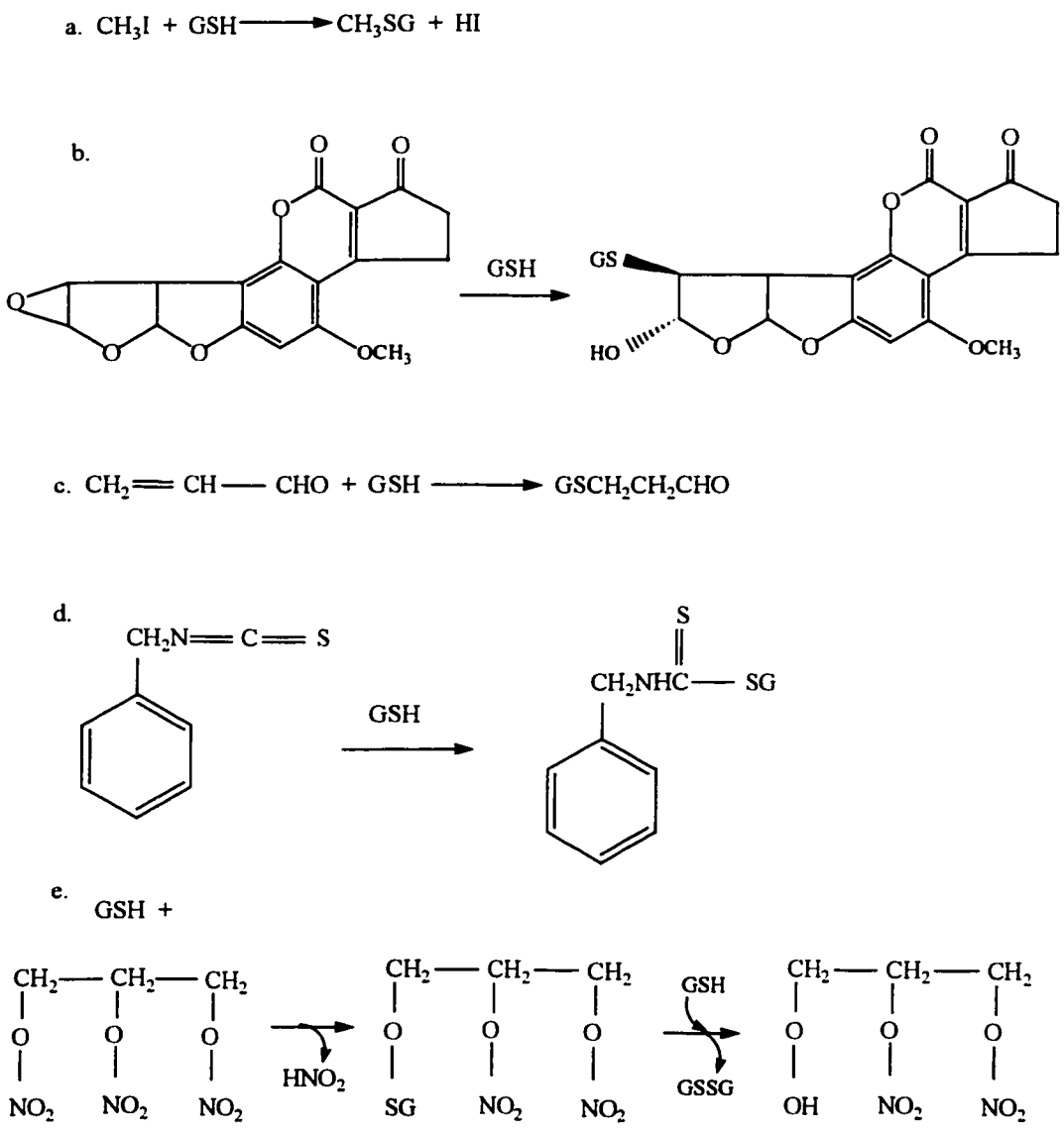

Figure 1.1: Typical examples of reactions catalyzed by GSTs. The conjugation of GSH to (a) industrial carcinogen methyliodide, (b) hepatocarcinogen aflatoxin-8,9-oxide, (c) oxidative by-product acrolein, (d) dietary constituent benzyl isothiocyanate, and (e) anti-anginal agent nitroglycerin.

high activity with organic hydroperoxides, epoxides, and α,β-unsaturated carbonyls, respectively (Prohaska, et al., 1977; Mannervik, et al., 1985b; Armstrong, 1994).

As alluded to earlier, GSTs also provide a protective role against oxidative stress. Specifically, these enzymes can catalyze the reduction of fatty acid, phospholipid, and nucleic acid hydroperoxides (Ketterer, 1988; Prohaska, et al., 1977). The glutathione peroxidase activity of GSTs toward 5-hydroperoxyeicosatetraenoic acid (5-HPETE), an important intermediate in the 5-lipoxygenase pathway, has been described (Jakobsson, et al., 1997; Zhao, et al., 1999; Chang, et al., 1987; Nicholson, et al., 1993). Thus, GSTs are important in the biosynthesis of physiologically relevant compounds such as leukotriene A_4 and prostaglandin H_2. In addition, GSTs catalyze the glutathione-dependent isomerization of Δ^5-3-ketosteroids and cis-trans isomerization of maleylacetone (Keen, et al., 1978).

The role of GSTs in cells is not only limited to detoxification. Glutathione S-transferase was given the name 'ligandin' due to its ability to bind to a wide variety of hydrophobic ligands, both covalently and non-covalently. For instance, the ligandin role of GST in liver is that of storage proteins for hydrophobic, endogenous compounds such as cortisol, bilirubin, heme, bile acids, and steroids (Habig, et al., 1974; Kirsch, et al., 1975; Listowsky, et al., 1988).

The considerable interest in the structural, mechanistic, and clinical studies of GSTs is primarily due to their role in cytotoxic drug resistance. Many of the drugs used in cancer chemotherapy are alkylating agents, which are metabolized to GSH conjugates (Hayes, et al., 1990; Tew, 1994). Therefore, the development of drug resistance could be

an impediment to many chemotherapeutic protocols. Overexpression of GSTs in many cancer cells has been observed, and it may further contribute to drug resistance (Hayes, et al., 1995). As a result, GST has become an important target for rational drug design, specifically in the design of isoform-specific inhibitors.

1.2.2 Structure

The X-ray crystal structures of six of the eight classes of cytosolic GSTs (A-, M-, P-, T-, S-, and O-class) have been determined in the presence of GSH, GSH conjugates, or transition state analogs (Cameron, et al., 1995; Ji, et al., 1992; Reinemer, et al., 1992; Rossjohn, et al., 1998; Ji, et al., 1995; Board, et al., 2000). Although the sequence identity between classes is low, the overall topology is similar (Figure 1.2). Each class consists of two domains. The N-terminal domain comprises the first one-third of the sequence and has a βαβαββα structural motif common to thioredoxin superfamily fold (Murzin, et al., 1995). This domain serves as a binding site for glutathione (G-site). Most of the interactions of polar groups in GSH with one of the subunits of the enzyme involve hydrogen bonds and salt-bridges. However, two of these interactions involve residues (Asp-101 and Arg-131) from the opposite subunit of the dimeric enzyme (Sinning, et al., 1993). Consequently, the completion of the G-site is dependent on dimerization of the enzyme. This may explain, in part, why catalytically active monomers have never been observed.

The remaining two-thirds of GST is the C-terminal domain, which is helical and provides the structural elements for the hydrophobic xenobiotic binding site (H-site).

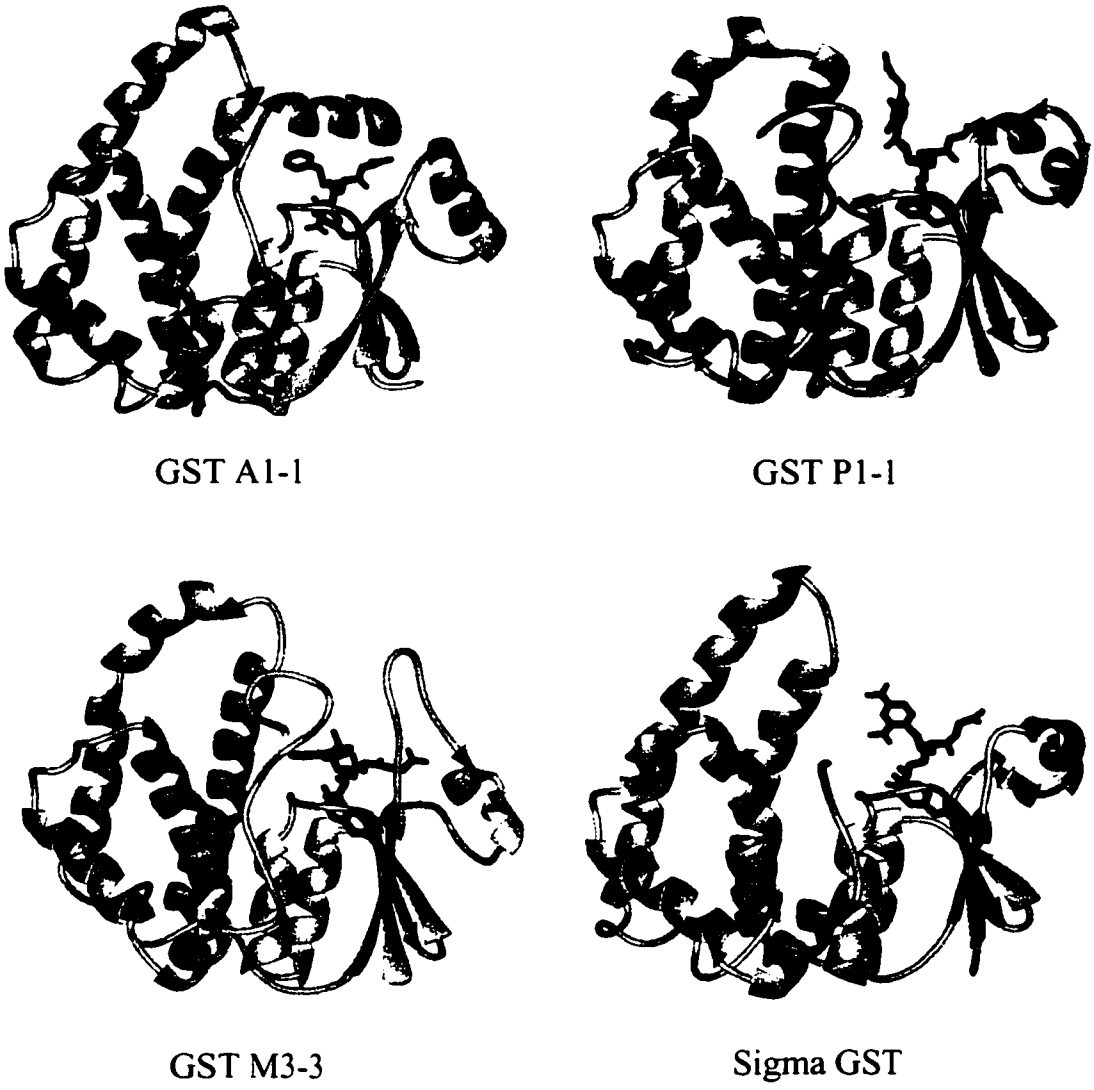

Figure 1.2: Ribbon representations of the three-dimensional structures of human GST A1-1, human GST P1-1, rat GST M3-3, and squid Sigma GST in complex with S-benzylglutathione, ethacrynic acid-glutathione conjugate, (9S,10S)-9-(S-glutathionyl)-10-hydroxy-9,10-dihydrophenanthrene, and 1-(S-glutathionyl)-2,4-dinitrobenzene, respectively. The ligand and active site Tyrosine in each structure are shown in magenta and blue, respectively. The structures were derived from PDB files 1GUH (alpha), 2GSS (pi), 2GST (mu), and 1GSQ (sigma).

This domain consists of a bundle of 5 helices and defines the substrate specificities of the various isoenzymes. Of the two domains, the C-terminal domain in GSTs exhibits the most structural variation. For example, the M- and P-class GSTs are shorter than the A-class by some 5-13 residues at the C-terminus. Furthermore, the active sites of M-class and A-class GSTs are confined by two flexible loops (mu-loop) and amphipathic α9 helix, respectively (Ji, et al., 1992; Cameron, et al., 1995). These structural elements serve to constrict the access of substrate to the active site. The active site in hGST2-2 is also closed by a long C-terminal helix extension, which undergoes large conformational changes to allow substrate binding and release (Jemth, et al., 1999; Rossjohn, et al., 1998). In comparison to the P-, T-, and S-class GSTs, the access of solvent to the active site of A-class GST is restricted by its unique, flexible C-terminal helix (Figure 1.2).

1.3 Glutathione S-Transferase A1-1

As the most abundant isoform in the liver, GST A1-1 is the major contributor to drug metabolism (Hayes, et al., 1995; Awasthi, et al., 1994). Because liver is the major site of metabolism of drugs/xenobiotics, it is at great risk for oxidative stress as a result of reactive oxygen species (ROS) formation. Presumably, the high constitutive expression of GST A1-1 serves a dual purpose in order to meet the detoxification needs of the liver. In this case, this isoform is not only efficient in catalyzing the conjugation of relevant endogenous and exogenous electrophiles to GSH, but also provides protection against lipid peroxidation (Zhao, et al., 1999).

Table 1.1: Sequence alignments of hGST A1-1 and rGST A1-1[a]

```
                          10                  20                  30
hGST A1-1   MAEKPKLHYF NARGRMESTRWLLAAAGVEFEE
rGST A1-1   MSGKPVLHYF NARGRMECIRWLLAAAGVEFEE
                    β1                  α1

                    40                  50                  60
hGST A1-1   KFIKSAEDLDKLRNDGYLMFQQVPMVEIDGMKL
rGST A1-1   KLIQSPEDLEKLKKDGNLMFDQVPMVEIDGMKL
            β2          α2                      β3          β4

                70                  80                  90
hGST A1-1   VQTRAILNYIASKYNLYGKDIKERALIDMYIEG
rGST A1-1   AQTRAILNYIATKYDLYGKDMKERALIDMYSEG
                    α3

            100                 110                 120                 130
hGST A1-1   IADLGEMILLLPVCPPEEKDAKLALIKEKIKNR
rGST A1-1   ILDLTEMIIQLVICPPDQREAKTALAKDRTKNR
                α4                                              α5

                    140                 150                 160
hGST A1-1   YFPAFEKVLKSHGQDYLVGNKLSRADIHLVELL
rGST A1-1   YLPAFEKVLKSHGQDYLVGNRLTRVDIHLLELL
                                                        α6

                170                 180                 190
hGST A1-1   YYVEELDSSLISSFPLLKALKTRISNLPTVKKFL
rGST A1-1   LYVEEFDASLLTSFPLLKAFKSRISSLPNVKKFL
                                    α7                  α8

            200                 210                 220
hGST A1-1   QPGSPRKPPMDEKSLEEARKIFRF
rGST A1-1   QPGSQRKPAMDAKQIEEARKVFKF
                β5                  α9
```

[a]Indicated in bold is the catalytic residue, Tyr-9. Phe-10 and Phe-220 are shown in italics. Underlined residues correspond to major secondary elements, α-helix and β-strand. The references for the sequences are: hGST A1-1 (Board, et al., 1987) and rGST A1-1 (Pickett, et al., 1984).

Comparison of the amino acid sequences of the rat and human isoforms of A1-1 indicates only 77% identity (Table 1.1). However, many of the amino acid differences between the two GSTs are conservative. This suggests that rGST A1-1 is an ortholog of hGST A1-1. In contrast, the sequence identity of rGST A1-1 compared to other rat forms, such as A3-3 and A5-5, is only 68%. Meanwhile, both rat GST A3-3 and A5-5 share ~75% sequence identity with hGST A1-1. Interestingly, rGST A3-3 and rGST A5-5 are ~91% identical. Although the focus of this thesis is not on substrate selectivity of A-class GSTs, it is interesting to note that some forms of the enzymes within the same class and same species show catalytic activity differences for some substrate but not for others. For example, rGST A5-5 is very efficient in catalyzing the conjugation of aflatoxin B_1-8,9-epoxide (AFBO) to GSH, while rGST A3-3 and hGST A1-1 are 1,320-fold and 2,200-fold less active in catalyzing the same reaction (McDonagh, et al., 1999). Moreover, the catalytic activities of rGST A3-3 and rGST A5-5 toward CDNB are similar, but vary by 3-10-fold in comparison to both hGST A1-1 and rGST A1-1 (McDonagh, et al., 1999; Wang, et al., 1992).

In addition to the C-terminal helix, there are other unique features of GST A1-1 that distinguish it from other classes. As described earlier, the conserved hydrogen bond between the catalytic hydroxyl group of Tyr-9 and the thiol group of GSH facilitates the formation of nucleophile, thiolate anion GS^-. In GST A1-1, there is an additional first-sphere electrostatic interaction with the sulfur of GSH (Figure 1.3). The positive charge on the side chain of Arg-15 is hydrogen bonded to the sulfur, contributing to the

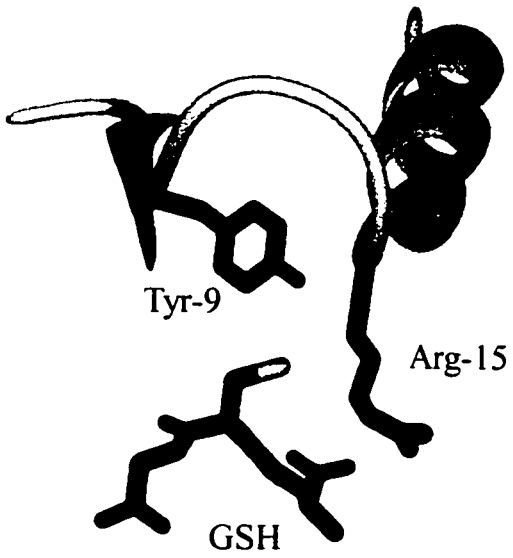

Figure 1.3: First-sphere electrostatic interactions in hGST A1-1. The sulfur of GSH forms hydrogen bonds with the phenolic hydroxyl group of Tyr-9 (3.3 Å) and the N^{ε} of the guanidinium group of Arg-15 (3.8 Å). In addition, the hydroxyl group of Tyr-9 is linked by a hydrogen bond to the main chain amide NH of Arg-15 (3 Å). Values enclosed in parentheses represent the distances between functional groups in GSH and Tyr-9, GSH and Arg-15, or Tyr-9 and Arg-15 (PDB file 1GUH).

electrostatic interactions at the active site (Bjornestedt, et al., 1995). Consequently, the electrostatic potential near the thiolate will not only assist in lowering the pK_a of bound GSH but also stabilize the nucleophile. Removal of the side chain of Arg-15 dramatically reduces the catalytic efficiency of the enzyme (Stenberg, et al., 1991).

The exact mechanistic role of active site Tyr in catalysis, especially with respect to the position of protons in the binary [GST•GSH] complex is still in dispute. Does the proton in the hydroxyl group of Tyr serves as a hydrogen bond donor or as a hydrogen bond acceptor? Shown below are equations illustrating these two situations.

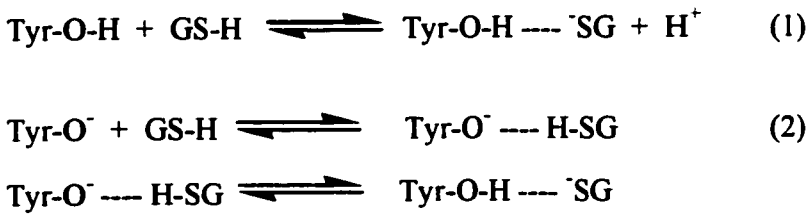

In equation 1, the hydroxyl group of Tyr donates a hydrogen bond to stabilize the thiolate anion in the ground and transition states. On the other hand, equation 2 describes a situation in which the tyrosinate anion ($Tyr\text{-}O^-$) serves as a general base and abstracts a proton from the thiol group. Following this process is a proton transfer from the thiol group to the tyrosinate anion between the ground state and transition state. In both equations, the nucleophilic thiolate necessary for catalysis is formed.

Another unique feature of GST A1-1 is the unusually low pK_a of catalytic Tyr (Atkins, et al., 1993; Bjornestedt, et al., 1995; Dietze, et al., 1996a). The spectroscopic pK_as for the human and rat A1-1 isoforms are respectively 8.1 and 8.3, which are significantly lower than the pK_a of 10.3 for tyrosine in solution. For the A1-1 isoform, a highly conserved Arg-15 contributes to the lowering of catalytic Tyr pK_a through electrostatic effects (Bjornestedt, et al., 1995). Specifically, the phenolic hydroxyl of Tyr-9 is hydrogen bonded to the amide NH of Arg-15, and it is involved in electrostatic interaction with the guanidinium group of Arg-15. In light of the unusually low pK_a in GST A1-1, the role of a general base (eq 2) was considered for the catalytic Tyr. However, the pK_a of bound GSH in rGST A1-1 (~7.4) is actually higher compared to other classes of GSTs, suggesting that proton may be equally shared [Tyr-O•••H•••⁻SG] rather than localized to either Tyr-9 or GSH (Dietze, et al., 1996b).

In contrast, the catalytic Tyr in GST M1-1 has a normal pK_a of 10.2 and is predominantly protonated at physiological pH. Based on solvent deuterium isotope effects studies, the general base mechanism has been ruled out. In this case, the primary function of Tyr is to donate a hydrogen bond and stabilize the GS^- anion (eq 1) (Parsons, et al., 1996). Similarly, the kinetic studies on hGST A1-1 substituted with fluorinated tyrosine analogs indicate a pH-dependence of catalytic activity that is not very different from the wild-type enzyme (Thorson, et al., 1998), thereby ruling out general base mechanism. The major conclusion drawn from the linear free energy correlation was that the shared proton resides near the phenolic oxygen as in equation 1. However, one issue that has not been previously addressed by these studies is the functional role of the anomalous pK_a of catalytic Tyr in A-class GSTs, which is ultimately the focus of the present project.

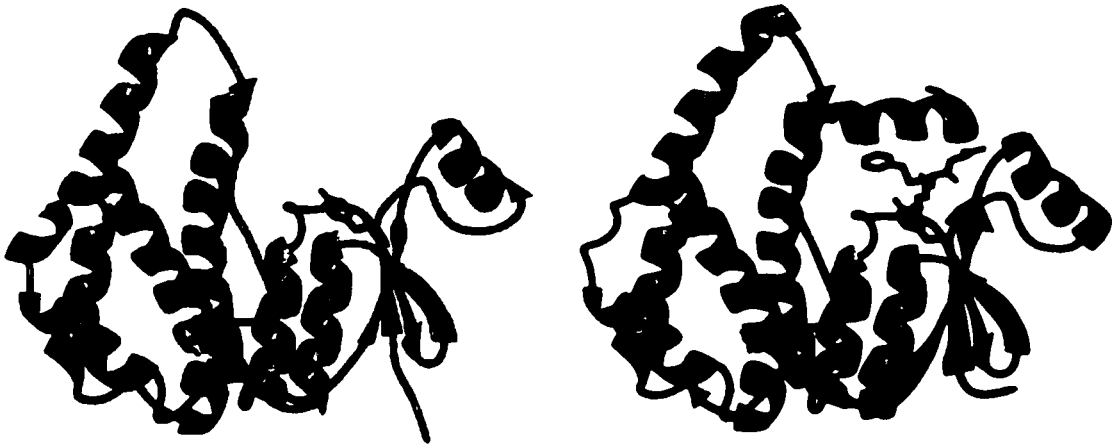

Figure 1.4: Ribbon diagrams of hGST A1-1 in the absence (left) and presence (right) of ligand. The ligand in the bound enzyme is S-benzylglutathione (magenta). Note the presence of C-terminus over the active site containing catalytic Tyr-9 (blue). Structures were derived from PDB files 1GSD and 1GUH.

As alluded to earlier, a structural feature unique to the A-class GSTs is a C-terminal helix that serves as a lid or cap over the active site in the presence of ligand (Figure 1.4). This helix serves as a kinetic barrier to the binding and dissociation of substrates and products (Nieslanik, et al., 1999). Based on the X-ray crystal structures of hGST A1-1 in complex with GSH product conjugate, the aromatic side chain of Phe-220 at the C-terminus is packed near the catalytic Tyr-9 and Phe-10 (Cameron, et al., 1995; Sinning, et al., 1993). In contrast, the C-terminus is crystallographically invisible in the absence of ligand and in the rGST A1-1 crystal structure in complex with G-site ligand,

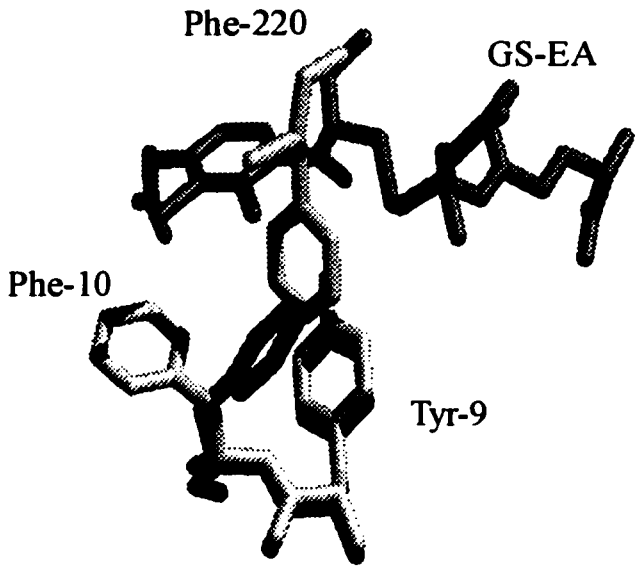

Figure 1.5: Local dynamics of hGST A1-1 near the catalytic Tyr-9. In the apo hGST A1-1, Phe-10 is above Tyr-9 (black) and the C-terminus is disordered (not visible). Upon addition of the ethacrynic acid conjugate GS-EA, Phe-10 moves to allow Phe-220 (light gray) within the C-terminus to occupy the space above Tyr-9. The schematic representations were from the coordinates of PDB files 1GSD and 1GSE.

glutathione sulfonate (GSO_3^-) (Cameron, et al., 1995; Adman, et al., 2001). Moreover, NMR studies suggest that the C-terminus is heterogenous until both G-site and H-site are occupied (Lian, 1998; Allardyce, et al., 2000).

A closer inspection of the crystal structures of apo-enzyme and ligand-bound enzyme indicates another feature that is particularly unique to A-class GSTs. In the apo-enzyme structure, the edge of Phe-10 is packed against the face of Tyr-9, forming an apparent aromatic-aromatic interaction specifically known as edge-to-face electrostatic interaction (Figure 1.5) (Burley, et al., 1985). Upon ligand binding, the side chain of Phe-10 moves away in order to accommodate the side chain of Phe-220 as the C-terminus 'closes' over the active site. Essentially, the aromatic interaction between Phe-10 and Tyr-9 in the apo-enzyme is replaced by a less intimate Phe-220/Tyr-9 interaction in the enzyme-bound complex.

There are several data that suggest the existence of various conformational states of the C-terminus of GST A1-1. NMR and equilibrium binding studies illustrate that the nature of ligands, such as GSH, CDNB, EA and GS-EA, bound at the active site changes the environment at the C-terminus (Lian, 1998; Adman, et al., 2001). For example, the presence of either G-site ligand (i.e., GSH) or H-site ligand (i.e., CDNB) at the active site results in multiple conformations, as evinced by the presence of multiple peaks or resonances for the Phe-222 amide (Lian, 1998). Only when G- and H-sites are occupied simultaneously that the C-terminus become less mobile. Additionally, stopped-flow experiments suggest that G-site ligand induces a conformational change within the C-terminus, despite the fact that this region was not visible in the [rGSTA1-1•GSO_3^-]

complex (Allardyce, et al., 1999; Dirr, et al., 1999; Adman, et al., 2001). Moreover, Phe-220 is the only residue within the C-terminal helix that does not undergo a positional shift in all of the crystal structures with visible helix. In fact, the structural rearrangement that occurs upon GSH conjugate binding may favor the 'closed' conformation, in which an aromatic interaction between Phe-220 and Tyr-9 is formed. On the other hand, the edge-to-face interaction between Phe-10 and Tyr-9 shifts the equilibrium of the C-terminus to a more dynamic or 'open' state. Therefore, the position of Phe-10 relative to Tyr-9 and Phe-220 will likely dictate the conformational status of the C-terminal helix.

Taken together, the structural studies suggest that Phe-10 plays a critical role in the ligand-dependent dynamics of the C-terminus. Furthermore, Phe-10 may modulate the ionization properties of catalytic Tyr-9. This may then provide a molecular mechanism for the unusually low pK_a of this active site residue. One fundamental issue that will be addressed in this project is the functional significance of the anomalous pK_a of Tyr-9. Is the ionization state of Tyr-9 coupled to the dynamics of the C-terminus? How are ligand binding and dissociation affected by the ionization state of Tyr-9? The dissection of each of these subjects will hopefully bring an insight into the role of the unusually low pK_a of Tyr-9 in the function of GST A1-1.

1.4 Outline

There are three sections in this thesis. Chapter 2 describes the structural and functional contributions of Phe-10 in the unusually low pK_a of active site Tyr-9 and in the dynamics of the C-terminal helix. Available X-ray crystal structures of GST A1-1

indicate that the electropositive ring edge of Phe-10 is in van der Waals contact with the electronegative face of Tyr-9 in the absence of ligand. Moreover, structural data indicate that in the presence of ligand, the aromatic ring of Phe-10 is displaced to accommodate the ring of Phe-220 within the active site. The results presented within illustrate that electrostatic interaction between two aromatic rings are indeed sufficient to contribute to the lowering of pK_a of Tyr-9, and Phe-10 modulates the binding of GSH product conjugate by affecting both steps of the binding reaction.

Several data, including those presented in Chapter 2, suggest that the ionization state of Tyr-9 is closely linked to the dynamics of C-terminus. The functional significance of the anomalous pK_a of Tyr-9 has not been directly addressed previously. The focus of Chapter 3 is to determine the role of the ionization properties of Tyr-9 in ligand binding. The results indicate that the ionization state of Tyr-9 controls the conformational status of the C-terminus, thereby altering the rates of ligand binding and dissociation as well as binding affinities of ligand.

While the focus of Chapters 2 and 3 had been on the structure-function studies of rGST A1-1, the focus of Chapter 4 is on understanding the mechanism of thioester GSH conjugate hydrolysis mediated by human GSTs. Out of the four thioester GSH conjugates investigated, only the thioester conjugate of ethacrynic acid (EA), namely ESG, showed considerable hydrolysis by hGST P1-1. In contrast, hGST A1-1 is 3-fold slower in catalyzing the hydrolysis of a similar thioester conjugate. Interestingly, the incubation of hGST P1-1 and hGST A1-1 with ESG for 1 hour resulted in 21% and 10% decrease, respectively, in enzymatic activity toward 1-chloro-2,4-dinitrobenzene (CDNB)

as a substrate. However, the mechanism by which ESG inhibits hGST P1-1 is possibly complicated by a reaction in which the products of hydrolysis, namely EA and GSH, are subsequently conjugated to form GS-EA, which has been shown previously to be a potent inhibitor of P-class GST. Whether or not the two reactions, namely ESG hydrolysis and Michael addition of released products, occur in the same active site of hGST P1-1 is still unclear.

CHAPTER 2

CONTRIBUTION OF AROMATIC-AROMATIC INTERACTIONS TO THE ANOMALOUS pK_a OF TYROSINE-9 AND THE C-TERMINAL DYNAMICS OF GLUTATHIONE S-TRANSFERASE A1-1

2.1 Introduction

One of the most fundamental differences among the GST classes is the interaction of protein with the sulfur of cofactor GSH. With the exception of theta class GST, the A-, M-, P-, and S-classes have a tyrosine residue that serves as a hydrogen bond donor to the sulfur which essentially lowers the pK_a of the thiol group in the binary [GST•GSH] complex (Ji, et al., 1995; Liu, et al., 1992; Kolm, et al., 1992; Wang, et al., 1992). In contrast, the T-class GST, which is believed to be the evolutionary precursor to the other GST classes, utilizes the hydroxyl group of a serine to activate the thiol group of the bound GSH (Wilce, et al., 1995; Board, et al., 1995). As previously described, the A-class GSTs have recruited the side chain of Arg-15 into the inner coordination sphere of the sulfur. In all cases, the reactive species in the binary complex is the thiolate anion GS^-, which accepts a hydrogen bond from the hydroxyl group of Ser or Tyr as well as the guanidinium group of Arg-15 in the A-class enzyme.

The unsually low pK_a of catalytic Tyr is a feature common to both A-class and P-class GSTs. In the A-class GSTs, the stabilization of Tyrosinate-9 by the side chain of Arg-15 in the binary complex and the proximity of the amide NH of this residue contribute to the lowering of this pK_a. The X-ray crystal structures of hGST A1-1 and

rGST A1-1 indicate that the hydroxyl group of Tyr-9 is, respectively, separated from the amide NH of Arg-15 by 2.8 Å and 2.9 Å, which are well within hydrogen bonding distances. Removal of the side chain of Arg-15 had a pronounced effect on the ionization behavior of Tyr-9 (Bjornestedt, et al., 1995).

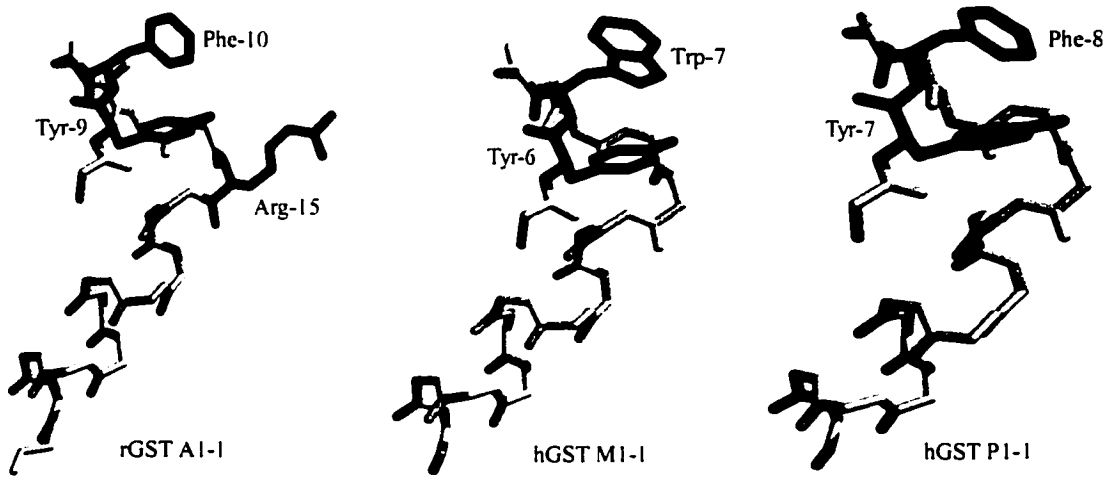

Figure 2.1: Schematic diagrams of aromatic-aromatic interactions in GSTs. The edge-to-face electrostatic interaction between catalytic Tyr (blue) and an adjacent aromatic residue (magenta) is more pronounced in the GST A1-1 isoform. Specifically, the electropositive ring edge of Phe-10 is directly above the electronegative π-cloud of Tyr-9. Note that none of the ring edges of the aromatic residues analogous to Phe-10 in GST M1-1 and GST P1-1 (Trp-7 and Phe-8, respectively) are oriented toward the π-cloud of catalytic Tyr. The unique Arg-15 in the GST A1-1 is indicated in red. Structures were derived from PDB files 1EV9, 1GTU, and 14GS.

Structural information has indicated that the C-terminus in the GST A1-1 isoform undergoes a ligand-dependent conformational change. The putative aromatic cluster implicated in the C-terminal dynamics includes Tyr-9, Phe-10, and Phe-220. In addition to the presence of Tyr-9 in the active site, another feature shared by the A-, M-, and P-class GSTs is a conserved aromatic residue at position 10 (Figure 2.1) (Sinning, et al.,

1993). A close inspection of the crystal structures of these GST classes (Cameron, et al., 1995; Ji, et al., 1992; Reinemer, et al., 1992; Sinning, et al., 1993; Adman, et al., 2001) indicated two pieces of information that ultimately served as the foundation of part of this thesis project. (1) In the apo-enzymes, only the A-class GSTs, specifically the A1-1 isoform, exhibited an edge-to-face electrostatic interaction between residues 9 and 10. Notably, the electrostatic interaction between the two aromatic residues was more pronounced in rGST A1-1 than in hGST A1-1 (Figure 2.2). The corresponding aromatic residues in the P-class and M-class GSTs were not optimally situated to form an edge-to-face electrostatic interaction. (2) In addition, inspection of the unbound and conjugate-bound structures in GST A1-1 indicated that Phe-10 was the only residue not contained in

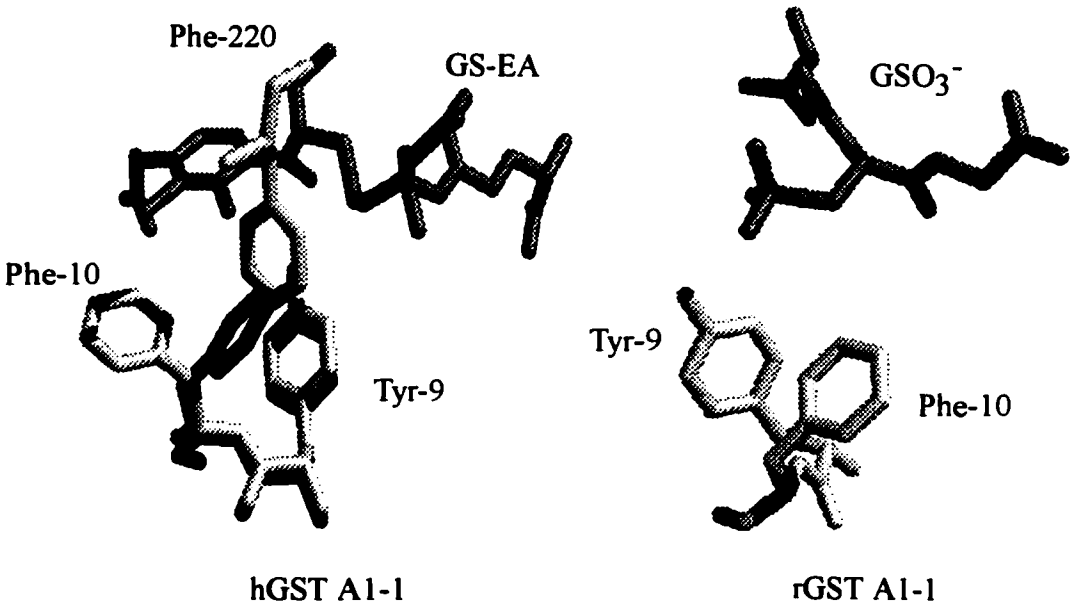

Figure 2.2: Comparison of edge-to-face electrostatic interaction in GST A1-1. Similar to hGST A1-1, the rGST A1-1 exhibits an edge-to-face interaction between the ring edge of Phe-10 and the π-cloud of Tyr-9. However, the Phe-10 in the [rGSTA1-1•GSO_3^-] complex makes a steeper angle with and is closer to the center of the aromatic ring of catalytic Tyr.

the C-terminus that exhibited significant rearrangement. In contrast, the relative orientation of the corresponding residue in the P-class and M-class GSTs (Phe and Trp, respectively) did not change at all.

Previous studies have shown that mutations at Phe-220 of GST A1-1 resulted in modest changes in the pK_a values of Tyr-9 and bound GSH as well as in the dynamics of the C-terminus (Atkins, et al., 1997; Gustafsson, et al., 1999; Dietze, et al., 1996b). Interestingly, these mutations modulated the ionization state of Tyr-9 and GSH even though residue 220 is highly disordered in the apo-enzyme and in the GSO_3^- complex. Moreover, biochemical studies suggest that a disordered C-terminus contributes to the local active site environment in the GSH complex (Lian, 1998; Allardyce, et al., 2000; Allardyce, et al., 1999).

Given all of the unique features of GST A1-1, it is conceivable that the ionization properties of Tyr-9 are modulated by its interaction with Phe-10. Additionally, the available crystal structures suggest that Phe-10 plays a critical role in ligand-dependent dynamics of the C-terminal helix. In order to explore the role of Phe-10 in modulating Tyr-9 pK_a and ligand binding, site-directed mutants of rGST A1-1 containing F10A, F10L, and F10Y substitutions were characterized. Our results underscore the importance of edge-to-face electrostatic interaction between the electropositive ring edge of Phe-10 and the negatively charged π-cloud of Tyr-9 in the stabilization of tyrosinate anion. Furthermore, removal of aromatic side chain at residue-10 significantly reduced the rate of GSH conjugate binding. The effects of Phe-10 substitutions were large for both steps

of biphasic binding reaction, suggesting the importance of aromatic interactions in orchestrating the dynamics of the C-terminus.

2.2 Materials and Methods

2.2.1 Chemicals

Glutathione (GSH), 1-chloro-2,4-dinitrobenzene (CDNB), 2-(N-morpholino)ethanesulfonic acid (MES), N-(2-hydroxyethyl)piperazine-N'-2-ethanesulfonic acid (HEPES), 3-(cyclohexylamino)-2-hdyroxy-1-propanesulfonic acid (CAPSO), and glutathione sulfonate (GSO_3^-) were obtained from Sigma (St. Louis, MO). The Michael adduct of ethacrynic acid and glutathione (GS-EA) was synthesized, and its purity analyzed as previously described (Nieslanik, et al., 1999).

2.2.2 Site-directed Mutagenesis

The Phe-10 mutants of rGST A1-1 were constructed by PCR-based amplification of a fragment spanning the *Eco*RI and *Bgl*II restriction sites contained in the linearized pKKGTB34 or pKKGTB34-W21F plasmid. Construction of the pKKGTB34 plasmid has been described previously (Wang, et al., 1989). Similarly, the Phe-220 mutants and the C-terminal truncation mutant were constructed by PCR-based amplification of a fragment spanning the *Bgl*II and *Sal*I restriction sites contained in the aforementioned plasmids (Dietze, et al., 1996a). The sequences of the oligonucleotide primers encoding the F10Y, F10A, and F10L mutants are shown below.

5'-GTGCTTCACTAC**TA**CAATG*CTCGAG*GCAGAATGGAG-3' F10Y

5'-GTGCTTCACTAC**GC**CAATG*CTCGAG*GCAAATGGAG-3' F10A

5'-GTGCTTCACTAC**CTG**AATGCCCGGGGCCAGA-3' F10L

Indicated in bold letters and italic letters are the mismatched codons and unique *Xho*I sites, respectively. All primers spanned the *Eco*RI site. The final PCR product was digested with *Eco*RI and *Bgl*II and subcloned into pKKGTB34 or pKKGTB34-W21F plasmids that were digested with similar set of restriction enzymes. Conditions for the PCR reactions were 10 mM $(NH_4)SO_4$, 20 mM Tris (pH 8.3), 3 mM $MgSO_4$, 200 μM each dNTP, 0.1% Triton X-100, 10 ng of linearized template, and 1 unit of Vent DNA polymerase (New England Biolabs). The cycle profiles were 94°C for 1 min, 65°C for 1 min, and 72°C for 1 min for 25 cycles, followed by 10 min at 72°C. All mutants were validated by DNA sequencing.

2.2.3 Protein Expression and Purification

The expression and purification of rGST A1-1 mutants have been described (Dietze, et al., 1996b). Briefly, *E. coli* AB1899 cells harboring the plasmid were used to express wild-type or mutant proteins. The proteins were purified by using a GSH affinity column and a diethylaminoethyl anion exchange (DEAE) column. Fractions containing GST were pooled and then chromatographed on a gel filtration column (Sephadex G75) to remove GSH. Mutant proteins purified by this method were pure on the basis of SDS-PAGE. To ensure that the C-terminus was not proteolyzed during *E. coli* expression, the mutant proteins were analyzed via liquid chromatography-electrospray ionization mass

spectrometry (LC-ESI MS). All mutants were full length, showing the expected molecular mass.

2.2.4 Ab Initio Model Calculations

The model calculations described below were performed as described previously (Dietze, et al., 1996a). The Tyr-9 and Phe-10 were modeled as p-cresol and benzene, respectively, using the coordinates of the non-hydrogen atoms of rat or human GST A1-1 as indicated (PDB files 1EV4 and 1GUH). Geometry optimization was performed with the Hartree-Fock theory and the 3-21G* basis set. The coordinates of Phe-10 in rat GST A1-1 were used as templates for p-cresol-10, isobutane-10, and methane-10 to provide the mimics of Tyr-10, Leu-10, and Ala-10, respectively. The structures of these models, in complex with p-cresol-9, were optimized as indicated above. Single point energy calculations of the proton affinity were performed with the 6-31+G* basis set. The recovered energies are those required to remove a proton from p-cresol-9.

2.2.5 Steady-State Kinetics

Enzymatic activity was determined spectrophotometrically with 1 mM CDNB and 1 mM GSH as described (Habig, et al., 1974b). The kinetic parameters for CDNB and GSH were measured at pH 6.5 and 25°C, using the following conditions: (a) 0.1-3 mM CDNB in the presence of 1 mM GSH and (b) 0.1-4 mM GSH in the presence of 1 mM CDNB. The k_{cat} and K_M values were determined by fitting the collected data to the Michaelis-Menten equation via Enzfitter program (Biosoft®).

2.2.6 Spectroscopic Determination of Tyr-9 pK_a

The pK_a of Tyr-9 was determined by both fluorescence and UV absorbance spectroscopy. Because the pK_a values determined by the two methods were identical within experimental error, only those obtained by fluorescence were reported. Fluorescence titrations were performed as described previously (Atkins, et al., 1993). Briefly, samples contained 1 μM GST in a mixed buffer of 35 mM MES/35 mM Tris/35 mM CAPSO at various pH and 25°C. The pK_a values were determined from the fluorescence intensity at 305 nm of excitation spectra, as well as from the spectral center of mass of emission spectra. Fluorescence titrations were also carried out at 5°C in the absence and presence of 1.5 mM S-hexylgluathione. For difference absorbance spectroscopy, samples contained 10 μM GST in the same mixed buffer system. The absorption intensity at 295 nm due to tyrosinate was monitored at 0.5 pH unit intervals between pH 5.5 and 9.5. Titration data were fitted to an equation describing single ionization via Enzfitter.

2.2.7 Spectroscopic Determination of GSH pK_a

The pK_a of GSH bound to mutant protein was determined as described (Graminski, et al., 1989). Briefly, the UV difference spectra of samples containing 10 μM GST in the absence and presence of 400 μM GSH were determined via Cary 3E spectrophotometer. Samples were prepared in 50 mM MES/50 mM HEPES/50 mM Tris/ 1 mM EDTA at various pH. The spectra of the binary [GST•GSH] complex were

measured between 230 and 300 nm. The absorption intensity at 239 nm due to thiolate formation was monitored at 0.25 pH unit intervals between pH 5.5 and 8.

2.2.8 GST Binding and Dissociation Kinetics

Binding and dissociation experiments were performed via BioLogic SFM/QFM stopped-flow fluorometer as described previously (15). The rate constants for the binding reaction were measured by the decrease in protein fluorescence after rapid mixing of an equal volume of 2 μM GST and 20-400 μM GS-EA at 15°C. Kinetic data were analyzed and fitted to a single (eq 1) or double (eq 2) exponential decay equation: where a_1 and a_2 are the amplitudes of the two observed rate constants k_{obs1} and k_{obs2}, t is the time, and C is the offset.

$$f(x) = a_1 e^{-k_{obs1} t} + C \qquad (1)$$

$$f(x) = a_1 e^{-k_{obs1} t} + a_2 e^{-k_{obs2} t} + C \qquad (2)$$

Under conditions when two rate constants were experimentally observed, the rapid association and dissociation rates, k_1 and $k_{-1(calc)}$, were fitted to an equation (eq 3) describing the linear dependence of k_{obs1} on GS-EA concentration:

$$k_{obs1} = k_{-1(calc)} + k_1[GS - EA] \qquad (3)$$

The association and dissociation rates of the slower step of the binding reaction, k_2 and $k_{-2(calc)}$, were fitted to an equation (eq 4) describing the hyperbolic dependence of k_{obs2} on GS-EA concentration:

$$k_{obs2} = k_{-2(calc)} + \frac{k_2}{1 + (K_1 / [GS - EA])} \qquad (4)$$

In cases where a single rate constant was observed, plots of k_{obs} versus GS-EA concentration also fit best to a hyperbolic curve (eq 5):

$$k_{obs2} = k_{-2(calc)} + \frac{k_2[GS-EA]}{K_1+[GS-EA]} \qquad (5)$$

The dissociation of product from the [GST•GS-EA] complex was monitored by the increase in fluorescence intensity after rapid mixing of an equal volume of 2 μM complex and 5 mM of trapping agent, GS-sulfonate (GSO_3^-). The dissociation rate constants, $k_{-1(exp)}$ and $k_{-2(exp)}$, were measured directly from a single (eq 1) or double (eq 2) exponential fit to the raw data.

2.3 Results

2.3.1 Molecular Basis for the Low pK_a of Tyr-9 in GST A1-1

The electrostatic contribution of Arg-15 in the stabilization of tyrosinate-9 of hGST A1-1 has been described (Bjornestedt, et al., 1995). Substituting the side chain of Arg-15 with hydrophobic side chain, as in the R15L mutant, resulted in Tyr-9 pK_a of 8.8, which was significantly below the pK_a of 10.3 for tyrosine in solution. Thus, we hypothesized that other electrostatic interactions contribute to the ionization properties of Tyr-9. Notably, the first-sphere interaction between the electropositive ring edge of Phe-10 and the π-cloud of Tyr-9 may contribute to the unusually low pK_a of the latter.

The contribution of edge-to-face electrostatic interactions between aromatic residues in stability of protein structure has been shown in previous studies (Burley, et al., 1985; Kretsinger, et al., 1973; Babu, et al., 1985; Hertzberg, et al., 1985). The

packing between aromatic rings within proteins is considered to be energetically favorable, providing an estimate of ~0.5-1 kcal/mol of interaction energies in solution (Burley, et al., 1988; Burley, et al., 1985).

The energetic contribution of aromatic-aromatic interactions is highly dependent on distance and orientation (Burley, et al., 1985; Burley, et al., 1988; Mecozzi, et al., 1996; Mitchell, et al., 1994; Gallivan, et al., 1999). To determine whether or not the edge-to-face electrostatic interaction between Phe-10 and Tyr-9 is favorable, *ab initio* calculations were performed with model compounds superimposed on the three-dimensional coordinates of the residues in the apo structure of hGST A1-1 and the [rGSTA1-1•GSO_3^-] complex. Tyr-9 and Phe-10 were mimicked by p-cresol and benzene, respectively. The non-hydrogen atoms were constrained to the coordinates of the protein, followed by geometry optimizations of neutral and deprotonated p-cresol-9. In addition, the F10Y, F10A, and F10L mutations were mimicked by p-cresol, methane, and isobutane, respectively, and the proton affinities of Tyr-9 for each were also calculated. Cyclohexane was used as a non-aromatic mimic of Phe-10. During the geometry optimizations, cyclohexane was observed to adopt several conformations, which stabilized the phenolate (Tyrosinate-9) more than the methane (Ala-10) or isobutane (Leu-10) but less than the benzene (Phe-10). The results of the gas-phase calculations are shown on Table 2.1, with an average value reported for several conformations of cyclohexane. These calculations neither represent the absolute magnitude of aromatic-aromatic interactions in the active site of protein nor predict the pK_a values for the active site Tyr-9 of GST A1-1 or Phe-10 mutants discussed below.

Nonetheless, these calculations should provide a qualitative estimate of the sign and relative magnitude of the energetic effects on the pK_a of Tyr-9 upon mutation of Phe-10.

The results presented on Table 2.1 indicate that the orientation and distance of Phe-10 and Tyr-9 observed in the crystal structures of rGST A1-1 are sufficient to stabilize the tyrosinate anion, thereby lowering the pK_a of Tyr-9. On the other hand, model calculations with aliphatic constituents, such as alanine (modeled by methane) or leucine (modeled by isobutane), suggest that the acidity of Tyr-9 would be decreased. Similarly, model calculations with the hGST A1-1 coordinates underscore the importance of the orientation of aromatic residues in edge-to-face electrostatic interactions. In the human isoform, the aromatic ring of Phe-10 is oriented toward Tyr-9 at a less steep angle than the rGST A1-1. In fact, the Phe-10 in hGST A1-1 is more parallel with Tyr-9, with its ring edge oriented toward the phenolic hydroxyl group. As a result, the model calculations suggest that the pK_a of Tyr-9 would decrease in hGST A1-1 compared to the rat isoform, although by a very small amount (Table 2.1). Interestingly, this is observed experimentally (Bjornestedt, et al., 1995; *vide infra*). Apparently, the direct electrostatic interaction between the ring edge of Phe-10 and the hydroxyl group of Tyr-9 may contribute to the low pK_a in hGST A1-1. Moreover, it was observed that if the coordinates of Phe-10 were not constrained to the crystal structure of human isoform, then the ring of Phe-10 turned toward the center of Tyr-9 ring to make a steeper angle. This observation underscores the importance of such electrostatic interactions in some conformations.

Table 2.1: Gas-Phase Proton Affinities for Tyr-9 from Model Calculations[a]

	Tyr-9-OH → Tyr-9-O$^-$ + H$^+$	
Model	Proton affinity (kcal/mol)	ΔE (kcal/mol)
p-cresol-9	447.05	
human GST A1-1		
p-cresol-9/benzene-10	365.74	-81.31
rat GST A1-1		
p-cresol-9/benzene-10	368.44	-78.61
p-cresol-9/p-cresol-10	392.47	-54.58
p-cresol-9/cyclohexane-10	394.57	-49.76
p-cresol-9/isobutane-10	471.88	+24.83
p-cresol-9/methane-10	548.82	+101.76

[a]Energy required to remove a proton from Tyr-9. The non-hydrogen atoms of p-cresol-9 and benzene-10, which serve as mimics of Tyr-9 and Phe-10, were constrained to the coordinates of [rGSTA1-1•GSO_3^-] complex (Adman, et al., 2001). The optimized structures of p-cresol-10, isobutane-10, methane-10, and cyclohexane-10 provide mimics of tyrosine, leucine, alanine, and non-aromatic residue, respectively. Similarly, the non-hydrogen atoms of p-cresol-9 and benzene-10 in the hGST A1-1 model were constrained to the coordinates of the human isoform with bound S-benzylglutathione (Sinning, et al., 1993).

2.3.2 Characterization of Phe-10 Mutants

In order to determine the role of edge-to-face electrostatic interaction between

Phe-10 and Tyr-9 in rGST A1-1, three amino acid substitutions were made (i.e., F10Y, F10L, and F10A). In these studies, the W21F mutant was used as a "wild-type" template. The steady-state kinetic parameters for the true wild-type and the W21F mutant are shown on Table 2.2. As previously described, the fluorometrically silent Phe in the W21F mutant facilitates in the spectroscopic characterization of Tyr-9 (Atkins, et al., 1993). In most spectroscopic studies, the W21F is the wild-type reference. In contrast, the true wild-type is used as a reference for the stopped-flow studies.

As part of the initial characterization of Phe-10 mutants, the steady-state kinetic parameters were determined for the conjugation reaction of GSH to CDNB. The recovered parameters on Table 2.2 indicate that Phe-10 mutants result in modest increase in K_M for CDNB but a slightly more pronounced increase in K_M for GSH. As expected for a mutant that retains the edge-to-face interaction, the k_{cat} for F10Y is comparable to that of wild-type. In contrast, the k_{cat} for F10A mutant is significantly reduced by 4-fold. The effects on turnover rates are presumably due to an increase in pK_a of GSH at the active site and alterations in ligand-dependent desolvation. Meanwhile, the effects on K_M may result from ligand-dependent conformational changes at the C-terminus and at Phe-10.

Table 2.2: Steady-State Parameters of rGST A1-1 and Site-Directed Mutants

Enzyme	k_{cat} (s^{-1})	K_M (μM)	k_{cat}/K_M (mM^{-1} s^{-1})
		CDNB	
WT[a]	52 ± 2	560 ± 60	93 ± 6
W21F[a]	47 ± 5	520 ± 50	90 ± 9
F10Y:W21F	43 ± 2	753 ± 119	57 ± 2
F10A:W21F	12 ± 1	585 ± 119	20 ± 4
F10L:W21F	25 ± 2	479 ± 66	51 ± 1
W21F:F220Y	55 ± 7	410 ± 40	134 ± 4
W21F:F220I	14 ± 2	300 ± 14	47 ± 6
		GSH	
WT[a]	51 ± 2	310 ± 30	164 ± 12
W21F[a]	62 ± 6	370 ± 30	167 ± 12
F10Y:W21F	43 ± 1	1014 ± 133	42 ± 1
F10A:W21F	12 ± 1	714 ± 94	17 ± 3
F10L:W21F	26 ± 1	551 ± 98	47 ± 3
W21F:F220Y	65 ± 7	331 ± 19	196 ± 19
W21F:F220I	14 ± 2	330 ± 31	42 ± 7

[a]Values taken from Wang, et al., 1992.

2.3.3 *Spectroscopic Determination of Tyr-9 pK_a in Apo and S-hexylglutathione-Bound GST A1-1*

The pK_a of active site Tyr-9 in each of the mutants was compared to the wild-type by employing fluorescence methods previously described (Atkins, et al., 1993; Dietze, et al., 1996b). Briefly, the titration method exploits the different absorption and emission properties of tyrosine and tyrosinate. Tyrosine has absorption maxima at 225 nm (ϵ = 8200 cm^{-1} M^{-1}) and 278 nm (ϵ = 1350 cm^{-1} M^{-1}), while tyrosinate has absorption maxima at 244-255 nm (ϵ = 11,000 cm^{-1} M^{-1}) and 295 nm (ϵ = 2350 cm^{-1} M^{-1}). Moreover, the emission maxima of tyrosine are in the 305-315 nm range, compared to 330-350 nm for tyrosinate. Thus, the contribution of tyrosinate to the total fluorescence intensity of the protein can be assigned unequivocally by monitoring the excitation and emission wavelengths. Figure 2.3 shows the typical spectra for wild-type and Phe-10 mutants at several pHs. The results from fluorescence titration are summarized on Table 2.3. The pK_a of Tyr-9 in each mutant was also determined by UV spectroscopy (Bjornestedt, et al., 1995). Essentially, the pK_as recovered from such method were identical to those obtained by fluorescence. As hypothesized, the pK_a of Tyr-9 in the F10Y mutant was comparable to the pK_a in wild-type. Removal of an aromatic ring, such as in the F10A mutant, increased the pK_a of Tyr-9 by ~1 pK_a unit, which corresponds to an increase in $\Delta\Delta G$ for ionization of Tyr-9 of +1.4 kcal/mol. The hydrophobic side chain substitution in F10L mutant resulted in increased pK_a, with $\Delta\Delta G$ for ionization of +0.5 kcal/mol.

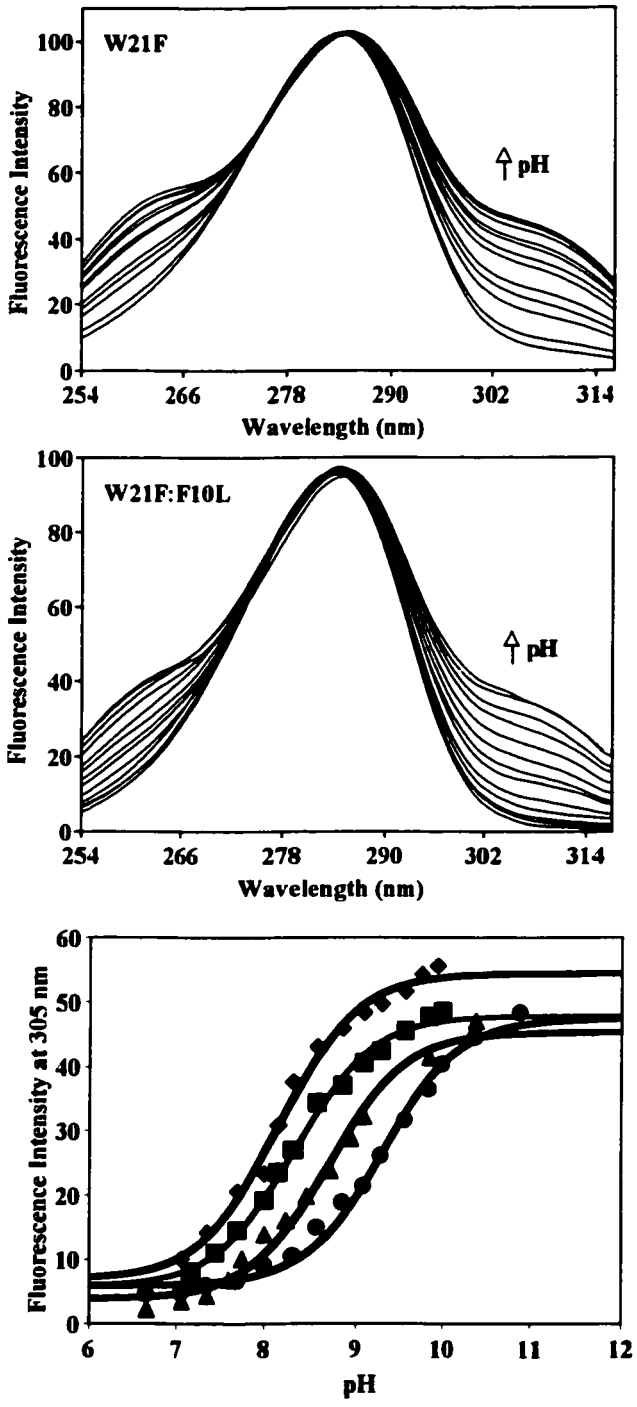

Figure 2.3: Titration of Tyr-9 in Phe-10 mutants. Normalized excitation spectra of W21F and F10L:W21F at variable pHs. The spectral bands at 258 nm and 305 nm result from tyrosinate formation in W21F (squares), W21F:F10Y (diamonds), W21F:F10L (triangles), and W21F:F10A (circles).

For comparison, the pK_a of Tyr-9 in each Phe-220 mutant, namely F220Y and F220I, was determined. As noted earlier, crystal structures indicate that Phe-220 displaces Phe-10 in the helix-closed conformation with GSH conjugates bound at the active site. Both F220Y and F220I substitutions decreased the pK_a of Tyr-9 in the free enzyme (i.e., apo rGST A1-1) (Table 2.3). These results are analogous to the pK_a values reported for hGST A1-1 containing the F220A and F220T substitutions (Gustafsson, et al., 1999). Interestingly, the substitution with non-aromatic side chain at Phe-10 had the opposite effect on Tyr-9 than substitution at Phe-220. Together, these results suggest that aromatic interactions between Phe-10 and Tyr-9 are necessary in lowering the pK_a of the phenolic group of the latter. Meanwhile, aromatic interactions involving Phe-220 in the apo-enzyme are not necessary. In fact, the pK_a of Tyr-9 is even lower with non-aromatic residue at position 220 (Atkins, et al., 1997; Gustafsson, et al., 1999; Table 2.3).

As noted above, the Phe-10/Tyr-9 interactions in the apo-enzyme are replaced by Phe-220/Tyr-9 interactions in several structures containing GSH conjugates, with closed C-terminal helix. However, the Phe-220/Tyr-9 interaction is less intimate than Phe-10/Tyr-9 interaction, in that the ring of Phe-220 is not in van der Waals contact with the radius of Tyr-9. Rather, the ring edge of Phe-220 is ~3 Å from the center of Tyr-9. In such a position, Phe-220 could still provide a weak electrostatic stabilization of Tyr-9, whose pK_a would be expected to remain low. To examine this possibility, the pK_a of Tyr-9 with bound S-hexylglutathione (S-hexyl GSH) was determined in each mutant. This ligand was previously shown to induce closure of the C-terminus (Adman, et al.,

Table 2.3: pK_a Values for Tyr-9 in Disordered and Ordered States

Enzyme	pK_a Tyr-9[a] open	$\Delta\Delta G$[b] (kcal/mol)	pK_a Tyr-9[c] closed	$\Delta\Delta G$[d] (kcal/mol)
W21F	8.3 ± 0.2		9.0 ± 0.3	
F10Y:W21F	8.2 ± 0.2	-0.1	9.2 ± 0.1	+0.3
F10A:W21F	9.4 ± 0.1	+1.4	9.6 ± 0.1	+0.8
F10L:W21F	8.7 ± 0.1	+0.5	9.5 ± 0.1	+0.7
W21F:F220Y	7.9 ± 0.1	-0.3	8.3 ± 0.1	-0.9
W21F:F220I	7.7 ± 0.2	-0.6	8.4 ± 0.1	-0.8
Δ209-222	8.0 ± 0.2	-0.2	8.5 ± 0.1	-0.7

[a]pK_a for the apoenzyme. [b]$\Delta\Delta G = (-RT \ln K_d)$ for apo W21F minus $(-RT \ln K_d)$ for the apo form of the mutant entry. [c]pK_a for the Tyr-9 in the presence of 1.5 mM S-hexylGSH. [d]$\Delta\Delta G = (-RT \ln K_d)$ for the [W21F•S-hexylGSH] complex minus $(-RT \ln K_d)$ for the S-hexylGSH complex of the mutant entry.

2001; Le Trong, et al., 2002). As summarized in Table 2.3 and Figure 2.4, the pK_a of Tyr-9 remains significantly below the pK_a of free tyrosine in solution. The increase of only 0.7 pK_a unit in wild-type upon addition of ligand suggests that the pK_a of Tyr-9 remains lower than normal Tyr and that ~5% of complex remains unprotonated at equilibrium at physiological pH. Qualitatively, the Phe-10 mutations, F10A and F10L, have similar effect on Tyr-9 pK_a in the apo-enzyme as for the bound rGST A1-1. On the other hand, the pK_a of Tyr-9 in the F10Y mutant increased for the bound state.

Similarly, the effect of Phe-220 in the S-hexyl GSH complex with a closed C-terminus is an increase in Tyr-9 pK_a. Interestingly, the pK_as in Phe-220 mutants are lower than in the [W21F•S-hexylGSH] complex. In fact, removal of aromatic ring at Phe-220 resulted in a pK_a of Tyr-9 that is even lower than the bound wild-type. It appears that the aromatic-aromatic interaction between Phe-10 and Tyr-9 in the apo-enzyme is not functionally replaced by Phe-220/Tyr-9 interaction in the closed conformation. However, Phe-10 is necessary to maintain a low Tyr-9 pK_a in [GST•ligand] complex, presumably by anchoring the C-terminus in its closed conformation.

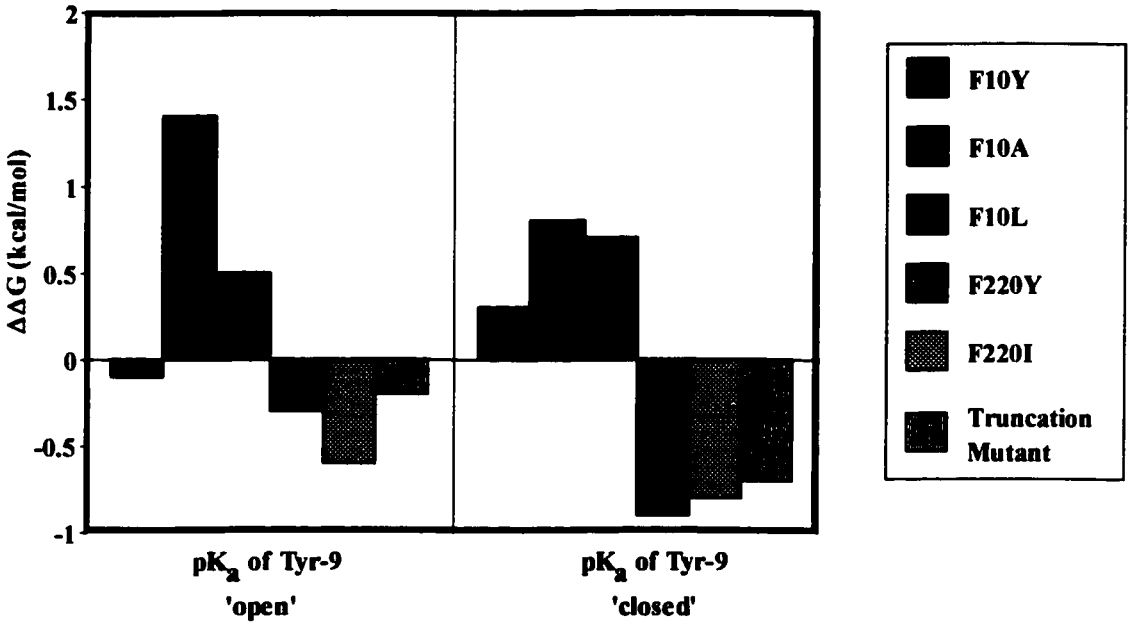

Figure 2.4: Effects of Phe-10 and Phe-220 substitutions on ΔG for ionization of Tyr-9. In the apo-enzyme and S-hexyl GSH complex, the non-aromatic mutations cause an increase in Tyr-9 pK_a. Mutations within, or truncation of, the C-terminus has the opposite effect.

2.3.4 Spectroscopic Determination of [GST•GSH] pK_a

In principle, any interaction that affects the first-sphere hydrogen bonding interaction between the hydroxyl group of Tyr-9 and the thiol group of GSH will determine the pK_a of the latter. A decrease in the acidity of Tyr-9 would be expected to weaken the Tyr-OH•••$^-$SG hydrogen bond, thus increasing the pK_a of GSH. Inasmuch as the Phe-10/Tyr-9 interactions are maintained in the [GST•GSH] complex, the pK_a of bound GSH is expected to change upon mutations at Phe-10. To explore this possibility, the pK_a of GSH in the binary complex was determined by UV difference spectroscopy, monitoring thiolate absorption at 239 nm (Graminski, et al., 1989; Dietze, et al., 1996a). In comparison to the wild-type (W21F), the pK_a of GSH in the F10Y mutant is not significantly altered, as expected for a mutant with no significant change in Tyr-9 pK_a (Table 2.4). In contrast, F10A and F10L mutants increased the pK_a of GSH,

Table 2.4: pK_a Values of the Thiol Group of Enzyme-Bound Glutathione in rGST A1-1 and Site-Directed Mutants

Enzyme	pK_a of GSH	Enzyme	pK_a of GSH
W21F	7.46 ± 0.06	W21F:F220Y	7.02 ± 0.05
F10Y:W21F	7.38 ± 0.08	W21F:F220I	8.32 ± 0.04
F10A:W21F	7.76 ± 0.18	Δ209-222	7.72 ± 0.11
F10L:W21F	7.73 ± 0.13		

although the change in pK_a was small and outside the range of experimental error. Obviously, the effects of Phe-10 mutations are more pronounced on the pK_a of Tyr-9. Nonetheless, the linear free energy relationship, with Bronsted coefficient $\alpha = 0.37$ ($r^2 = 0.88$), between the pK_a of bound GSH and the pK_a of free Tyr-9 in W21F and various mutants illustrate the contribution of Tyr-9 hydrogen bond to the ionization of GSH (Figure 2.5).

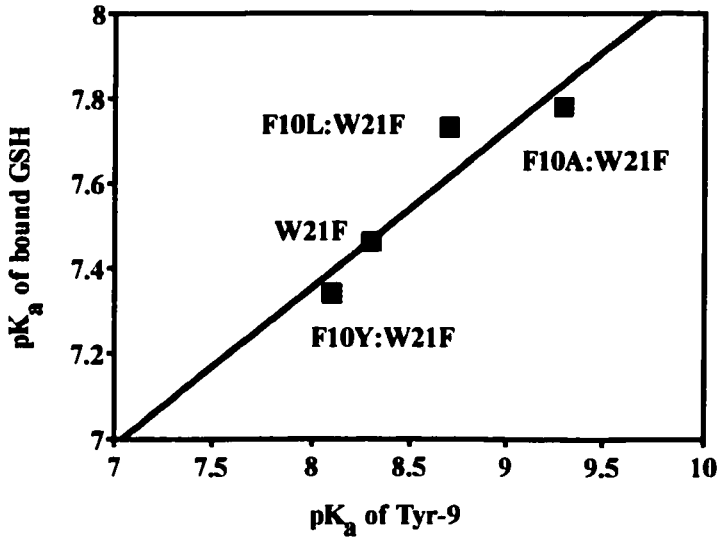

Figure 2.5: Linear free energy relationship between the pK_a of free Tyr-9 and the pK_a of enzyme-bound GSH in various rGST A1-1 site-directed mutants. The slope of the linear plot represents the Bronsted α value (0.37), which measures the sensitivity of GSH ionization to the pK_a of Tyr-9, and thus reflects the strength of hydrogen bond shared between them. The values of α are usually between 0 and 1, with negligible hydrogen bond yielding a value of 0 and strong hydrogen bond yielding a value of 1.

2.3.5 Ionization Properties of C-Terminal Truncation Mutant

As alluded to earlier, X-ray structures suggest that there are no specific

interactions between the C-terminus and active site residues in the apo-enzyme and [GSTA1-1•GSO_3^-] complex (Cameron, et al., 1995; Sinning, et al., 1993; Adman, et al., 2001). However, Phe-220 substitutions indicate modest changes in the pK_as of Tyr-9 and GSH via an apparent poorly understood mechanism (Atkins, et al., 1997; Gustafsson, et al., 1999). In principle, the observed changes in the F10A substitution could be due to indirect effects transmitted through the C-terminus. In this case, substitution at Phe-10 could alter the conformational space near Tyr-9 that is sampled by the C-terminus and thereby alter the pK_as of Tyr-9 and bound GSH. To test this possibility, the pK_as of Tyr-9 and GSH for a C-terminal truncation mutant which lacks the last 13 residues, namely Δ209-222, were measured. Similar truncation mutants in GST A1-1 and GST A2-2 have been characterized in previous studies wherein the proteins were found to be structurally intact but functionally impaired (Nieslanik, et al., 1999; Board, et al., 1991). The binding and dissociation of product conjugate GS-EA with Δ209-222 mutant have been characterized previously by stopped-flow kinetics (Nieslanik, et al., 1999). This mutant has specific activity which is ~20% of the wild-type enzyme. Moreover, the rate of binding of GS-EA to this mutant was comparable to the wild-type, but the release of the same ligand was more rapid than the wild-type. Table 2.4 indicates that the pK_as of Tyr-9 and bound GSH for Δ209-222 were essentially similar to the wild-type. Apparently, the C-terminus is not the critical determinant of the pK_as of Tyr-9 and GSH. Therefore, the observed effects for the Phe-10 mutants are not likely to be due to indirect effects transmitted through the C-terminal helix.

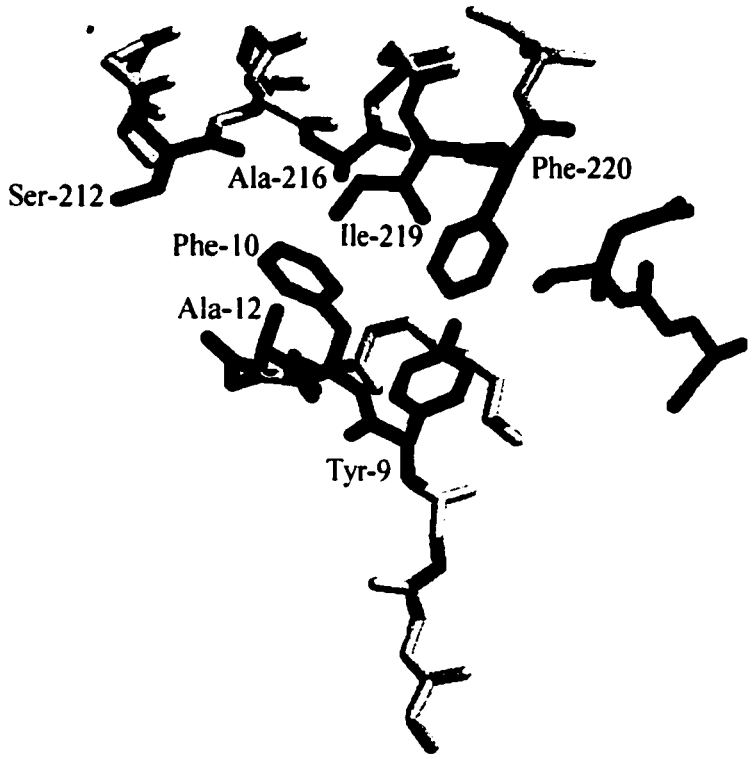

Figure 2.6: Hydrophobic pocket within the active site of hGST A1-1. In the presence of ligand, the aromatic side chain of Phe-10 fits into a hydrophobic pocket formed by Ala-12, Ser-212, Ala-216, and Ile-219. This accommodation also supports the aromatic side chain of Phe-220. The bound ligand in this crystal structure is GS-EA. Indicated in red is the glutathione moiety of the bound GS-EA. For clarity, the structure of the ethacrynic acid (EA) was not shown.

2.3.6 Kinetics of Ligand Binding and Dissociation

The available X-ray structures indicate that Phe-10 is a critical component of ligand-dependent dynamics of the C-terminus. This residue must be completely displaced from its interaction with Tyr-9 in order to bring the C-terminus over the active

site. One interesting possibility deduced from the ionization properties of Tyr-9 in the apo-enzyme and ligand-bound F10A mutant (Table 2.3) is that the C-terminus adopts a closed conformation even in the absence of ligand. Removal of the aromatic side chain at residue-10 would shift the conformational ensemble toward the 'closed' but 'disordered' states and thereby decrease the population of the 'open' states available for ligand docking. In the ligand-bound (closed) state, the aromatic side chain of Phe-10 fits into a hydrophobic pocket formed by Ala-12, Ser-212, Ala-216, and Ile-219 (Figure 2.6). This accommodation, in turn, creates a hydrophobic pocket for Phe-220. Mutation at Phe-10 may perturb the hydrophobic pocket necessary to stabilize the 'closed and ordered' C-terminus. This would then decrease the affinity and rates of ligand binding. To test this hypothesis, the kinetics of ligand binding and dissociation were determined via stopped-flow fluorescence.

As previously described for rGST A1-1 and hGST A1-1, the binding of GSH conjugates follows a biphasic mechanism (Scheme 2.1), which includes a bimolecular

$$\text{GST} + \text{GS-EA} \underset{k_{-1}}{\overset{k_1}{\rightleftharpoons}} [\text{GST}\cdot\text{GS-EA}]_{\text{disordered}} \underset{k_{-2}}{\overset{k_2}{\rightleftharpoons}} [\text{GST}\cdot\text{GS-EA}]_{\text{ordered}}$$

Scheme 2.1

Table 2.5: Kinetic Parameters for GS-EA Binding to rGST A1-1 WT and Site-Directed Mutants at 15°C

	WT[a]	F220Y[a]	F220I[a]	F10A[a]	F10Y[a]	F10L
Amp_1[b]	0.0091	0.0029	0.0074	0.013		0.0045
k_1 (μM^{-1} s^{-1})[c,d]	6.11	7.92	4.81	0.41		0.65
Amp_{-1}	0.0043	0.0044	0.0037	0.0098		0.0077
$k_{-1(exp)}$ (s^{-1})[c]	15.9	9.37	20.44	8.04		13.3
$k_{-1(calc)}$ (s^{-1})[d]	14.7	6.84	24.22	9.81		14.1
K_1 (μM^{-1})	2.60	1.18	4.25	19.6	2.03	22.1
Amp_2	0.051	0.082	0.032	0.046	0.034	0.025
k_2 (s^{-1})[d]	17.6	29.6	10.2	0.811	26.3	1.28
Amp_{-2}	0.018	0.022	0.021	0.013	0.014	0.011
$k_{-2(exp)}$ (s^{-1})[c]	1.51	0.77	4.26	0.59	8.1	0.48
$k_{-2(calc)}$ (s^{-1})[d]	1.89	0.83	6.96	0.51	11.9	0.51
K_2[g]	0.086	0.026	0.42	0.73	0.026	0.42
K_d (μM)[h]	0.19	0.03	1.25	8.25	0.48	6.05

[a]Values were taken from Nieslanik, 2000. [b]Amplitude values refer to the magnitude of the pre-exponential terms for the rate constants k_1, $k_{-1(exp)}$, k_2, and $k_{-2(exp)}$, as determined from stopped-flow experiments. [c]The rate constants for all enzymes were determined from duplicate or triplicate experiments, where 15-30 scans were averaged. The standard deviation was less than ±0.8 for k_1, ±0.7 for k_{-1}, ±0.9 for k_2, and ±0.5 for k_{-2}. [d]Kinetic binding and dissociation constants were determined by curve fitting the k_{obs} *vs.* GS-EA plots to eqs 3 and 4. [e]Rates of GS-EA dissociation were directly determined from a fit of the raw data to a single or double exponential equation. [f]K_1 is determined from the ratio $k_{-1(exp)}/k_1$ or eq 5. [g]K_2 is determined from the ratio $k_{-2(exp)}/k2$. [h]Equilibrium dissociation constants were determined from $K_{d(calc)} = K_1[k_{-2}/(k_2 + k_{-2})]$.

docking step (k_1, k_{-1}) and a slower unimolecular isomerization step (k_2, k_{-2}) that corresponds to the ordering and closure of the C-terminus (Nieslanik, et al., 1999; Nieslanik, et al., 2001). The concentration-dependence of GS-EA on the observed rate constants (k_{obs}) were determined and fitted to relevant equations as described in Section 2.2.7. In general, the binding and dissociation of GS-EA in each mutant, except for F10Y, were biphasic. The rates of docking and isomerization steps in the F10A and F10L mutants were dramatically reduced in comparison to the wild-type (Table 2.5). In contrast, the F10Y mutation resulted in rate constants for the docking step that were sufficiently fast to be experimentally observed. The rate constants for the isomerization step (k_2, k_{-2}) in the F10Y mutant were faster than for the wild-type. Figure 2.7 illustrates that the approach to equilibrium after addition of GS-EA to wild-type and F10A is dramatically slower in the latter. Clearly, non-aromatic substitutions at Phe-10 result in

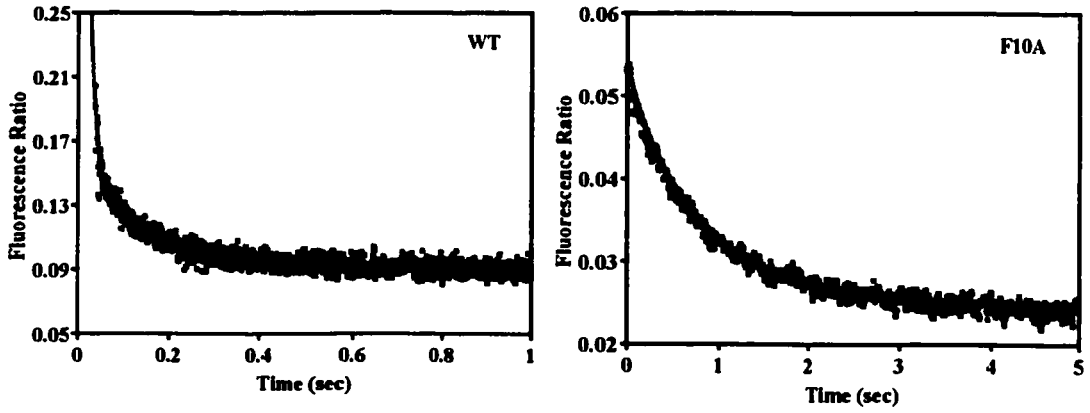

Figure 2.7: Kinetics of GS-EA binding. The stopped-flow data are shown for the approach to equilibrium for wild-type (left) and F10A (right). Ligand binding and dissociation are slowed dramatically upon substitution at Phe-10. Note the different time scales. The recovered parameters are summarized in Table 2.5.

significantly reduced rates in both steps of the ligand binding reaction as well as decreased equilibrium binding affinity.

In general, the effects of Phe-220 substitutions were less pronounced than those of Phe-10 substitutions. In fact, Phe-220 substitutions have greater effect on the second step of the ligand binding reaction, although the F220I mutation also affects the first step. The largest effects in the later stages of the reaction in the Phe-220 mutants are not surprising since the C-terminus contributes to important packing interactions with the rest of the protein residues at the active site as the reaction progresses to the final, closed state.

2.4 Discussion

2.4.1 The Role of Phe-10 in the Modulation of Tyr-9 and GSH pK_as

The available X-ray structures and amino acid sequences of the A-, M-, and P-class GSTs indicate that an aromatic residue adjacent to catalytic Tyr is conserved. However, only the A-class GSTs, particularly the A1-1 isoforms, exhibit an edge-to-face electrostatic interaction between the catalytic Tyr and adjacent residue. In both hGST A1-1 and rGST A1-1, the residue next to catalytic Tyr-9 is a phenylalanine, and both isoforms exhibit an anomalous pK_a of Tyr-9 (8.1 and 8.3, respectively) compared to that of free tyrosine in solution (10.3). However, a closer inspection of the crystal structures of apo hGST A1-1 and [rGSTA1-1•GSO_3^-] complex indicates that the aromatic ring of Phe-10 in the rat isoform is oriented at a steeper angle with Tyr-9 and is farther from the phenolic hydroxyl group (Figure 2.1). The angles formed by the rings of Tyr-9 and Phe-

10 are ~60° and 40° for the rat and human isoforms, respectively. In the hGST A1-1, the electropositive ring edge of Phe-10 is significantly closer to the Tyr-9 hydroxyl group and may, in fact, participate in an on-face electrostatic interaction. The *ab initio* calculations presented here (Table 2.1) suggest that the slightly lower pK_a of Tyr-9 in the human isoform is due, in part, to the difference in orientations of the aromatic rings.

Interestingly, the aromatic-aromatic interactions observed in GST A1-1 are not required for the even lower pK_a of catalytic Tyr in the GST A4-4, which in this case is ~6.7 (Nilsson, et al., 2000). In hGST A4-4, the residue adjacent to catalytic Tyr is a proline. The available X-ray structure of GST A4-4 suggests that Pro is not capable of lowering the pK_a of Tyr via an aromatic edge-to-face interaction. Although the present work does not provide an explanation for the unusually low pK_a of catalytic Tyr in GST A4-4, it is interesting to note that the C-terminus in this isoenzyme is static and adopts a more open conformation even in the apo-enzyme (Nilsson, et al., 2000). Apparently, GST A1-1 and GST A4-4 have evolved multiple and different mechanisms for achieving a low Tyr pK_a.

The results presented here indicate that Phe-10 plays an important role in lowering the pK_a of Tyr-9 in GST A1-1 although it is not the only determinant. As discussed earlier, Arg-15 has a functional role in lowering the pK_a of Tyr-9 in the GST A1-1 isoform. In addition to the electrostatic stabilization conferred by the guanidino group of Arg-15, its amide NH provides additional stability to Tyr-9 in the apo-enzyme. The *ab initio* gas phase calculations in the present studies show the potential of weakly polar interactions between two aromatic residues in lowering the pK_a of the phenol.

Recent studies indicate that aromatic-aromatic interactions are characterized by electrostatic and van der Waals interactions (Gervasio, et al., 2002). In fact, the binding energy between two aromatic structures involved in nonclassical hydrogen bond, such as the one described between Phe-10 and Tyr-9, is dominated by electrostatic contribution. The importance of electrostatic interactions between the electronegative π-ring of aromatic residues and electropositive groups, such as cations or protons, in proteins has been demonstrated previously (Mecozzi, et al., 1996; Mitchell, et al., 1994; Gallivan, et al., 1999). In fact, the role of weakly polar interaction between the hydroxyl proton of a Thr and aromatic ring of Tyr-6 in GST M1-1 has been shown to modulate the pK_a of bound GSH (Liu, et al., 1993). The removal of on-face hydrogen bond by substitution of Thr with aliphatic side chain resulted in increased kinetic pK_a of GSH by 0.7 pK_a unit. Obviously, this effect was substantially larger than the effects of F10A and F10L substitutions, which increased the spectroscopic pK_a of GSH by only 0.3 pK_a unit compared to wild-type. It appears that the local environment of different GSTs results in differential coupling between the pK_a of Tyr-9 and pK_a of GSH. Notably, the large changes observed in the Tyr-9 pK_as of rGST A1-1 have 'buffering' effects on the pK_a of GSH, such that a change in the pK_a of the latter is less pronounced. In contrast, the pK_a of GSH in GST M1-1 is more sensitive to the change in electrostatic environment of Tyr-6.

As the results presented on Tables 2.3 and 2.4 suggest, the C-terminus is not a major determinant of Tyr-9 pK_a, as substitutions at Phe-220 led only to modest changes in the pK_a of Tyr-9 in the apo-enzyme and GSH in its binary complex. But more

importantly, the results obtained for the C-terminal truncation mutant indicate that the C-terminus is not necessary to stabilize the Tyrosinate-9 in the apo-enzyme or GS^- in the binary complex. Although the magnitude of change in Tyr-9 pK_a of the Phe-220 mutants of rGST A1-1 and hGST A1-1 have been small, each mutant decreased the pK_a of Tyr-9. Thus, if the anomalous pK_a of Tyr-9 has a functional role, there is no evolutionary driving force to decrease it further.

In all of the X-ray structures inspected, only Phe-10 indicated a significant positional shift in going from apo-enzyme to ligand-bound enzyme. The position of Tyr-9 remains invariant, including the hydrogen bond it shares with Arg-15. In addition to its functional role in lowering Tyr-9 pK_a, Phe-10 may play a structural role, in which it stabilizes the closed conformation in the presence of GSH conjugates, such as S-hexyl GSH and GS-EA. Although the putative role of edge-to-face electrostatic interactions in protein stability is well appreciated, the effect of Phe-10 in Tyr-9 pK_a is not due to hydrophobic interactions. If this was truly the case, then substitutions of Phe-10 with Ala and Leu should decrease the hydrophobicity of Tyr-9 environment and result in Tyr-9 that is more solvated. Because the ionization of Tyr-9 is more energetically favored in a solvated environment, one would expect a decrease in the pK_a of Tyr-9 in such Phe-10 substitutions. However, this was not experimentally observed. Therefore, the electrostatic interaction between the aromatic rings of Phe-10 and Tyr-9 is the major contributor to the low pK_a of the latter.

The indirect interaction of Phe-10 with Tyr-9 in the presence of S-hexyl GSH also contributes to the low pK_a of Tyr-9. As noted earlier, S-hexyl GSH induces a closed

conformation, wherein the active site environment is likely to be desolvated. In such environment, the electrostatic interaction with Arg-15 would be strengthened, thus favoring the ionization of Tyr-9 compared to Tyr in solution. Apparently, the contribution of Phe-10 to Tyr-9 ionization changes from first-sphere electrostatic interaction in the open conformation to indirect second-sphere electrostatic interaction in the closed conformation.

2.4.2 The Role of Phe-10 in the Dynamics of C-Terminal Helix

Indubitably, the dynamics of the C-terminus in GST A1-1 influence the binding and release of ligand. NMR studies suggest that when H-site and G-site are occupied simultaneously, the C-terminus become less mobile compared to the apo-enzyme and binary complex of the protein (Lian, 1998). Thus, the C-terminus samples a number of conformational states.

A thermodynamic profile (Figure 2.8) describing the binding and dissociation of GS-EA in Phe-10 and Phe-220 mutants can be constructed from the recovered rate constants shown on Table 2.5. This was achieved by employing the transition state theory, which relates Gibbs free energy of activation ($\Delta G^{\neq}$) to the rate constant of reaction (k) via the following equation: $\Delta G^{\neq} = -RT \ln (kh/k_BT)$, where h is the Planck's constant, k_B is the Boltzmann constant, R is the molar gas constant, and T is the temperature (Moore, et al., 1981). In the ligand-free enzymes, the free energies of all proteins were normalized, as any difference in the absolute free energies due to mutation is likely to be negligible. The effects of Phe-10 mutations are apparent in both steps of

transition of the C-terminus. Particularly, the removal of aromatic side chain from residue-10, as in the F10A and F10L mutants, dramatically reduced the rates of ligand docking (k_1, k_{-1}) and isomerization steps (k_2, k_{-2}). In fact, the 8-fold increase in the equilibrium constant K_1 in both mutants is due to decreased k_1, indicating that the

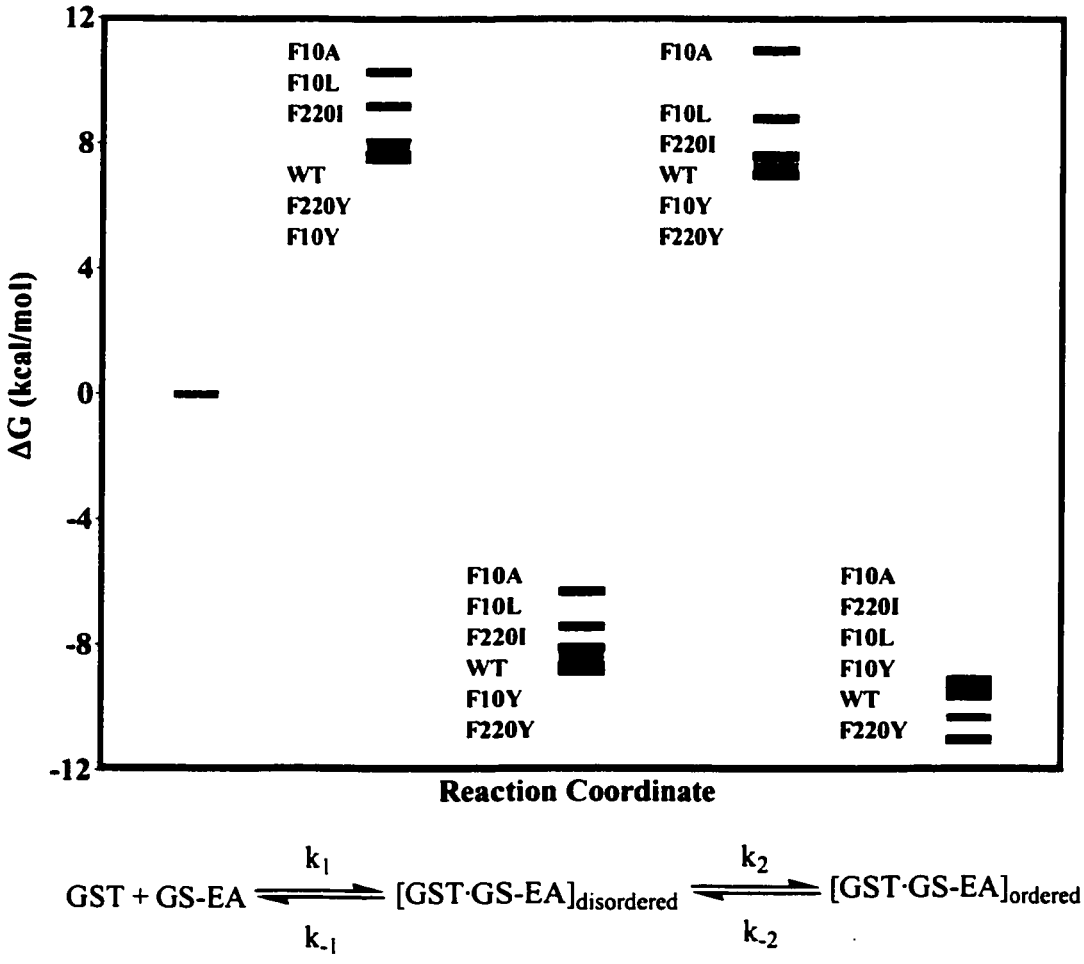

Figure 2.8: Free energy diagram for the reaction coordinate of Phe-10 and Phe-220 mutants. The free energies of the individual proteins were derived as described in the text and have been normalized in the ligand-free state (left).

unbound mutants are likely to adopt a closed conformation, which is similar to the conformation observed in the conjugate-bound structures. The effects of Phe-10 substitutions on the second step of the binding reaction (k_2, k_{-2}) are also quite pronounced. In terms of free energies, the transition state for the second step is destabilized by 1.5-3.6 kcal/mol, while the ground state for the 'ordered' equilibrium complex is destabilized by 0.8-1.2 kcal/mol. In general, the mutations at Phe-220 primarily affect the second step of the binding reaction, as expected for a residue whose position does not change much in several complexes with GSH conjugates. The transition state for the second step of the binding reaction is destabilized in the F220I mutant by only 0.3 kcal/mol, while this step is stabilized in the F220Y mutant by the same magnitude. Likewise, the ground state of closed conformation in the F220I mutant is destabilized by 0.6 kcal/mol, while such conformation is stabilized in the F220Y mutant by 0.4 kcal/mol compared to the wild-type enzyme. Altogether, the available data suggest that Phe-10 affects the kinetics of the C-terminal closure as well as the equilibrium between the open and closed states of the enzyme. Thus, Phe-10 plays a vital role in guiding the C-terminus to its final closed conformation.

2.4.3 Unified Model of Ionization State of Tyr-9 and C-Terminal Dynamics

In light of the X-ray structures of [rGSTA1-1•GSO_3^-] complex and the contribution of Phe-10 in the anomalous pK_a of Tyr-9, reinterpretation of previous high-pressure experiments is warranted. Initially, it was speculated that the pressure-dependent ionization of Tyr-9, together with the observation that Phe-220 could

contribute to the low pK_a of [GST•GSH] complex, resulted in additional interaction that would cause residue-220 within the disordered C-terminus to interact more efficiently with Tyr-9, thus favoring the ionization of the latter (Atkins, et al., 1997). This suggestion was based on previous studies in which the 'molten globule' states with significant void volume between interstitial spaces in poorly packed structural elements have 'high-volume' states compared to folded 'native' states (Vidugiris, et al., 1998; Vidugiris, et al., 1995). Although some proteins with molten globule states are moderately compressed by pressure compared to native states, others are quite sensitive to it (Nolting, et al., 1993; Vidugiris, et al., 1995; Vidugiris, et al., 1998). On the basis of these studies and available X-ray structures of hGST A1-1, the C-terminus was presumed to have features analogous to molten globules and that pressure may cause the helix to close to a more native-like state, in which residue-220 is properly oriented to lower the pK_a of GSH through aromatic-aromatic interaction or other electrostatic interactions.

Furthermore, the pressure-dependent ionization of Tyr-9 occurred at pressures well below those typically required to unfold proteins or peptides (Weber, 1986; Atkins, 1994). At such low pressures, however, protein-protein complexes may be disrupted. Interestingly, proteins have been shown to 'condense' or become more tightly packed at low pressures before they unfold at higher pressures (Cioni, et al., 1996). The earlier speculation was based on the observation that Phe-220 substitutions altered Tyr-9 pK_a, as confirmed by others (Gustafsson, et al., 1999).

As illustrated in the present studies, Phe-10 is the major determinant of the low Tyr-9 pK_a. The *ab initio* model calculations, together with the experimental results,

provide significant insights: (1) the aromatic-aromatic interaction between Phe-10 and Tyr-9 lowers the pK_a of the latter, (2) the movement of Phe-10 allows the C-terminal helix to close, and (3) the C-terminal open conformations predominate when Tyr-9 is ionized. Consequently, open conformations with intact Phe-10/Tyr-9 interactions are favored when Tyr-9 is deprotonated. This is, in fact, consistent with the observation that the C-terminal truncation mutant has a slightly lower pK_a of Tyr-9 than the wild-type.

In light of this new information, the initial speculation concerning the effect of pressure on the dynamics of the C-terminus is incorrect. Apparently pressure causes the C-terminus to open without necessarily unfolding. The increase in solvation of the C-terminus and the active site may explain the observed effects of pressure. This reinterpretation is in accord with the suggestion of Gustafsson and co-workers (Gustafsson, et al., 1999).

There are several studies that suggest that the ionization state of Tyr-9 and GSH and the dynamics of the C-terminus are coupled (Gustafsson, et al., 1999; Nieslanik, et al., 2000). The model on Figure 2.9 summarizes the available structural, spectroscopic, and thermodynamic information. In the apo-enzyme and GSH complex, the aromatic ring edge of Phe-10 is packed against the face of Tyr-9, lowering the pK_a of the latter. Moreover, Phe-10/Tyr-9 interaction prevents the closure of the C-terminus. At atmospheric pressure, Phe-10 and Phe-220 compete for the immediate space next to Tyr-9. Upon addition of pressure, the C-terminus 'opens', with the Phe-10/Tyr-9 interaction predominating to a greater extent, and thereby causing the Tyr-9 pK_a to be further reduced. The binding of GSH conjugate to the active site 'closes' the C-terminus. In

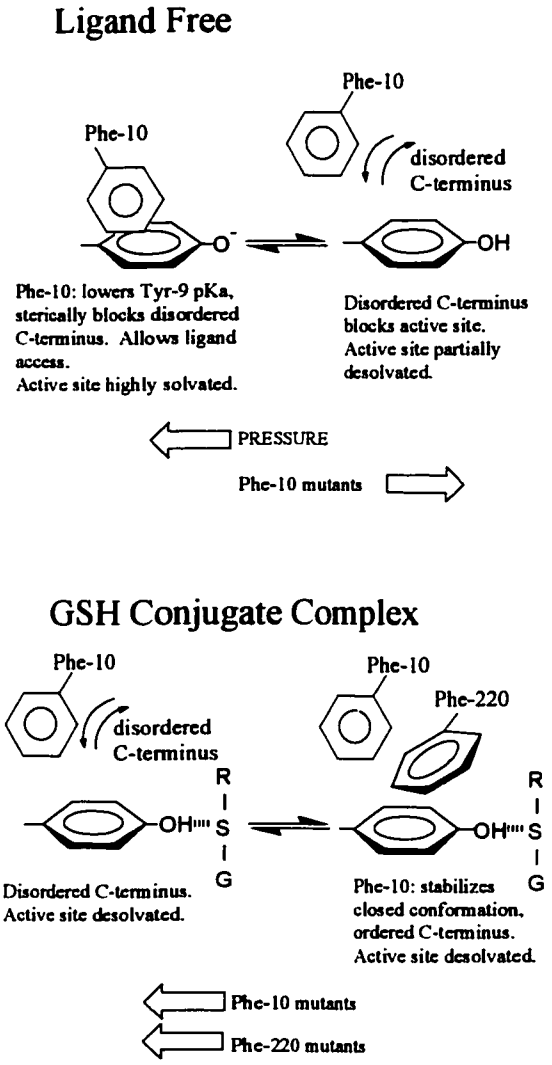

Figure 2.9: Functional role of Phe-10 in C-terminal dynamics of the apoenzyme and GSH conjugate-bound GST A1-1. In the apoenzyme, the interaction of aromatic ring edge of Phe-10 with the aromatic π-cloud of catalytic Tyr-9 directly lowers the pK_a of the latter residue. As long as this interaction is intact, the disordered C-terminus is prevented from sampling a conformational space over the active site. Phe-10 also plays an important role in the GSH conjugate (R-S-G) complex by allowing the aromatic ring of Phe-220 to interact with the active site. The effects of hydrostatic pressure (Atkins, et al., 1997) and mutations at Phe-10 and Phe-220 (Atkins, et al., 1997; Gustafsson, et al., 1999) in the C-terminal dynamics are also indicated. Apparently, the F220Y mutant is an exception, in that it stabilizes the closed conformation.

such conformation, Phe-10 indirectly stabilizes the Tyrosinate-9, presumably by providing part of the hydrophobic pocket into which Phe-220 is docked.

The observed effects on the Tyr-9 pK_as in the Phe-220 mutants are likely to be due to the conformational status of the C-terminus. Because all Phe-220 mutations result in further decrease of Tyr-9 pK_a in the apo-enzyme, the open conformations are presumed to be favored. This is consistent with the increased on-rate for GSH observed in the F220A and F220T mutants (Gustafsson, et al., 1999). Although the effect of F220I substitution on Tyr-9 pK_a is similar to F220A and F220T mutations, the rate of GS-EA binding is decreased. The difference in results probably reflects the different conformational requirements for GSH binding *vs.* GSH-conjugate binding. In the present studies, the effects of Phe-220 mutations on ligand binding rates are smaller than those found in Phe-10 mutations. It appears that these point mutations alter the pre-equilibrium between conformational states in the apo-enzyme, and different conformers preferentially bind ligands. Among the Phe-220 and Phe-10 mutants, the F220Y mutant is the only one with decreased GSH pK_a and decreased K_2 value, suggesting a more tightly closed C-terminus. Although the possibility of on-face hydrogen bond with Tyr-9 has been suggested in the F220Y mutant, this is unlikely the case in the apo-enzyme. However, such interaction could not be ruled out in the presence of GSH-conjugate.

Thermodynamic studies suggest that the C-terminus of GST A1-1 contributes to catalysis by active site desolvation, which occurs during the early stages of ligand binding (Nieslanik, et al., 2001). Presumably, the open conformations of the C-terminus are favored by the ionization of Tyr-9, at which time the active site becomes solvated. In

contrast, protonation of Tyr-9 promotes desolvation of the active site and ordering of the C-terminus. Together, these results indicate that Phe-10 plays a critical role in orchestrating the ionization of Tyr-9, the solvation of active site, and the conformational dynamics of the C-terminus.

CHAPTER 3

THE FUNCTIONAL SIGNIFICANCE OF THE ANOMALOUS pK_a OF TYR-9 IN GLUTATHIONE S-TRANSFERASE A1-1: PARALLEL PATHWAYS FOR PRODUCT DISSOCIATION

3.1 Introduction

Although the functional role of the anomalous pK_a of catalytic Tyr-9 (8.1-8.3) in the A-class GST has not been identified, the structural basis for Tyr-9 ionization is reasonably well understood. For the A-class GSTs, the proximity of amide NH of Arg-15 to the hydroxyl group of Tyr-9 is believed to contribute to the low pK_a of the latter residue via a hydrogen bond. In addition, the guanidinium side chain of Arg-15 contributes via electrostatic effects (Bjornestedt, et al., 1995). Site-directed mutagenesis studies on hGST A1-1 indicate that substitution of Arg-15 with Leu resulted in a Tyr-9 pK_a of 8.8, which is significantly below the pK_a of free Tyr (10.3) in solution. However, this modest change in pK_a led us to hypothesize that other interactions might contribute to the ionization of Tyr-9. As described in Chapter 2, Phe-10 has, in fact, an important contribution to the ionization state of Tyr-9. Specifically, the edge-to-face electrostatic interaction between Phe-10 and Tyr-9 facilitates the ionization of tyrosyl hydroxyl group in the apo-enzyme (Ibarra, et al., 2001). Removal of this interaction by mutagenesis dramatically altered the ionization behavior of Tyr-9 at the active site. In this case, the Tyr-9 pK_a of F10A mutant increased by ~1 pK_a unit compared to the wild-type enzyme.

Together, these structural features including Phe-10 and Arg-15 are likely to account for the unusually low pK_a of Tyr-9.

The functional significance of the dynamic C-terminus of GST A1-1 in enzyme catalysis has been demonstrated in steady-state studies in which product release was determined to be the rate-limiting step of the catalytic cycle (Nieslanik et al., 1998). As previously described for hGST A1-1, wild-type rGST A1-1, and several mutants, the binding of GS-EA follows a 2-step mechanism, which includes a fast docking step (k_1, k_{-1}) and a slower isomerization step (k_2, k_{-2}) that corresponds to the ordering and closure of the C-terminus (Scheme 2.1). Indirect evidence suggests an intimate link between the ionization state of Tyr-9 and the dynamics of the C-terminus. For example, the C-terminal truncation mutant (Δ209-222) in the rGST A1-1 has a Tyr-9 pK_a that is modestly lower than the wild-type, suggesting that the solvated active site in this mutant facilitates ionization of Tyr-9 (Ibarra, et al., 2001). In fact, the rate of docking of GS-EA to this mutant was described by a single docking step, and its release was more rapid (Nieslanik, et al., 1999). Moreover, the conservative substitution at Tyr-9 (Y9F) significantly reduced the rate constants for the second step of the ligand binding reaction, indicating the importance of phenolic hydroxyl in the isomerization of the C-terminus. In other studies, the Y9F mutant exhibited increased affinity for GSH product conjugate and CDNB (Allardyce, et al., 1999). Overall, these results suggest that the ionization state of Tyr-9 contributes to the C-terminal dynamics, and that the helix is open preferentially when Tyr-9 is ionized or unprotonated. One possible implication is that ligands will preferentially bind to or dissociate from the ionized state of the enzyme.

Although previous studies suggest that the ionization state of Tyr-9 controls the dynamics of the C-terminus of GST A1-1, there has been no direct evidence that supports the hypothesis that ligand binding is also governed by the ionization state of Tyr-9. Possibly, the Y9F mutant has altered ligand binding properties due to subtle mutation-induced structural changes rather than ionization-dependent effects. The objectives of the present chapter were to determine directly whether (1) local conformational changes at the C-terminus are in fact due to the ionization properties of the active site Tyr-9 and (2) the extent and rate of ligand binding and release are coupled to the ionization state of Tyr-9. The results indicate that the binding and release of ligand are tightly coupled to the ionization of Tyr-9 at the active site. Therefore, these results provide a clear functional role for the unusual pK_a of Tyr-9.

3.2 Materials and Methods

3.2.1 Chemicals and Instrumentation

GSH, EA, MES, CAPSO, and GSO_3^- were obtained from Sigma (St. Louis, MO). Synthesis of GS-EA was described previously (Nieslanik, et al., 1999). As in Chapter 2, the stopped-flow experiments were performed with a BioLogic SFM/QFM fluorimeter, while steady-state fluorescence was performed with an Aminco SLM-8100 spectrofluorimeter.

3.2.2 F222W Site-Directed Mutants

The construction of W21F:F222W has been previously described (Nieslanik, et

al., 2001). The triple mutant Y9F:W21F:F222W was constructed by subcloning the available W21F:F222W insert, which was acquired from *Bgl*II and *Sal*I digests, into a Y9F:W21F plasmid that has been linearized with similar set of restriction enzymes. Originally, the single and double Y9F mutants were generated by PCR-based amplification of a fragment spanning the *Eco*RI and *Bgl*II restriction sites contained in the linearized pKKGTB34 or pKKGTB34-W21F plasmid (Wang, et al., 1989). All mutants employed in the present studies were validated by DNA sequencing.

3.2.3 Protein Expression and Purification

The expression and purification of wild-type rGST A1-1 and its various mutants have been described previously (Ibarra, et al., 2001). The purity of each protein was assessed by SDS-PAGE. Enzymatic activity of each mutant was assessed as described in previous studies (Habig, et al., 1974).

3.2.4 Determination of Conformational Transition in GST A1-1

The fluorescence properties of two reporter mutants of rGST A1-1, W21F:F222W and Y9F:W21F:F222W, were monitored to determine whether conformational changes at the C-terminus correlate with the ionization of Tyr-9 at the active site. For each mutant, the emission spectra were monitored at excitation wavelength of 295 nm, with slit widths of both monochromators set to 4 nm. In contrast to the previously employed tyrosine titration method (Atkins, et al., 1993), here the emission properties of tryptophan were exploited to determine the nature of the surrounding environment of this residue. The

pH-dependence of Trp emission was monitored in 2 μM GST prepared in a mixed buffer of 35 mM MES/35 mM Tris/35 mM CAPSO at 25°C. The pK_a values were determined by fitting the spectral center of mass, emission peak intensity, relative intensity at 305 nm, and relative intensity at 345 nm vs. pH to an equation describing single ionization via Enzfitter. Parallel fluorescence titrations were also performed in the presence of 200 μM S-hexylglutathione.

3.2.5 Equilibrium Binding Studies

The equilibrium dissociation constants (K_D) for the Michael addition product GS-EA were determined by the decrease in the fluorescence of W21F:F222W, Y9F:W21F:F222W, and Δ209-222 upon ligand binding. During the titration experiments, serial dilutions of equilibrated [GST•GS-EA] complex, consisting initially of 0.5 μM GST and 100 μM GS-EA in a mixed buffer system at pH 6.5 and 9, were made. The steady-state emission of each protein at 25°C was monitored at an excitation wavelength of 295 nm, using slit widths of 4 nm. The observed fluorescence intensity at each dilution was corrected for the emission intensity of a reference buffer. The mole fraction of GS-EA bound to total protein was determined from the ratio of change in protein intensity when a ligand is bound and the emission intensity of the free enzyme. This fraction is further corrected for the dilution factor. K_D values were then derived from an eq (1) via DeltaGraph 4:

$$\nu = P * \frac{[GS-EA]_{free} / K_D}{1 + ([GS-EA]_{free} / K_D)} + C \qquad (1)$$

where ν is the mole fraction of GS-EA bound to protein and P and C are the upper plateau and lower plateau, respectively, of the ν vs. $[GS\text{-}EA]_{free}$ plot.

3.2.6 GST Binding and Dissociation Kinetics

Stopped-flow fluorescence studies were performed to determine the rates of ligand binding and dissociation as described in previous studies (Ibarra, et al., 2001; Nieslanik, et al., 1999; Nieslanik, et al., 2000; Nieslanik, et al., 2001). Briefly, the rate constants for the binding reaction were measured by monitoring the decrease in protein fluorescence after rapid mixing of equal volumes of 2 μM GST and 6.25-100 μM GS-EA at 15°C and various pH. The multicomponent buffer used in these pH-dependent studies was 35 mM MES/35 mM Tris/35 mM CAPSO to ensure constant ionic strength. Kinetic data were analyzed and fitted to a single or double exponential decay equation as described in Chapter 2. In cases where two rate constants were experimentally observed, the rapid association and dissociation rates, k_1 and $k_{-1(calc)}$, were fitted to an equation (eq 2) that describes the linear dependence of k_{obs1} on GS-EA concentration:

$$k_{obs1} = k_{-1(calc)} + k_1[GS-EA] \qquad (2)$$

It should be noted that the $k_{-1(calc)}$ values derived from the binding experiment and the above equation are different from $k_{-1(exp)}$ values that were directly determined from the dissociation experiments. The association and dissociation rates of the slower step of the binding reaction, k_2 and $k_{-2(calc)}$, were determined from a hyperbolic dependence (eq 3) of k_{obs2} on GS-EA concentration:

$$k_{obs2} = k_{-2(calc)} + \frac{k_2}{1 + (K_1 / [GS - EA]} \qquad (3)$$

Alternatively, a single observed rate, k_{obs}, could be plotted against GS-EA concentration to yield a hyperbolic curve fit (eq 4):

$$k_{obs2} = k_{-2(calc)} + \frac{k_2[GS - EA]}{K_1 + [GS - EA]} \qquad (4)$$

The dissociation of product from the [GST•GS-EA] complex was measured by monitoring the increase in fluorescence intensity after rapid mixing of equal volumes of 2 μM complex and 4 mM of the trapping agent, GSO_3^-. The dissociation rate constants, $k_{-1(exp)}$ and $k_{-2(exp)}$, were measured from a single or double exponential fit to the raw data.

3.3 Results

3.3.1 Characterization of C-Terminal Dynamics by Fluorescence

The previous studies on the anomalous pK_a of catalytic Tyr-9 in rGST A1-1 suggest that the ionization state of the tyrosyl hydroxyl group influences the dynamics of the C-terminus (Ibarra, et al., 2001; Atkins, et al., 1997). In both human and rat isoforms, the native Trp-21 near the domain-domain interface serves as a probe of global microconformational changes that occur upon ligand binding (Dirr et al., 1999; Wang, et al., 1993). However, to directly investigate the localized structural changes at the C-terminus, the W21F:F222W mutant was constructed and characterized (Nieslanik, et al., 2001). The kinetics of ligand binding and dissociation for this mutant are comparable to the wild-type enzyme, suggesting that global changes in protein conformation are

coupled to local conformational changes at the C-terminus. Thus, the W21F:F222W mutant serves as a faithful mimic of ligand binding to the wild-type.

In order to determine the relationship between the ionization state of Tyr-9 and C-terminal dynamics, the W21F:F222W mutant was titrated between pH 7 and 10 to monitor the fluorescence emission properties of the terminal Trp. The emission of Trp, which absorbs at 275-295 nm and emits light at 340-353 nm, is very sensitive to its local environment and is often used as a direct probe of conformational changes in protein (Lakowicz, 1999). The changes in the emission spectra of Trp-222 in the site-directed mutants reflect the polarity of the surrounding environment. Figure 3.1 summarizes the typical emission spectra for the W21F:F222W and Y9F:W21F:F222W mutants at several pHs. The emission intensity decreases and the spectrum is red-shifted up to 7 nm with

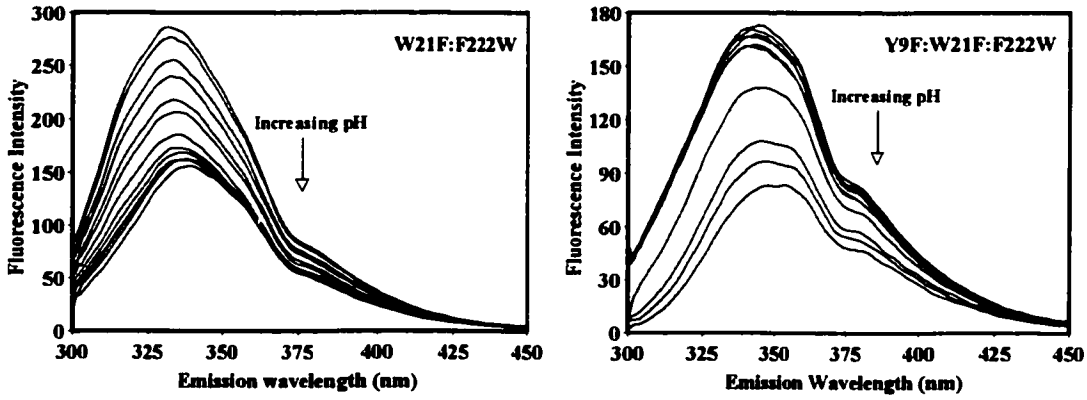

Figure 3.1: Emission of Trp-222 in the C-terminus of rGST A1-1 mutants. The fluorescence emission spectra of W21F:F222W (left) and Y9F:W21F:F222W (right) are shown at variable pHs. While the emission spectra of W21F:F222W was very sensitive to pH in the range of 7-8, the emission of Y9F:W21F:F222W was constant except at higher pHs.

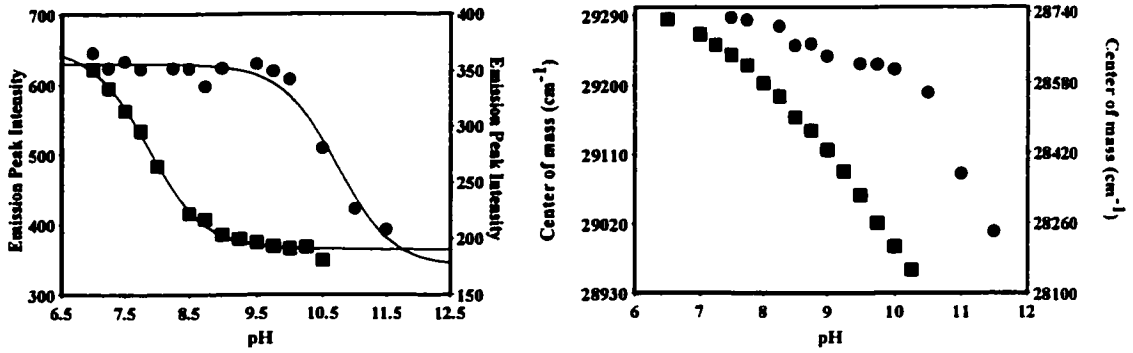

Figure 3.2: pH-dependence of conformational transition. The pH-dependence of the emission peak intensity (left) and the spectral center of mass (right) in the W21F:F222W (squares) and Y9F:W21F:F222W (circles) reflect the changes in the polarity of the active site. Note that the additional ordinate axis on the right applies to the Y9F:W21F:F222W mutant. The recovered pK_a values (Table 3.1) are for the spectral transition based on peak intensity.

increasing pH in the W21F:F222W mutant. In contrast, the emission intensity of Y9F:W21F:F222W mutant remained relatively constant, except at the very high pHs, at which the maximal spectral red-shift was approximately 2 nm. Clearly, the W21F:F222W exhibits a large pH-dependent change in environment only when Tyr-9 is present. From the fluorescence titrations employed, the pK_a values for this transition could be determined by fitting the spectral peak intensity, relative intensity at 305 nm or relative intensity at 345 nm against pH via single ionization model (Figure 3.2). The average pK_a values recovered from all curve fittings based on intensity change are 7.9 and 10.5 for W21F:F222W and Y9F:W21F:F222W, respectively (Table 3.1).

A more sensitive measurement of polarity at the active site of the enzyme is the pH-dependence of spectral center of mass, which closely resembles the trend observed in

Table 3.1: Recovered pK_a Values for Trp-222 Spectral Transition in the Free and Bound rGST A1-1 Mutants

Enzyme	pK_a[a] free	pK_a[b] bound
W21F:F222W	7.9 ± 0.1	9.3 ± 0.1
Y9F:W21F:F222W	10.5 ± 0.1	10.8 ± 0.1

[a]Recovered pK_a in the apo-enzyme. [b]Recovered pK_a in the presence of 200 μM S-hexylglutathione.

the pH-dependence of peak intensity (Figure 3.2). However, the spectral center of mass in W21F:F222W does not reach a plateau after pH 9.5. In fact, the center of mass continues to decrease even after pH 10. Presumably, at high pH, tyrosine residues in the protein become ionized, and contribute to the additional spectral red-shift as observed in the control Y9F:W21F:F222W mutant. Whereas tyrosine or tyrosinate would not contribute significantly to the change in intensity at the emission maximum of Trp-222, their spectral signals would contribute to the overall spectral center of mass. Therefore, an accurate pK_a for the conformational transition based on Trp-222 parameters could not be obtained. Although the spectral center of mass data could not be fitted to an equation yielding a pK_a, they clearly demonstrate a change in Trp polarity in the pH range of 7.5-8.5, which does not occur in the triple mutant. In addition, the overall pK_a recovered from the intensity data of W21F:F222W most likely reflects the pK_a of active site Tyr-9. Although the catalytic Tyr in the triple mutant had been removed, the apparent pK_a of 10.5 is probably due to seven other tyrosines present in the protein that become ionized at very high pH.

As described in Chapter 2, the binding of S-hexylglutathione (S-hexyl GSH) to GST A1-1 has been shown to induce closure of the C-terminus, with Tyr-9 pK_a (~9) remaining lower than the pK_a of free tyrosine in solution. To determine the validity of these observations, the emission spectra of W21F:F222W and Y9F:W21F:F222W were also obtained in the presence of saturating concentration of S-hexyl GSH. The addition of S-hexyl GSH in the titration experiments does not interfere with the emission measurements. If the pH-dependent changes observed with W21F:F222W correlate with the ionization of Tyr-9 in the apo-enzyme, and if ionization is a major determinant of helix dynamics, then spectral changes would still be observed in the presence of S-hexyl GSH, but at a higher pH. The recovered pK_a values for the conformational transition (Table 3.1) indicate an increase of 1.4 pK_a unit for the ligand-bound W21F:F222W compared to the apo-enzyme, in excellent agreement with previously observed ligand-dependent increase in Tyr-9 pK_a. This increase suggests that, at equilibrium, ~3% of the conjugate-bound W21F:F222W remains unprotonated at pH 7.5. Also, the triple mutant Y9F:W21F:F222W was titrated with ligand at each pH, in order to determine whether the observed pH-dependence was related to Tyr-9 ionization. As expected for a mutant with no ionizable group at residue 9, the bound conjugate had little effect on the apparent pK_a for the conformational transition of the triple mutant.

Together, these spectroscopic studies demonstrate that the local conformational equilibria of the C-terminus are pH-dependent in addition to being ligand-dependent. Moreover, this pH-dependence exhibits an apparent pK_a equivalent to the pK_a of Tyr-9

(~8) in the apo-form and pK_a of ~9 for the ligand-bound form, and such pH-dependent behavior is eliminated upon removal of the Tyr-9 phenolic hydroxyl.

3.3.2 Binding Affinity of GS-EA

Equilibrium binding studies were explored as an initial strategy to determine whether GSH conjugates bind preferentially to or dissociate from the ionized, open form of GST A1-1. These studies were performed at pH 6.5 and 9 where the active site Tyr-9 in bound rGST A1-1 (pK_a ~9.3) is completely protonated and significantly unprotonated (ionized), respectively. The protein was found to be unstable at highly basic conditions, and therefore, equilibrium binding studies beyond pH 9 were not pursued. The ligand employed in equilibrium studies was GS-EA, for which we have previously characterized the binding mechanism in detail and which has been shown to be a high affinity ligand of rGST A1-1 via pre-steady state kinetics and equilibrium studies (Nieslanik, et al., 1999; Nieslanik, et al., 2001). Moreover, crystal structures demonstrate that the helix is 'closed' and ordered with GS-EA bound. The maximal emission intensities of W21F:F222W and Y9F:W21F:F222W at pH 6.5 were measured at 333 nm and 330 nm, respectively, at varying ratios of GS-EA:protein. In the presence of GS-EA, these emission maxima blue-shifted to 321 nm, as previously shown (Le Trong, et al., 2002). At pH 9, only the W21F:F222W mutant exhibited red-shifted emission spectra. Equilibrium ligand binding studies were also performed on the C-terminal truncation mutant, Δ209-222, for comparison. Typical binding isotherms, from which K_D values were determined, are shown on Figure 3.3. The recovered K_D values are reported in

Table 3.2. At pH 6.5, the W21F:F222W mutant yielded a K_D of 3.3 μM, which is comparable to a previously determined K_D of wild-type via steady-state fluorescence (Nieslanik, et al., 1999). The K_D for GS-EA significantly increased by 2.5-fold at pH 9, indicative of lower affinity at equilibrium when Tyr-9 is ionized. In previous studies, the C-terminal truncation has been shown to exhibit Tyr-9 pK_a that is slightly lower than the wild-type (Ibarra, et al., 2001). Moreover, with an open, solvent-accessible active site, GS-EA was found to bind to the Δ209-222 mutant (K_D ~6.4 μM) with 3-fold increased K_D compared to the wild-type enzyme (Nieslanik et al., 1999). In the present studies, the measured K_D for GS-EA in this mutant is 8.4 μM at pH 6.5, which is 2.5-fold greater

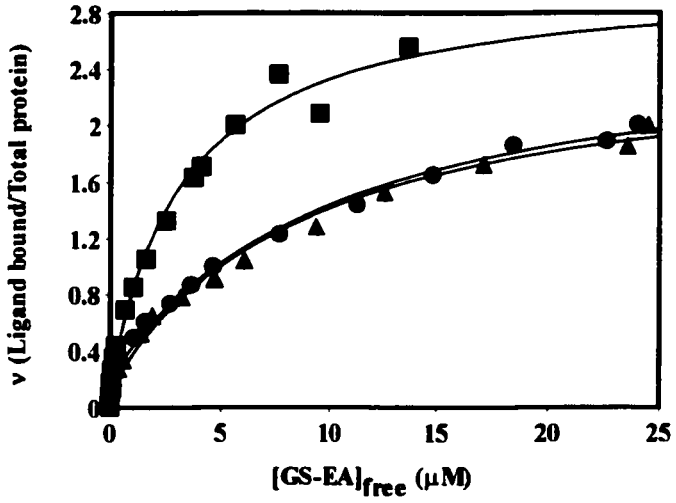

Figure 3.3: Equilibrium binding of GS-EA to rGST A1-1 mutants at pH 6.5. The fluorescence of W21F:F222W (squares), Y9F:W21F:F222W (circles), and C-terminal truncation mutant (triangles) in complex with GS-EA was monitored at excitation wavelength of 295 nm. The K_D values for GS-EA were determined from nonlinear regression fits to the mole fraction of GS-EA bound to protein vs. concentration of free GS-EA via eq 1, as described in Section 3.2.5.

Table 3.2: Equilibrium Binding Dissociation Constants for GS-EA at 25°C

Enzyme	K_D (μM) at pH 6.5	K_D (μM) at pH 9
W21F:F222W	3.3 ± 0.4	10.3 ± 0.6
Y9F:W21F:F222W	9.7 ± 0.1	9.7 ± 0.2
Δ209-222	8.4 ± 0.2	8.4 ± 0.1

than W21F:F222W. Thus, physical truncation of the C-terminus or increased pH lowers the ligand affinity to a similar extent. As expected for a mutant lacking the C-terminus to restrict the access of solvent and ligand at the active site, the Δ209-222 mutant did not show a pH-dependence of K_D (Table 3.2). Similarly, the Y9F:W21F:F222W mutant showed no apparent pH-dependence, as K_D values at pH 6.5 and 9 remained essentially unchanged. The recovered K_D values in the present studies, particularly with the triple Y9F mutant at pH 6.5, are different from the previously determined values for the single Y9F mutant with a different GSH conjugate, 7-glutathionyl-4-nitrobenzo-2-oxa-1,3-diazole (GS-NBD). The K_D values for the Y9F:W21F:F222W mutant are at least 3-fold higher than the values suggested from the previous studies (Nieslanik, et al., 2000). This discrepancy may be attributed to the difference in fluorescence properties of Trp-222 and Trp-21 in the ligand-bound Y9F:W21F:F222W ([GS-EA•GST] complex) and the Y9F mutant ([GS-NBD•GST] complex), respectively. Moreover, the subtle difference in the nature of binding of GS-EA and GS-NBD in the two separate studies may contribute to the difference in K_D values. Nonetheless, the lack of pH-dependence of K_D for GS-EA, along with spectroscopic pK_a of 10.5 for the conformational transition, suggest a

predominantly closed conformation in the Y9F:W21F:F222W mutant. But more importantly, the observed pH-dependence of K_D in the W21F:F222W mutant suggest that the ionization state of Tyr-9 controls the flexibility of the C-terminus, which in turn contributes to the K_D for ligand. However, when access to the active site is no longer limited by the C-terminus, such as in the Δ209-222 mutant, facile ligand binding and release follow. As a result, K_D is no longer dependent on pH in the absence of the C-terminus.

3.3.3 Kinetics of Ligand Binding and Dissociation

A more direct approach to examine the functional role of ionized Tyr-9 in C-terminal dynamics is a study of the pH-dependence of ligand binding. Stopped-flow fluorescence was employed to measure the individual rate constants that comprise the binding mechanism of GST A1-1 (Scheme 2.1). As described earlier, the binding of GS-EA to rGST A1-1 follows a two-step process, which includes a fast bimolecular docking step and a slow isomerization step that corresponds to the ordering and closure of the C-terminus. The binding and dissociation of GS-EA were monitored by the decrease and increase in protein fluorescence, respectively, as previously demonstrated in several manuscripts. The rate constants for the association and dissociation of GS-EA were determined by fitting to appropriate equations as described in Section 3.2.6.

As shown previously, the raw data for the wild-type fit best to double exponential equation, while the raw data for Y9F fit best to single exponential equation (Nieslanik, et al., 2000). Notably, the approach to equilibrium, as described by k_2 an k_{-2}, is

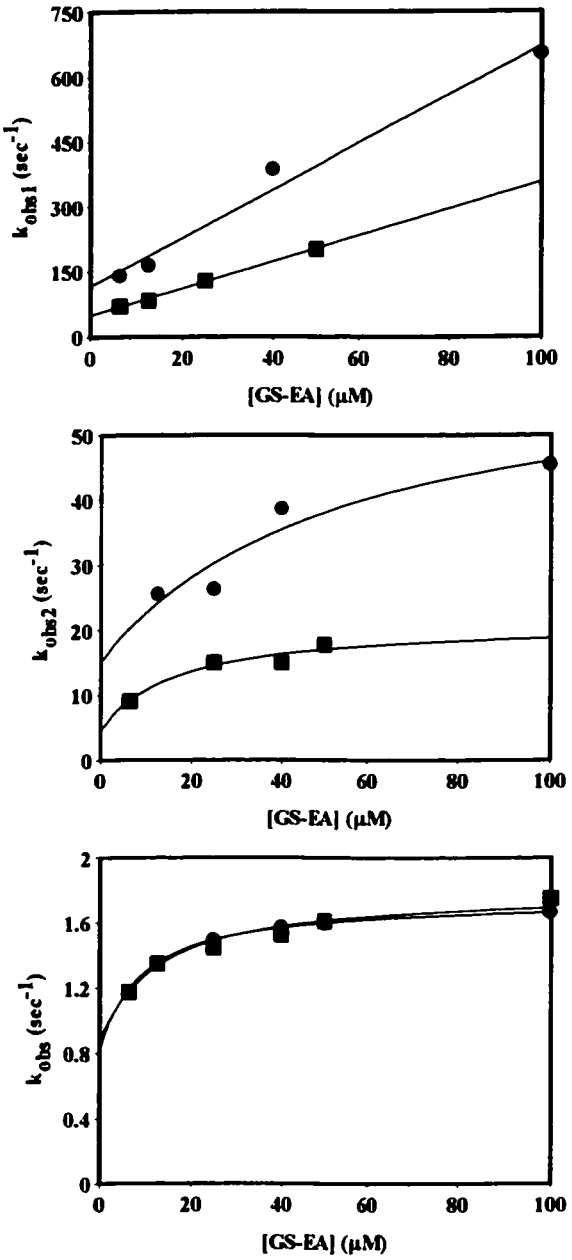

Figure 3.4: Kinetics of GS-EA binding to wild-type rGST A1-1 (top and middle) and Y9F mutant (bottom). The stopped-flow fluorescence data for GS-EA binding in wild-type and Y9F fit best to double exponential and single exponential decay, respectively. The rate constants k_{obs1} and k_{obs2} for wild-type showed linear dependence (eq 2) and hyperbolic dependence (eq 3), respectively, on GS-EA concentration ($R^2 = 0.99$ and $R^2 = 0.92$). Meanwhile, the single rate constant k_{obs} for Y9F mutant showed hyperbolic dependence (eq 4) on GS-EA concentration ($R^2 = 0.98$). Note that pH 6 (squares) and pH 9 (circles), the rate constants for wild-type showed apparent dependence on pH, while those of Y9F mutant were essentially identical at the extreme pHs. Kinetic parameters are reported in Table 3.3.

Table 3.3: Kinetic Parameters for GS-EA Binding to rGST A1-1 WT and Y9F at Variable pH and 15°C

	WT						
	pH 6	pH 6.5	pH 7	pH 8	pH 8.5	pH 9	pK_a[a]
k_1 (μM^{-1} s^{-1})	3.08	2.78	4.36	3.54	8.84	8.54	8.4
k_{-1} (s^{-1})	24.7	23.2	38.0	37.0	74.4	106	8.8
K_1 (μM^{-1})[b]	8.02	8.35	8.70	10.5	8.40	12.4	8.7
k_2 (s^{-1})	16.4	38.9	20.1	34.9	47.1	54.3	8.4
k_{-2} (s^{-1})	0.632	1.25	1.05	3.48	4.22	6.18	8.2
K_2[c]	0.039	0.032	0.052	0.100	0.090	0.114	7.4
$K_{D(calc)}$ (μM)[d]	0.30	0.26	0.43	0.95	0.69	1.27	7.7

	Y9F		
	pH 6	pH 8	pH 9
K_1 (μM^{-1})[e]	9.99	5.99	9.05
k_2 (s^{-1})	0.795	0.714	0.933
k_{-2} (s^{-1})[e]	0.925	0.681	0.804
K_2[c]	1.16	0.894	0.862
$K_{D(calc)}$ (μM)[d]	5.37	2.92	4.19

[a]The pK_a values recovered from each observed rate constant and equilibrium constant as a function of pH. [b]K_1 is determined from the ratio of k_{-1}/k_1. [c]K_2 is determined from the ratio k_{-2}/k_2. [d]Equilibrium dissociation constants were determined from $K_{D(calc)} = K_1[k_{-2}/(k_2 + k_{-2})]$. [e]$K_1$ and k_{-2} were determined from eq (6).

dramatically slower in the Y9F. The docking step could not be experimentally observed due to presumably fast k_1. Figure 3.4 shows the dependence of the observed rate constants on GS-EA concentration in wild-type and Y9F at pH 6 and 9. Although only single rate constant could be obtained from the raw data, the concentration-dependence of k_{obs} in the Y9F mutant yielded a hyperbolic curve, suggestive of two-step mechanism. Additionally, the rates of ligand binding were significantly increased at higher pH in the wild-type enzyme. In contrast, ligand binding at the extreme pHs, 6 vs. 9, is essentially

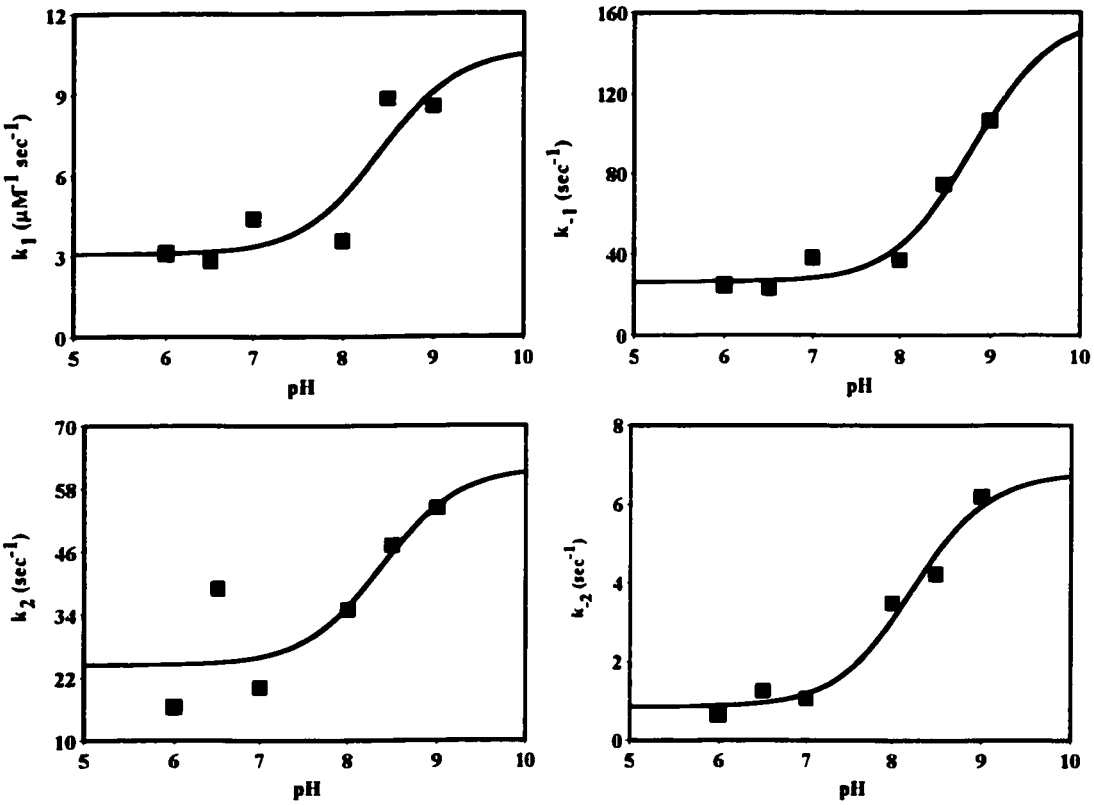

Figure 3.5: pH-dependence of observed rate constants for GS-EA binding (top left and bottom left) and dissociation (top right and bottom right) in rGST A1-1. Solid lines are nonlinear regression fits to single ionization model (Enzfitter). The recovered pKa values from each fit (Table 3.3) corresponded to the pKa of Tyr-9 in the ionized, open form of the enzyme.

identical in the Y9F mutant. As with spectral changes for Trp-222 and the equilibrium ligand binding titration, the pH-dependence observed in the double mutant is lost in the triple mutant. Apparently, Tyr-9 controls this pH-dependent behavior.

Upon the discovery of apparent pH-dependence of ligand binding and dissociation in the wild-type, other stopped-flow experiments were undertaken to determine if apparent pK_a values could be extracted from the recovered rate constants as a function of

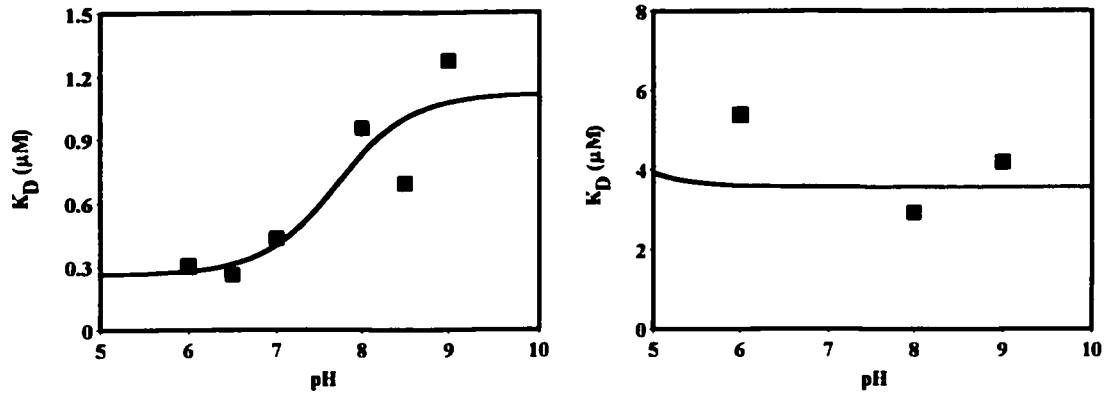

Figure 3.6: pH-dependence of equilibrium ligand binding. The dissociation of GS-EA from the wild-type rGST A1-1 (left) as a function of pH resulted in a pK_a of 7.7, which closely reflects the ionization of Tyr-9 in the open conformational state. In contrast, the Y9F (right) showed no apparent pH-dependence of ligand dissociation. Solid lines represent fits to single ionization model.

pH. The rate constants for the docking and isomerizations steps of binding reaction (Table 3.3) showed a pH-dependence and fitted well to a single ionization model, with recovered pK_a values ranging from 8.2 to 8.8 (Figure 3.5). From this set of rate constants, calculated equilibrium dissociation constants [$K_{D(calc)}$] could be obtained. Similarly, the calculated K_D values showed pH-dependence, resulting in an apparent pK_a of 7.7 (Figure 3.6). Apparently, all of the recovered pK_as (Table 3.3) reflect the ionization of Tyr-9, further suggesting that ligand docking and dissociation are favored in the open conformation of the enzyme. Due to difficulties in obtaining significant amounts of the Y9F proteins, which bind poorly to GSH affinity column, the kinetics of ligand binding and dissociation were determined at only three pHs. In contrast to the wild-type, the Y9F mutant indicated no apparent pH-dependence of rate constants (Table 3.3). Experimentally, the release of GS-EA from the active site of Y9F could not be

determined, as no apparent increase in protein fluorescence could be observed upon addition of excess trapping agent GSO_3^-. Presumably, this is due to high binding affinity of GS-EA to Y9F. However, the calculated K_Ds from the recovered rate constants were higher than those of the wild-type. As in the equilibrium binding studies, the calculated K_D values for the Y9F mutant may not represent the true equilibrium dissociation constant, as the $k_{-1(exp)}$ and $k_{-2(exp)}$ usually needed for $K_{D(calc)}$ could not be directly observed. Nonetheless, the apparent calculated K_Ds for GS-EA in Y9F were not significantly different at any given pH (Figure 3.6). Clearly, there is no indication that binding and dissociation of GS-EA in the Y9F depends on the ionization of a protein residue in this pH range.

3.4 Discussion

As already noted, there are many data that suggest indirectly a functional link between the anomalous pK_a of Tyr-9 and the dynamics of the C-terminus. For example, a coupling between Tyr-9 ionization and C-terminal dynamics is indicated by previous studies in which pressure-dependent ionization of Tyr-9, which was sensitive to C-terminal mutations, has been noted (Atkins, et al., 1997). Also, the rates of ligand binding and dissociation are dramatically altered in the Y9F mutant compared to the wild-type enzyme (Nieslanik, et al., 2000; Allardyce, et al., 1999; vide infra), further implicating a role for Tyr-9 in C-terminal dynamics. However, there has been no direct evidence regarding the functional significance of coupling between C-terminal dynamics and Tyr-9 ionization.

Although similar approaches (described below) have been used to address the pH-dependence of ligand binding to GST A1-1, the focus in those studies had been on the ionization state of GSH and how its binding and release were subsequently affected (Gustafsson, et al., 1999; Caccuri, et al., 1999; Caccuri, et al., 1998). In that case, the rates of ligand binding and release were dependent on whether or not the GSH at the active site of several GST isoforms was unprotonated. Apparently, the rates of GSH binding and release were faster at lower pH, where the ligand is mostly protonated. In contrast, the emphasis of the present studies is on the ionization state of active site Tyr-9 and how it controls the rates of binding and release of a GSH conjugate. No previous studies have directly investigated the role of Tyr-9 pK_a in binding mechanism.

To examine directly the relationship between the ionization state of Tyr-9 and the conformational status of the C-terminus, three approaches were exploited: (1) the pH-dependence of conformational dynamics of the C-terminus, as reported by an engineered Trp-222, (2) pH-dependent equilibrium binding studies, and (3) stopped-flow studies in which binding and dissociation of ligand were directly measured at variable pH. The W21F:F222W mutant serves as a good mimic of wild-type rGST A1-1, as its catalytic and binding properties are essentially identical to the wild-type (Nieslanik, et al., 2001). In previous studies, the Y9F mutant yielded an 8-12 fold decrease in the rates of isomerization (k_2, k_{-2}) of the C-terminus (Nieslanik, et al., 2000). Moreover, steady-state fluorescence indicated no appreciable Tyr ionization of this mutant at pH < 11 (Atkins, et al., 1993). In the present studies, a triple mutant, Y9F:W21F:F222W, was employed as an important control in our fluorescence titration studies, which monitored the emission

properties of Trp-222 at variable pHs. On the basis of emission properties of Trp-222, the local environments of the double and triple mutants were indeed different from each other. The decrease in the emission intensity and the red-shift in the spectrum of W21F:F222W from pH 7 to 9.5 are indicative of polar, solvent-accessible environment at higher pH. The pH-dependence of the emission profile was lost in the triple Y9F mutant. In addition, the dependence of Trp-222 spectral intensity on pH yielded an apparent pK_a of 7.9 in the W21F:F222W, which is remarkably close to the pK_a for the ionization of Tyr-9 at the active site. In contrast, the pH-dependence of spectral intensity in the Y9F:W21F:F222W mutant resulted in pKa of 10.5, which likely reflects the ionization of other tyrosines present in the protein at the extreme pHs. Apparently, the C-terminus of the triple Y9F mutant is significantly less solvated than W21F:F222W at pHs above 8, suggesting that the C-terminus in the former likely adopts a different conformation. This conclusion is further supported by similar studies in the presence of ligand known to induce closure of the C-terminus and alter the pK_a of Tyr-9. The increase in Tyr-9 pK_a of W21F:F222W, as a result of S-hexyl GSH binding, is not only consistent with our previous studies but also lends initial support to the hypothesis that the ionization of Tyr-9 also occurs to a limited extent, even with GSH conjugate bound. Indeed, the pH-dependence properties of W21F:F222W complexed with S-hexyl GSH are shifted to pK_a of 9.1, in agreement with the previously determined Tyr-9 pK_a of ligand-bound wild-type. Importantly, these are the first spectroscopic data that correlate local dynamics of the C-terminus with the ionization of Tyr-9.

The population of open and closed conformations in GST A1-1 will clearly contribute to the equilibrium ligand binding and dissociation. Perhaps more importantly, the equilibrium between open and closed forms could be expected to contribute to the rates of ligand dissociation and possibly binding. Because the apparent pK_as reported in Table 3.3 are based on a limited data set, and are therefore only estimates, the concentrations of each open and closed species at equilibrium cannot be quantitatively predicted. However, the present studies directly demonstrate that the relative affinity of a product conjugate is dependent on the ionization state of Tyr-9. In this case, ligand affinity decreases when Tyr-9 is increasingly ionized, as measured by K_D in the equilibrium binding studies of W21F:F222W. Inasmuch as the K_D values for GS-EA remain invariant in the C-terminal truncation mutant at pH 6.5 and 9, it appears that both C-terminus and Tyr-9 are critical determinants of the pH-dependence of ligand affinity at the active site. The importance of Tyr-9 in controlling the dynamics of the C-terminus is demonstrated clearly in the Y9F:W21F:F222W mutant, as removal of ionizable hydroxyl group led to no change in K_D as pH was increased from 6.5 to 9. In summary, the pH-dependence of GSH conjugate binding affinity is observed only when both C-terminus and Tyr-9 are simultaneously present.

Stopped-flow studies were performed to determine the pH-dependence of individual rate constants for the docking and isomerization steps of ligand binding reaction. Clearly, the data indicate that the binding and dissociation of GS-EA (k_1, k_{-1}) are pH-dependent, wherein the ligands bind faster to and dissociate from the ionized forms of the enzyme (Figure 3.5). Similarly, the forward and reverse rate constants for

the conformational changes of the binary complex (k_2, k_{-2}) are dependent on pH, yielding apparent pK_as that are similar to the ionization of Tyr-9 in the apo-enzyme. Based on the stopped-flow data, the equilibrium dissociation constants [$K_{D(calc)}$] for GS-EA were calculated. As expected, the calculated K_D for GS-EA in wild-type is pH-dependent with apparent pK_a of 7.9, which corresponds closely to the ionization of Tyr-9 in the apo-enzyme. In contrast, no pH-dependence of the calculated K_D was observed in the Y9F mutant. These kinetically determined K_D values show nearly the same pH-dependence as the experimental K_D values. Moreover, these results indicate that GS-EA, at equilibrium, will bind more tightly to the protonated conformation (low pH) of GST A1-1. As Tyr-9 becomes more ionized (high pH), the binding affinity of GS-EA decreases presumably due to an increase in K_2, which corresponds to the opening of the C-terminus. Clearly, the data demonstrate a pH-dependence of ligand dissociation, and that a pronounced increase in k_{-2} and K_2 at elevated pH depend on the presence and ionization of Tyr-9.

One unsatisfying aspect of the present studies is the uncertainty as to why the initial docking step (k_1, k_{-1}) is much faster for the Y9F mutant. The spectroscopic data suggest that the C-terminus occupies a more hydrophobic environment in the apo-form of this mutant, as it does in the ligand-bound W21F:F222W. If the C-terminus is 'closed' as in the GSH conjugate complex, then the initial docking step would be slow, rather than faster as observed. Although Y9F:W21F:F222W and W21F:F222W mutants have different C-terminal conformations in the apo-enzyme, the data do not provide additional structural detail. Possibly, the C-terminus in the triple mutant adopts a conformation that provide F222W with a hydrophobic environment, without it being 'closed' in a position

that sterically blocks ligand from entering the active site. Additional structural or spectroscopic studies may shed some light into this apparent inconsistency and explain the fast docking step for the Y9F mutant.

The new information obtained in this studies prompts an extension of the previous thermodynamic linkage 'box', describing the ionization of Tyr-9 and binding of ligands, to a thermodynamic linkage 'cube', which explicitly includes all possible states for ionization of Tyr-9, ligand binding, and C-terminal conformational states (Figure 3.7). According to this scheme, there are several conformations of the enzyme from which a ligand can dissociate. As noted previously, the release of GSH conjugate products is a critical determinant of enzymatic rate, and thus the C-terminal conformational states are of critical functional significance. In turn, these conformations are thermodynamically coupled to the ionization state of the active site Tyr-9. Therefore, the pK_a of Tyr-9 has mechanistic significance. At physiological pH, the pK_as of the apo-enzyme and ligand-bound enzyme would result in deprotonation of approximately 13-31% and 1-5% of active site tyrosine, respectively. As a result, both open and closed conformations of the enzyme are available for ligand binding and release. This situation is certainly applicable in the present studies, in which the dependence of GS-EA binding, dissociation, and affinity were monitored at pH 6 and 9. As depicted in Figure 3.7, the ionization of Tyr-9 results in several conformations, which are either disordered, open states (Open Tyr-9-O^-) or ordered, closed states (Closed Tyr-9-O^-). Our results with wild-type (or W21F:F222W) and Y9F mutant (or Y9F:W21F:F222W) indicate that GS-EA can bind to any of these states. However, preferential binding and dissociation of ligand, as

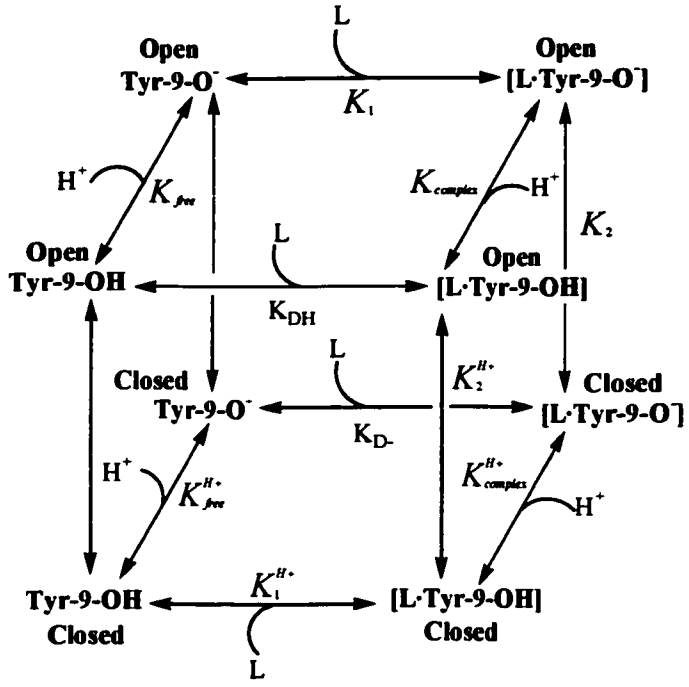

Figure 3.7: Thermodynamic "linkage" cube. Scheme describes the equilibrium binding of ligand in the open (top face) and closed (bottom face) states of rGST A1-1. The left and right sides of the cube represent the ionization states of Tyr-9 in the apo-enzyme and ligand-bound enzyme, respectively. Meanwhile, the front and back of the cube describes ligand binding and dissociation in the protonated and ionized forms of the enzyme, respectively.

measured by equilibrium constants K_1 and K_2 (Table 3.3 and Figure 3.7), were observed at pH 9 where the predominant species are deprotonated Tyr-9 with disordered, open C-terminus (Open Tyr-9-O$^-$) and ordered, closed C-terminus (Closed [L•Tyr-9-O$^-$]), respectively. As noted in the previous and present studies, Tyr-9 can undergo ionization even in the presence of ligand, although not to the same extent as in the apo-enzyme. The recovered pK_as in the ligand-bound enzymes were significantly below the pK_a of free tyrosine in solution, indicating that a small fraction of the complex remains unprotonated at equilibrium. Moreover, the unprotonated Tyr-9 in the open and closed [L•Tyr-9-O$^-$]

complex can be protonated again to yield a complex with disordered, open C-terminus (Open [L•Tyr-9-OH]) and ordered, closed C-terminus (Closed [L•Tyr-9-OH]), respectively. Binding affinity is also modulated by the ionization state of the Tyr-9 and conformational status of the C-terminus. Equilibrium binding and kinetic data suggest that binding affinity of ligand to a conformation with ionized Tyr-9 (K_{D-}) is reduced by 3-4 fold compared to a conformation with protonated Tyr-9 (K_{DH}). Because the recovered K_D values in the Y9F mutant remained essentially identical at pH 6 and 9, it is likely that the ligand affinity (K_{DH}) does not depend on the ionization of active site residue in this mutant. Although Figure 3.7 explains the pH-dependence of equilibrium binding, the model may appear oversimplified, as contributions of other ionizable groups on the ligand or possibly unknown protein residue have not been taken into account. One likely candidate is the γ-glutamyl group on the glutathione moiety, which has been shown to contribute to the pH-dependence of GSH binding in a lower pH range (Widersten, et al., 1996).

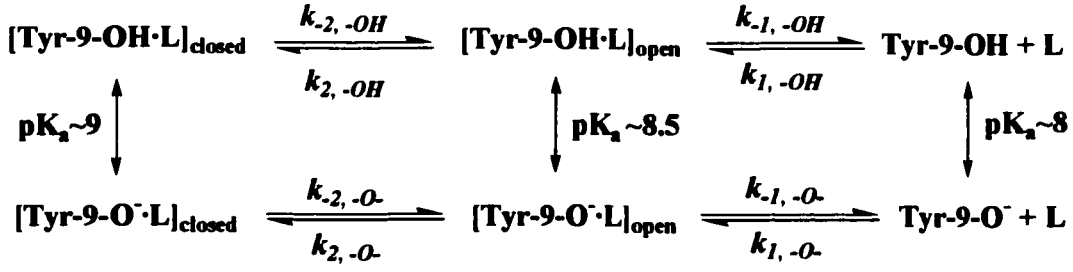

Figure 3.8: Scheme describing the parallel pathways for product dissociation. See text for details.

As an illustration of the mechanism by which multiple, linked equilbria can facilitate flux between ligand-bound and ligand-free states, consider the simplified Figure 3.8. As indicated in the scheme, there are parallel pathways for the release of product conjugate (L) from an enzyme with ionized Tyr-9 (bottom row) and enzyme with protonated Tyr-9 (top row). Figure 3.8 also depicts the pathway for product release from an enzyme with open active site, as exemplified by C-terminal truncation mutant (Δ209-222). In the presence of ligand that induces closure of the C-terminus, the active site Tyr-9 in the Δ209-222 mutant remains partly ionized with a pK_a of ~8.5, as determined from fluorescence titrations (Table 2.3). Because the flux from ligand-bound to ligand-free states is faster for the unprotonated enzyme, this pathway can contribute to the kinetic mechanism, even though the unprotonated forms of the enzyme do not predominate at equilibrium.

In summary, our results provide direct evidence that ligand binding and dissociation are facilitated in the ionized, open conformation of GST A1-1, which provides a parallel pathway for product dissociation. The kinetic and thermodynamic approaches undertaken here have been employed in other studies to identify which elementary steps in the ligand binding reaction are affected by pH as well as identify pK_as of important ionizable groups on protein and/or ligand (Hofmann, et al., 1996; Calugaru, et al., 2001; Hightower, et al., 1998; D'Souza, et al., 1995; Jeong, et al., 1994). In the present studies, the pH-dependence of individual rate constants in the binding reaction of GS-EA and equilibrium dissociation constants resulted in recovered pK_as that reflect the ionization of Tyr-9 in the apo-enzyme as well as the bound ezyme (Table 3.3).

In addition, the ionization state of Tyr-9 controls the conformational status of the C-terminus, thereby altering the rates of ligand binding and release, as well as binding affinities of ligand. It should be noted that the choice of ligand in the equilibrium and stopped-flow studies is actually a product conjugate. Therefore, the pH-dependence of K_D observed in the present studies reflects the extent of product release from the active site. Interestingly, among the kinetic parameters determined (Table 3.3), the rate constant k_{-2} showed a large change, by as much as 10-fold, upon deprotonation of Tyr-9. The results presented here do not directly demonstrate the role of Tyr-9 ionization in substrate *binding*. It will be interesting to determine whether substrate binding and dissociation will follow a similar trend, thus extending the functional significance of Tyr-9 ionization to the beginning of the catalytic cycle.

CHAPTER 4

THE HYDROLYSIS OF THIOL ESTER CONJUGATES MEDIATED BY GLUTATHIONE S-TRANSFERASES

4.1 Introduction

A major impediment in cancer treatment is the development of drug resistance, which is in part due to increased metabolic detoxification of cytostatic drugs. This problem is further exacerbated by high level or overexpression of glutathione S-transferases (GSTs) in tumors. The conjugation of chemotherapeutic agents, such as busulfan, melphalan, adriamycin, and fotemustine, have been reported to reduce the effectiveness of these drugs (Czwerwinski, et al., 1996; Kuzmich, et al., 1991; Brakenhoff, et al., 1994). Furthermore, overexpression of hGST P1-1 is often seen in carcinoma of the breast, colon, lung, kidney, and ovary although the functional or etiologic significance of this is unclear (Gilbert, et al., 1993; Chao, et al., 1992; Cole, et al., 1990; Harrison, et al., 1990; Green, et al., 1993). Several strategies have been explored to address such problems. Theoretically, drugs that are limited by GST-dependent metabolism may be 're-designed' to release the desired electrophilic functional groups and increase their duration of action. Alternatively, isoform-specific inhibitors may be used as adjuvants to chemotherapy in order to enhance the cytotoxicity of alkylating agents.

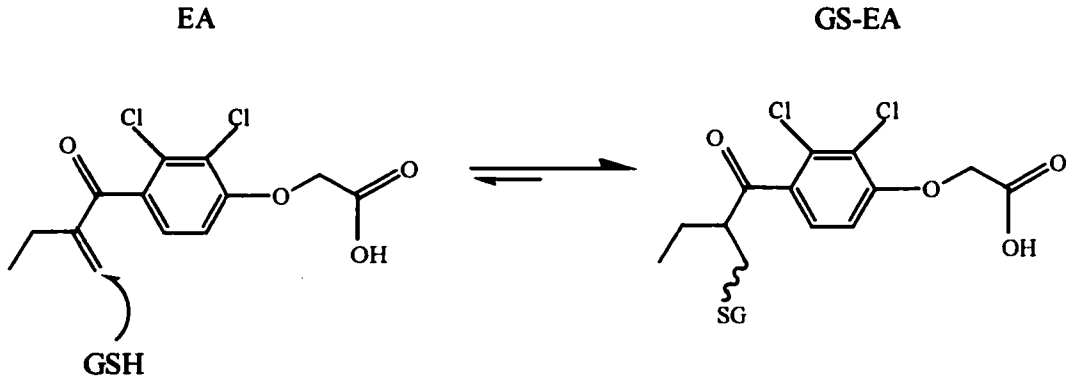

Figure 4.1: The conjugation of glutathione (GSH) with ethacrynic acid (EA) via Michael addition. The wavy line on the product conjugate GS-EA denotes the existence of two diastereomers.

Isoforms of the Alpha-, Pi-, and Mu-class GSTs are known to catalyze the conjugation of glutathione (GSH) to the Michael acceptor substrates such as ethacrynic acid (EA) (Figure 4.1). However, GSTs are also known to catalyze the release of GSH and electrophile from its conjugate as required by the Haldane relationship, which assumes reversibility of enzyme-catalyzed reaction (Fersht, 1999). Some examples of experimentally studied 'reverse' reactions include the hydrolysis of activated carbamate thiol esters and retro-Michael additions (Meyer, et al., 1995; Chen, et al., 1995). The utility of such reverse reactions can be envisioned as a way of delivering latent toxicants or drugs to tissues that express GSTs (Baillie, et al., 1991; Baillie, et al., 1994). In addition, GST-mediated reactions may be exploited in the design of prodrugs of specific GST inhibitors or cytostatic drugs. Therefore, it is essential to understand the mechanistic details of GSH conjugate hydrolysis.

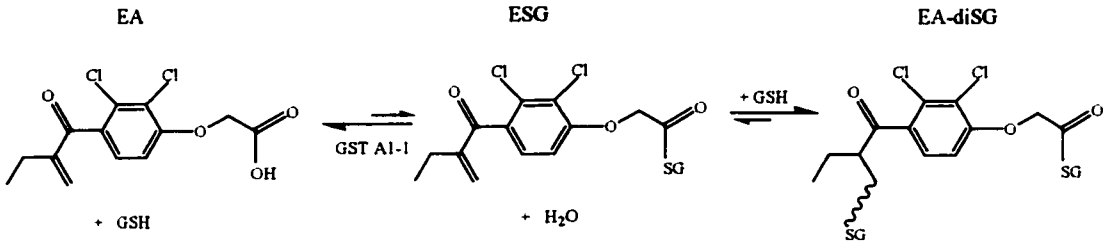

Figure 4.2: The rGST A1-1-catalyzed hydrolysis of thiol ester ESG. The formation of ESG is not catalyzed by the enzyme. At longer reaction times, the products from thiol esterase activity, namely EA and GSH, may react enzymatically or spontaneously to form the di-adduct, EA-diSG.

In previous studies, GST has been shown to catalyze the retro-conjugation reaction (Dietze, et al., 1998). A significant hydrolysis of the thiol ester formed from GSH and ethacrynic acid, glutathionyl ethacrynate (ESG), has been observed in rGST A1-1 (Figure 4.2). The enzyme does not catalyze the forward conjugation reaction to form ESG at any detectable rate. Rather, the enzyme efficiently catalyzes the thiol ester hydrolysis, thereby driving the reverse reaction to completion. The thiol esterase activity observed in these studies provides precedent for the metabolism of other GSH thiol esters commonly found *in vivo* (Shore, et al., 1995; Uotilla, et al., 1996; Crowl, et al., 1996). Hence, thiol ester hydrolysis may be exploited to deliver anticancer drugs to malignant cells overexpressing GSTs. Other labs have already explored similar strategies for delivering cytostatic drugs to tumors and demonstrated that the release of reactive phosphoramidates and GSH sulfone from GSH conjugates is mediated by GSTs (Lyttle, et al., 1994). In this case, general base catalysis by the active site tyrosine in P-class GST

has been proposed as the mechanism for hydrolysis. However, no experimental data have been reported to address this possibility other than the results presented in rGST A1-1 studies.

The studies on thiol esterase activity of rGST A1-1 have unequivocally shown the essential role of active site Tyr-9 (Dietze, et al., 1998). Substitution of this residue with Phe (Y9F) resulted in no detectable esterase activity. Thus, Tyr-9 appears to be critical to the hydrolytic reaction of rGST A1-1. Given the unusually low pK_a of Tyr-9 in A-class GSTs, there is a possibility that Tyrosinate-9 would serve as a nucleophile to yield an acylated protein adduct, followed by hydrolysis to regenerate Tyr-9. However, no acylated adduct could be identified with rGST A1-1. Nonetheless, it will be of great interest to determine the efficiency of other GST isoforms in catalyzing the hydrolytic reaction, especially those with active site Tyr exhibiting $pK_a > 10$.

In the present studies, the competence of human A-class and P-class GSTs in hydrolyzing ESG and a few other thiol esters was examined. Previous studies have shown that both EA and the Michael adduct GS-EA reversibly inhibit A- and M-class GSTs (Ploemen, et al., 1993). The P-class GST is also inhibited by EA and GS-EA, but the process is complex. In this case, the free EA is not only a competitive inhibitor, but it also forms a Michael adduct with Cys-47 of hGST P1-1, which yields a slowly reversible inhibited complex (Ploemen, et al., 1993; Phillips, et al, 1993). The present studies were designed to determine whether hGST P1-1 is inhibited by EA released from ESG, as monitored by activity assay and protein adduct via liquid chromatography electrospray ionization (LC-ESI) mass spectrometry. Additionally, the spectroscopic pK_a of catalytic

Tyr-7 in hGST P1-1 was determined to be comparable to that of A-class GST. However, given the unusually acidic pK_a of Cys-47 in hGST P1-1, it was hypothesized that this residue would be the primary site of covalent modification by EA. The potential role of Cys-47 in the thiol esterase activity will be discussed.

4.2 Materials and Methods

4.2.1 Chemicals

ESG and GS-EA were synthesized as previously described (Dietze, et al., 1998). Ethacrynic acid, diclofenac, flurbiprofen, and sulindac were purchased from Sigma (St. Louis, MO). The thiol esters of diclofenac, flurbiprofen, and sulindac (Diclofenac-SG, Flurbiprofen-SG, and Sulindac-SG, respectively) were generous gifts of Dr. Mark Grillo (Pharmacia, Kalamazoo, MI). HPLC solvents, such as acetonitrile (ACN) and methanol (MeOH), employed in the assays were of highest purity that was available commercially.

4.2.2 Protein Expression and Purification

The original clones of hGST A1-1 and hGST P1-1 were kind gifts of Dr. Kenneth Tew of the Fox Chase Center (Philadelphia, PA). For optimal expression, the hGST A1-1 was first subcloned into pKK233-3 vector, followed by transformation into AB 1899 *E. coli* strain. Likewise, the hGST P1-1 was subcloned into pET17b vector and expressed in either BL21(DE3) or BL21Codon. All *E. coli* strains were inducible with isopropyl-β-D-thiogalactopyranoside (IPTG). Wild-type hGST A1-1 proteins were purified as previously described (Ibarra, et al., 2001), while hGST P1-1 proteins were

purified as described by Chang and co-workers (Chang, et al., 1999). The purified hGST M2-2 and C47S hGST P1-1 were generous gifts of Dr. Theodore Bammler of the University of Washington, Department of Environmental Health and Dr. Mario Lo Bello of the University of Rome "Tor Vergata," Rome, Italy.

4.2.3 Thiol Esterase Activity Assay

Steady-state kinetics were performed by varying the concentrations of GSH thiol esters from 0.25 μM to 50 μM in the presence of 0.5 μM GST at 25°C. A 200-μl aliquot was immediately withdrawn after addition of the thiol ester and after incubation for 15 min to provide zero-time point and 15-min point, respectively. The reactions were stopped with equal volume of stop solution, consisting of 4:1 ACN:MeOH. The mixture was then centrifuged and kept on ice until analysis. Parallel incubations without GST were also performed to correct for nonenzymatic hydrolysis of each GSH thiol ester. All incubations were performed in 50 mM potassium phosphate, pH 7.

An isocratic HPLC system was employed to analyze each of the incubations. This system allowed chromatographic separation of GSH thiol esters from their parent compounds. Samples were loaded into 10 cm X 4.6 mm ID C18 reverse phase column (Alltech) via thermostated autoinjector (4°C). For the ESG and Sulindac-SG, a mobile phase of 50% 1:1 ACN:MeOH and 50% 50 mM potassium phosphate, pH 3.5 was employed, with UV detection at 230 nm. Meanwhile, the incubations with Flurbiprofen-SG and Diclofenac-SG were monitored at 245 nm, employing a mobile phase of similar organic solvent and 50% 50 mM potassium phosphate, pH 4.5. The detector response of

each compound was linear over the entire range of concentrations ($R^2 \geq 0.99$, data not shown).

4.2.4 GS-EA Conjugation Assay

The initial rates for the conjugation of GSH to ethacrynic acid (EA) in hGST P1-1, C47S hP1-1, and hGST A1-1 were determined spectrophotometrically at 25°C and pH 6.5 (Nuccetelli, et al., 1998; Habig, et al., 1974). For each isoform, the enzymatic rates were corrected for spontaneous reaction. The apparent kinetic parameters were determined by using the following conditions: (a) 0.05-0.5 mM EA in the presence of 1 mM GSH and (b) 0.05-1 mM GSH in the presence of 0.5 mM EA. The k_{cat} and K_M values were measured by fitting the collected data to the Michaelis-Menten equation via Enzfitter program.

4.2.5 Inhibition Studies

Because EA is a product of the hydrolysis and it is an established inhibitor of GSTs, the possibility of time-dependent inhibition was considered. To determine the time-dependent inhibition of GST by ESG, 0.25 μM protein was incubated with 5 μM ESG at 25°C for 5, 10, 20, 30, 40, 50, and 60 min. A 100-μl aliquot was withdrawn immediately after addition of ESG to provide a zero-time point. This aliquot and the subsequent aliquots from each time interval were transferred to a cuvette containing 1 mM CDNB and 1 mM GSH in 100 mM potassium phosphate, pH 6.5. The inhibition of CDNB conjugation was monitored at 340 nm via Cary3E spectrophotometer.

Additionally, the nature of the inhibition by ESG was determined by incubating GST with variable CDNB concentration (0.1-1 mM) in the presence of 5 μM ESG. The conjugation of CDNB with GSH (1 mM) was determined in duplicates as described above. The steady-state parameters were determined via the following modified Michaelis-Menten equation for mixed noncompetitive inhibition (Garrett, et al., 1996):

$$\upsilon = \frac{V_{max} * [S]}{\left(\frac{1+[I]}{K_I}\right) * K_M + \left(\frac{1+[I]}{K_I'}\right) * [S]}$$

where υ is the velocity, [I] is the inhibitor concentration, K_I is the E:I dissociation constant, and K_I' is the ES:I dissociation constant. All initial rates of conjugation were corrected for the enzyme concentration.

4.2.6 LC-ESI Mass Spectrometry

To determine whether GSTs are covalently modified by ESG, EA, or GS-EA, 5 μM proteins and 100 μM ESG in 50 mM potassium phosphate, pH 7 were incubated for 30 min, 60 min, and 24 hr at 25°C. Aliquots were taken at each time point, and equal volume of stop solution was added. For analysis in the mass spectrometer, these mixtures were diluted with the aforementioned buffer to give a final concentration of 1 μM protein and 25 μM ESG. Each protein was analyzed by electrospray ionization via Fisons VG Quattro II triple quadrupole mass spectrometer interfaced with Shimadzu HPLC system. The protein samples were loaded into 2.1 mm X 50 mm R2 Poros column, using an injection volume of 20 μl and carrier solvent of acetonitrile with 0.05%

trifluoroacetic acid (solvent A) and 0.05% trifluoroacetic acid (solvent B) at a flow rate of 0.3 ml/min. An initial mobile phase was held at 5% solvent A for 1 min followed by a linear gradient to 60% acetonitrile and 0.05% trifluoroacetic acid at 7 min. Operating parameters were capillary voltage of 3.5 kV, source temperature of 150°C, and cone voltage of 30V. The deconvoluted spectra were obtained by using the MaxEnt algorithm (Masslynx 3.4 software).

4.3 Results

4.3.1 Kinetics of Enzymatic Hydrolysis of Thiol Esters

Although the formation of GSH thiol ester, such as ESG, is not catalyzed by rGST A1-1, its hydrolysis is in fact mediated enzymatically (Dietze, et al., 1998). In the present studies, the thiol esterase activities of few human isoforms of GST were determined via an isocratic HPLC method. The rates of thiol ester loss after incubation with GST were monitored at various concentrations of substrate. Table 4.1 demonstrates that the rate of hydrolysis of ESG is faster for hGST P1-1 compared to hGST A1-1. In this case, the P-class is 3-fold and 16-fold more efficient, as measured by k_{cat}/K_M, than hGST A1-1 and rGST A1-1, respectively. This apparent efficiency is likely attributed to the significant turnover rate in hGST P1-1, as the apparent binding affinities of ESG (i.e., K_M) in both GST classes are identical.

The pK_a and unusual reactivity of Cys-47 (~4.2) has been known for some time (Lo Bello, et al., 1993). The mutation of this residue to serine or alanine had no dramatic effect on the affinity and turnover rate toward CDNB (Kong, et al., 1991; Lo Bello, et al.,

Table 4.1: Kinetic Parameters for the Hydrolysis of GSH Thiol Ester of Ethacrynic Acid (ESG) in Various GSTs[a]

Enzyme	Apparent k_{cat} (s^{-1})	Apparent K_M (μM)	k_{cat}/K_M (mM^{-1} s^{-1})
rGST A1-1[b]	0.0018 ± 0.0002	15.7 ± 1.6	0.11 ± 0.02
hGST A1-1	0.0068 ± 0.0020	11.9 ± 0.1	0.57 ± 0.13
hGST P1-1	0.0237 ± 0.0070	17.3 ± 9.8	1.80 ± 0.89
C47S hP1-1	0.0084 ± 0.0010	13.2 ± 3.4	0.66 ± 0.09
hGST M2-2	0.0073 ± 0.0010	6.5 ± 0.1	1.12 ± 0.19

[a]Kinetic data were derived from thiol esterase assay via HPLC for the enzymatic incubations containing 0.25-50 μM ESG as described in Materials and Methods. The enzymatic reactions were corrected for the nonenzymatic hydrolysis of ESG. Each reported parameter is an average of 2 or 3 separate experiments.
[b]Dietze, et al., 1998

1995; Chang, et al., 2001). In several studies of hGST P1-1, Cys-47 has been shown to be an important target of protein inactivation or modification. Given the reactivity of this residue, Cys-47 itself may participate in the hydrolysis of ESG, as suggested for the inactivation of hGST P1-1 by haloenol lactone (Mitchell, et al., 1998). As Table 4.1 indicates, the C47S substitution only led to a modest 2.8-fold decrease in k_{cat} and similar K_M for ESG compared to wild-type enzyme. This result suggests that Cys-47 is not the major determinant of thiol esterase activity.

In contrast, the experimental pK_a of catalytic Tyr-7 in hGSTP1-1 was largely unknown for many years. Recently, the pK_a of this residue was determined via established spectroscopic method (Ibarra, et al., 2001; Bjornestedt, et al., 1995). Figure 4.3 shows the pH-dependence of absorbance at 255 nm, which monitors the formation of

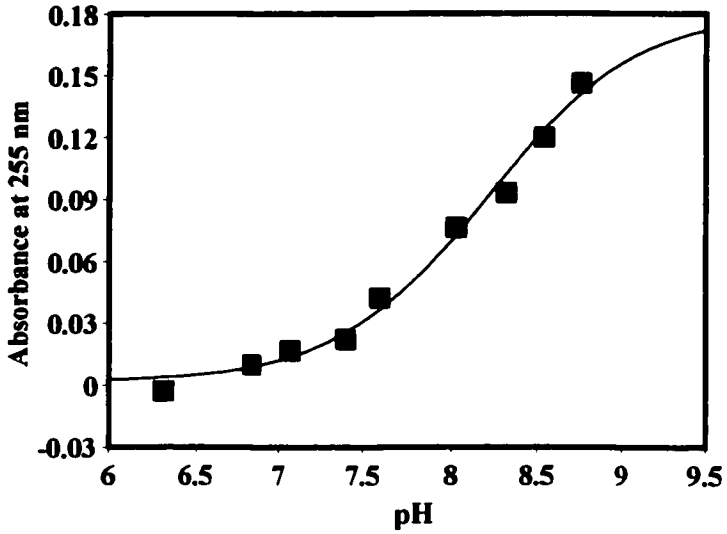

Figure 4.3: Titration of Tyr-7 in hGST P1-1 via UV difference absorption spectroscopy. The pH-dependence of absorbance at 255 nm reflects the formation of tyrosinate (R^2 = 0.99).

tyrosinate species with increasing pH. Nonlinear regression fit to the data indicated a spectroscopic pK_a of ~8.2, which is essentially the same as the pK_a of hGST A1-1.

In light of the identical pK_as of catalytic Tyr in A- and P-class GSTs, it is reasonable to speculate that this residue controls the hydrolysis of thiol ester in the latter class. In fact, the hydrolysis of ESG in rGST A1-1 has been attributed to Tyr-9, as substitution of this residue with Phe resulted in no detectable hydrolysis (Dietze, et al., 1998). To determine whether the efficiency of thiol esterase activity is largely due to the low pK_a of the catalytic Tyr, enzymatic incubations were also performed in the presence of hGST M2-2. As described in Chapter 1, M-class GSTs exhibit a normal tyrosine pK_a (~10.2) (Xiao, et al., 1996). On the basis of k_{cat}, the low pK_a of catalytic Tyr in P-class GST has only a modest advantage over the high pK_a in M-class, while the analogous

Table 4.2: Comparison of Thiol Esterase Activity in hGST P1-1 and hGST A1-1 with Various Thiol Ester Conjugates[a]

	hGST P1-1		
Thiol Esters	Apparent k_{cat} (s^{-1})	Apparent K_M (μM)	k_{cat}/K_M (mM^{-1} s^{-1})
ESG	0.0237 ± 0.0070	17.3 ± 9.8	1.80 ± 0.89
Flurbiprofen-SG	0.0130 ± 0.0050	73.7 ± 7.5	0.19 ± 0.09
Sulindac-SG	0.0120 ± 0.0030	32.3 ± 2.1	0.35 ± 0.08
Diclofenac-SG	0.0085 ± 0.0010	23.1 ± 6.2	0.41 ± 0.16
	hGST A1-1		
Thiol Esters	Apparent k_{cat} (s^{-1})	Apparent K_M (μM)	k_{cat}/K_M (mM^{-1} s^{-1})
ESG	0.0068 ± 0.0020	11.9 ± 0.1	0.57 ± 0.13
Flurbiprofen-SG	0.0038 ± 0.0003	12.8 ± 2.8	0.32 ± 0.09
Sulindac-SG	0.0061 ± 0.0003	17.2 ± 3.1	0.37 ± 0.05
Diclofenac-SG	0.0060 ± 0.0007	29.9 ± 6.1	0.21 ± 0.07

[a]Kinetic data were derived from thiol esterase assay via HPLC for the enzymatic incubations containing 0.25-50 μM GSH thiol ester as described in Materials and Methods. The enzymatic reactions were corrected for the nonenzymatic hydrolysis. Each reported parameter is an average of 2 or 3 separate experiments.

residue in A-class has no advantage (Table 4.1). However, as the k_{cat}/K_M values suggest, the efficiency of thiol esterase activity does not entirely depend on the low pK_a of catalytic Tyr. It is noteworthy that the apparent binding affinity of ESG to hGST M2-2 is increased by ~2.7-fold compared to hGST P1-1. This low K_M is essentially responsible for the apparent improved efficiency in M-class, despite its low turnover rate.

In addition to ESG, other thiol ester conjugates were characterized to determine if a hydrolytic reaction is a general phenomenon for human GSTs (Figure 4.4). The hydrolysis of the thiol esters of flurbiprofen, sulindac, and diclofenac in hGST P1-1 were not dramatically altered from the hGST A1-1 (Table 4.2). However, among the four thiol

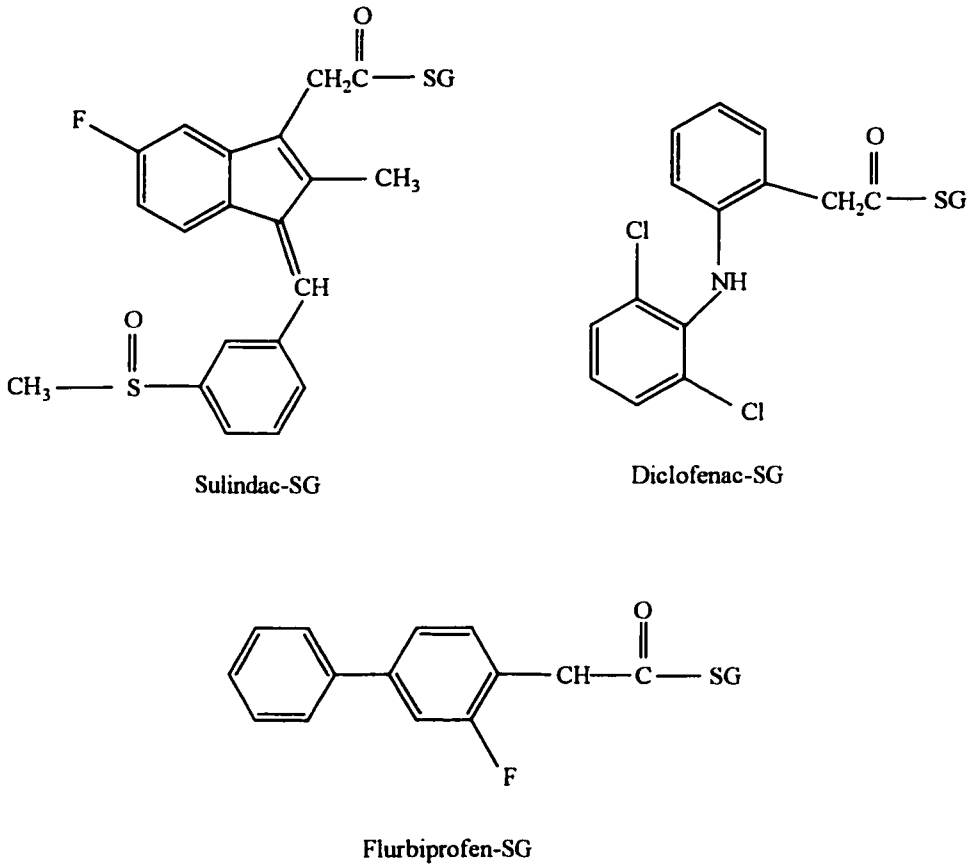

Figure 4.4: Structures of thiol esters Sulindac-SG, Diclofenac-SG, and Flurbiprofen-SG.

esters tested, hGST P1-1 was most selective for ESG. Meanwhile, hGST A1-1 did not exhibit any apparent substrate selectivity.

As a consequence of ESG hydrolysis, both EA and GSH are released. Subsequently, these hydrolytic products undergo conjugation reactions, which can occur enzymatically as well as spontaneously, to form the GSH conjugate GS-EA. The HPLC method and standard curves employed were sufficient to allow GS-EA formation to be monitored and quantified. Interestingly, a lag phase in GS-EA production for all GSTs

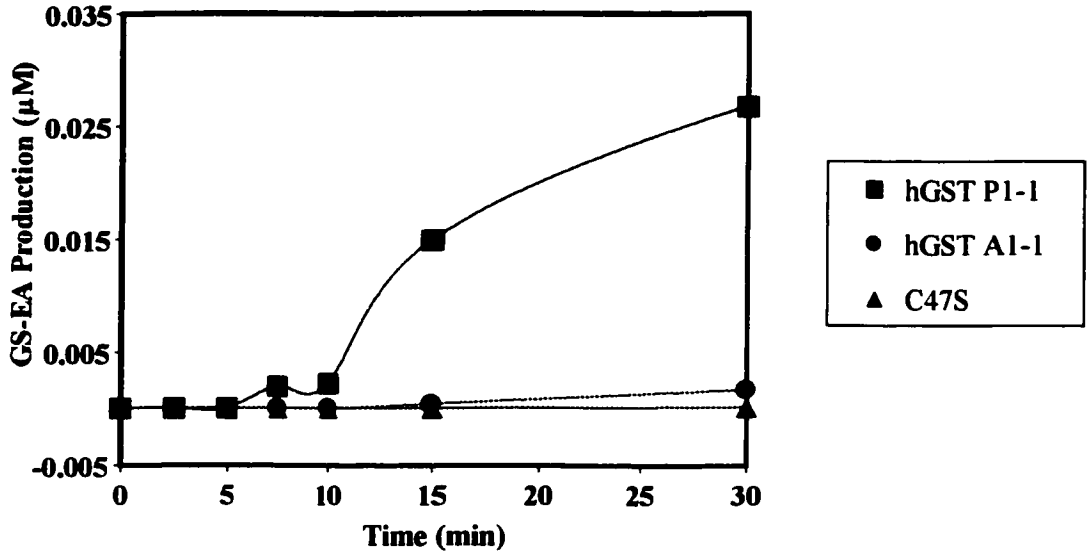

Figure 4.5: Time course of GS-EA formation following the hydrolysis of ESG. The formation of this GSH conjugate was not noted until 10 min after the incubation, with the hGST P1-1 showing the most activity.

was observed in the first 10 min (Figure 4.5). Thereafter, only the hGST P1-1 showed considerable increase in production of GS-EA.

4.3.2 GS-EA Conjugation

Possibly, the observed trend in the subsequent Michael addition (Figure 4.5) of the hydrolysis by-products, GSH and EA, could be explained by the relative binding affinity of each substrate at the active site of GSTs. Presumably, the Michael addition reaction does not occur until sufficient EA and GSH are released from ESG, thus explaining the observed initial lag phase in GS-EA formation. In the previous studies of hGST P1-1 and its C47S mutant as well as hGST A1-1, the kinetic parameters for the conjugation of GSH to CDNB indicated a slightly more pronounced difference in the K_M

Table 4.3: Steady-State Parameters for the Conjugation of EA to GSH by GSTs

Enzyme	k_{cat} (s^{-1})	K_M^{GSH} (μM)	K_M^{EA} (μM)	k_{cat}/K_M^{EA} (mM^{-1} s^{-1})
hGST P1-1	2.06 ± 0.01	65.6 ± 7.4	39.3 ± 11.9	57.7 ± 17.5
C47S P1-1	1.70 ± 0.12	177 ± 3	67.5 ± 14.8	26.1 ± 4.1
hGST A1-1	0.283 ± 0.012	137 ± 10	136 ± 17	2.11 ± 0.18
rGST A1-1[a]	0.048 ± 0.002	ND[b]	55 ± 10	0.87 ± 0.20

[a]Dietze, et al., 1998. [b]Not determined.

for GSH (1.6-8.5 fold change) than in the K_M for CDNB (1.5-fold change). To determine whether the apparent increased affinity of GSH to hGST P1-1 (compared to hGST A1-1 and C47S hP1-1) might contribute to its efficient GS-EA conjugation activity, steady-state kinetic parameters were determined. As the k_{cat} and k_{cat}/K_M values indicate (Table 4.3), the Michael addition reaction is much more efficient for the P-class GST, consistent with previous studies (Mannervik, et al., 1988; Ricci, et al., 1994). Although the C47S mutant had a modest effect on the turnover rate, its nearly 3-fold increase in the K_M for GSH compared to wild-type hGST P1-1 is likely to contribute to the mutant's decreased conjugation activity, as observed in Figure 4.5. Both C47S and hGST A1-1 showed comparable K_M for GSH (Table 4.3). Interestingly, these isoforms also showed similar trend in GS-EA formation, following the hydrolysis of ESG (Figure 4.5).

4.3.3 Inhibition of GSTs by ESG

In order to determine whether the catalytic activities of hGST P1-1 and hGST A1-1 were irreversibly inhibited by ESG, time course of inhibition was monitored with

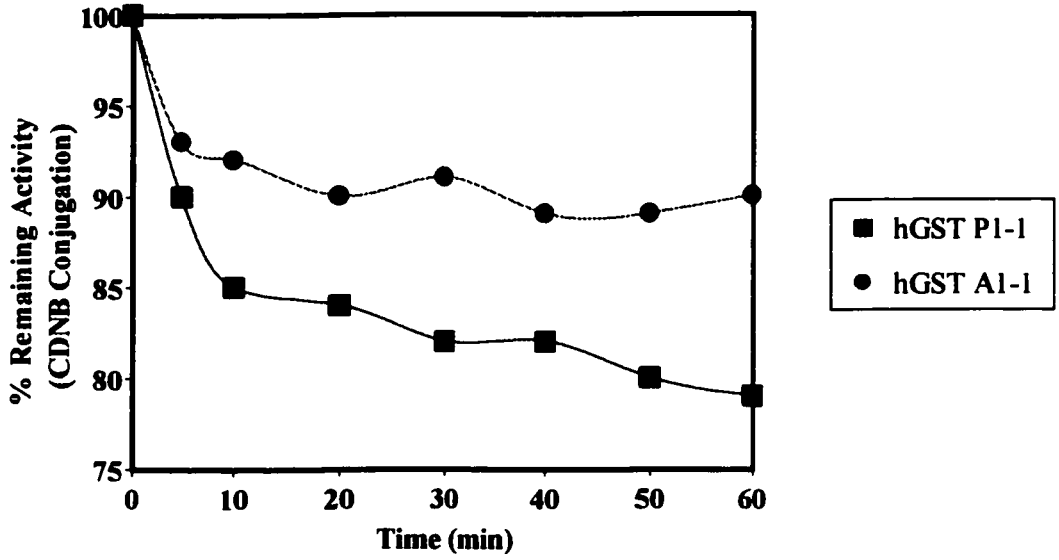

Figure 4.6: Time course of inhibition of human GSTs by ESG. The inhibitory activity of ESG was monitored via CDNB conjugation assay as described in Section 4.2.5. The results are an average of two incubations.

100 μM of thiol ester conjugate, which is ~6-fold greater than its K_M. As shown in Figure 4.6, both isoforms were inhibited by ESG. However, hGST A1-1 was inhibited at a slower rate than hGST P1-1. For instance, after 10 min of incubation with ESG, hGST A1-1 showed 92% of the original enzymatic activity toward CDNB conjugation compared to 85% of activity in hGST P1-1. After 1 hr, the observed remaining activities in A- and P-class were 90% and 79% of the original activity, respectively. As Figure 4.5 suggests, significant amount of GS-EA is already formed in incubations containing hGST P1-1. Presumably, the greater decrease in CDNB conjugation in hGST P1-1 is due to greater inhibition potency (K_I) of GS-EA than the parent compound EA (Awasthi, et al., 1993). This is reasonable considering that the K_M for either GSH or EA in P-class is two-fold to four-fold smaller than A-class (Table 4.3).

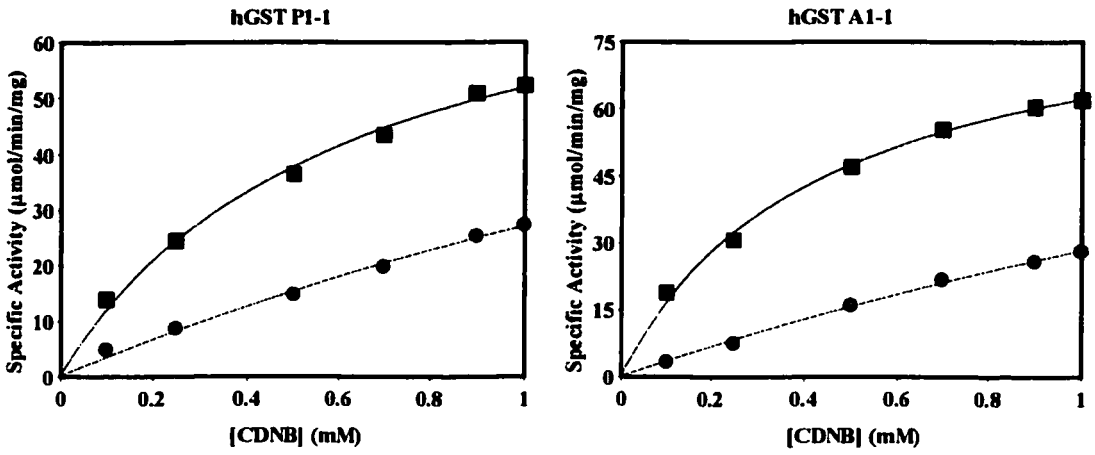

Figure 4.7: Substrate saturation curves for the GST-catalyzed conjugation of CDNB to GSH in the absence and presence of 5 µM ESG. The recovered kinetic parameters are reported in Table 4.4. Curve fits for the uninhibited (squares) and inhibited (circles) reactions were obtained via Michaelis-Menten equation and mixed noncompetitive inhibition equation, respectively, as described in Section 4.2.5.

Table 4.4: Steady-State Turnover of CDNB by hGST P1-1 and hGST A1-1 in the Absence and Presence of 5 µM ESG[a]

	hGST P1-1		hGST A1-1	
Parameters	- ESG	+ ESG	- ESG	+ ESG
V_{max} (µmol/min/mg)	82.86	69.55	89.45	70.01
K_M (µM)	602	363	442	364
K_I (µM)		183		182
K_I' (µM)		1740		2096

[a]Recovered parameters reflect the conjugation of 1 mM GSH to variable concentrations of CDNB in the presence of 9-13 nM of GSTs.

The time-dependent inhibition of GSTs (Figure 4.6) suggests that ESG may serve as an irreversible inhibitor. To determine further the mechanism by which ESG decreases the activity of human GSTs, enzyme kinetics were performed by varying the

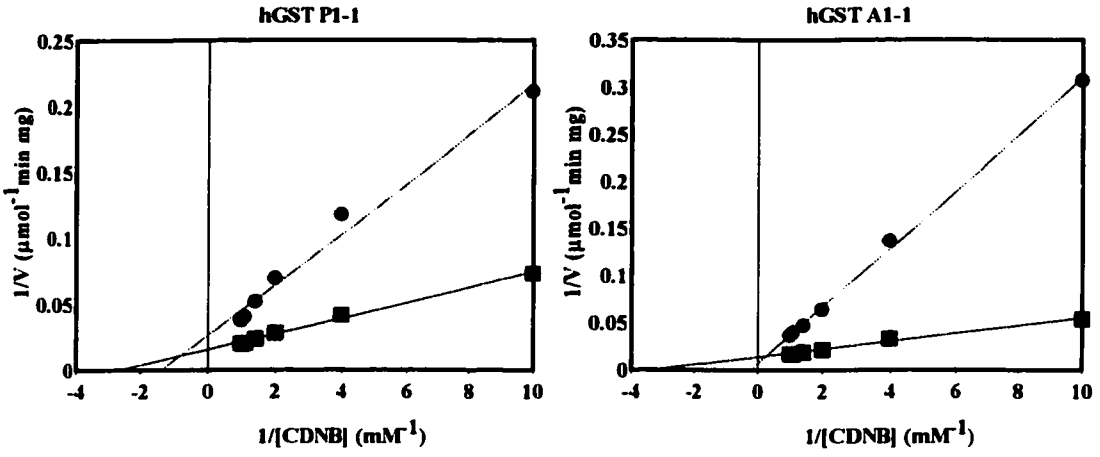

Figure 4.8: Lineweaver-Burk plots of mixed noncompetitive inhibition of hGST P1-1 and hGST A1-1 towards CDNB. Note that both x- and y-intercepts and the slope change in the presence of 5 µM ESG (circles).

concentration of CDNB in the presence of ESG below its K_M. In the presence of the thiol ester, both apparent V_{max} and K_M were altered, indicating a mixed inhibition (Figure 4.7, Table 4.4). Lineweaver-Burk plots clearly indicate a mixed noncompetitive inhibition of hGST P1-1, as apparent V_{max} decreased while apparent K_M increased (Figure 4.8). Similarly, hGST A1-1 indicated a mixed noncompetitive inhibition by ESG, resulting in increased apparent K_M and slightly increased apparent V_{max}. Interestingly, the turnover of CDNB in both GSTs is reduced by only ~20%, resulting in comparable apparent K_I values. Because of the apparent competing reactions within or near the active site, which include ESG hydrolysis and GS-EA conjugation, steady-state inhibition by ESG could not be achieved. Therefore, the results reported in Table 4.4 do not reflect the true inhibition parameters, as ESG is also a substrate for GST.

4.3.4 ESI-MS of Proteins

In comparison to the conjugation reaction, the enzymatic hydrolysis of ESG in human GSTs is slower. Nonetheless, the liberated EA from such reaction would be expected to form an adduct with Cys-47 of hGST P1-1, as previously observed in several studies (Ploemen, et al., 1993; Phillips, et al., 1993). Although the single Cys-112, located in the intersubunit cleft next to the hydrophobic substrate binding site of hGST A1-1, is not analogous to Cys-47, this residue is still a possible site of modification by virtue of its accessibility to solvent. To determine if P-class and A-class GSTs were modified by ESG or any of its liberated products (EA and GSH), overnight incubations with 20-fold molar excess of ESG were performed at 25°C. To monitor the progress of protein modification, aliquots were removed at different time points. In the incubation with hGST A1-1 (calc. 25,500 Da), approximately 50% and 100% of proteins had been glutathiolated (calc. 25,805 Da) after 60 min and 24 hr of incubation, respectively (Figure 4.9). In this case, a glutathiolated protein constitutes a mixed disulfide shared between a protein thiol and Cys of the tripeptide GSH. It is possible that in the prolonged incubation (i.e., 24-hr) with ESG, some of the proteins have been modified by EA (calc. 25,801 Da), which in this case would not be clearly distinguished from the glutathiolated proteins, given the resolution of the mass spectrometer. Recently, the effect of glutathiolation on the catalytic activity of hGST A1-1 had been determined, and it was found to have no effect (Lyon, et al., 2002). As in the rGST A1-1 studies, no transacylated adduct (calc. 25,785 Da) was observed, indicating that Tyrosinate-9 does

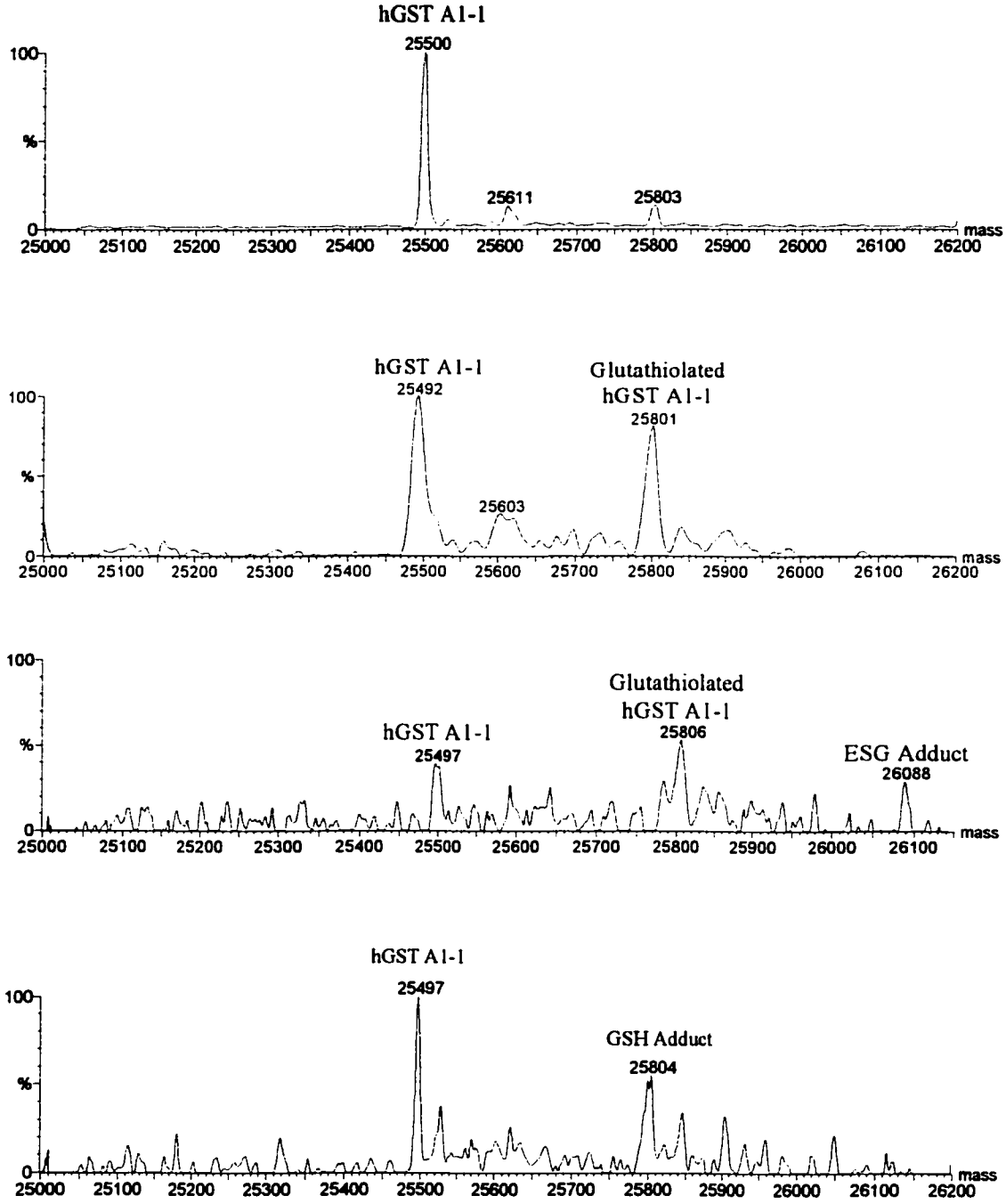

Figure 4.9: Electrospray ionization mass spectra of hGST A1-1 in the absence (first panel) and presence of ESG after 1 hour (second panel) and 24 hours (third panel) of incubation. Additionally, hGST A1-1 was incubated with glutathione overnight (fourth panel). Molecular mass additions of ~307 Da , ~301 Da, and ~591 Da relative to control protein correspond to glutathiolated adduct, EA adduct, and ESG adduct, respectively.

not get persistently acylated during the hydrolysis of ESG. However, a Michael adduct with ESG (calc. 26,093 Da) formed (~40%) following an overnight incubation.

In an otherwise identical incubation of hGST P1-1 (calc. 23,357 Da), no protein adducts could be identified after 30 min and 60 min of incubation with ESG. It was only after an overnight incubation that protein adducts became apparent from the ESI mass spectra. In this case, ~60% of proteins formed Michael adduct with EA (calc. 23,658 Da) (Figure 4.10). This protein modification was sufficient to cause >95% inhibition of hGST P1-1 activity toward CDNB (Figure 4.11). Surprisingly, glutathiolated adduct (calc. 23,664 Da) with hGST P1-1 could not be identified in incubations with ESG. In fact, glutathiolated protein was not detected from either enzyme stock or parallel incubation with GSH. Perhaps, the slightly lower K_M for EA (Table 4.3) and the depletion of GSH, as GS-EA is subsequently formed, may explain the absence of glutathiolated hGST P1-1 in the overnight incubations. As expected, incubation of C47S mutant of hGST P1-1 (calc. 28,208 Da) resulted in no formation of EA adduct (data not shown), indicating that Cys-47 is indeed the site of protein modification.

To determine whether the modification of hGST P1-1 by EA is reversible, dialysis experiments were performed. Any unreacted ESG and unbound hydrolysis by-products of this compound, namely EA and GSH, were removed by dialysis. After 24 hours of incubation with ESG, the hGST A1-1 and hGST P1-1 were inhibited by >95%. The activity of hGST A1-1 and hGST P1-1 were recovered by 78% and 39%, respectively, after overnight dialysis in 50 mM potassium phosphate, pH 7 at 4°C (Figure 4.11). Previous studies indicate that incubation of GSTs with EA resulted in almost

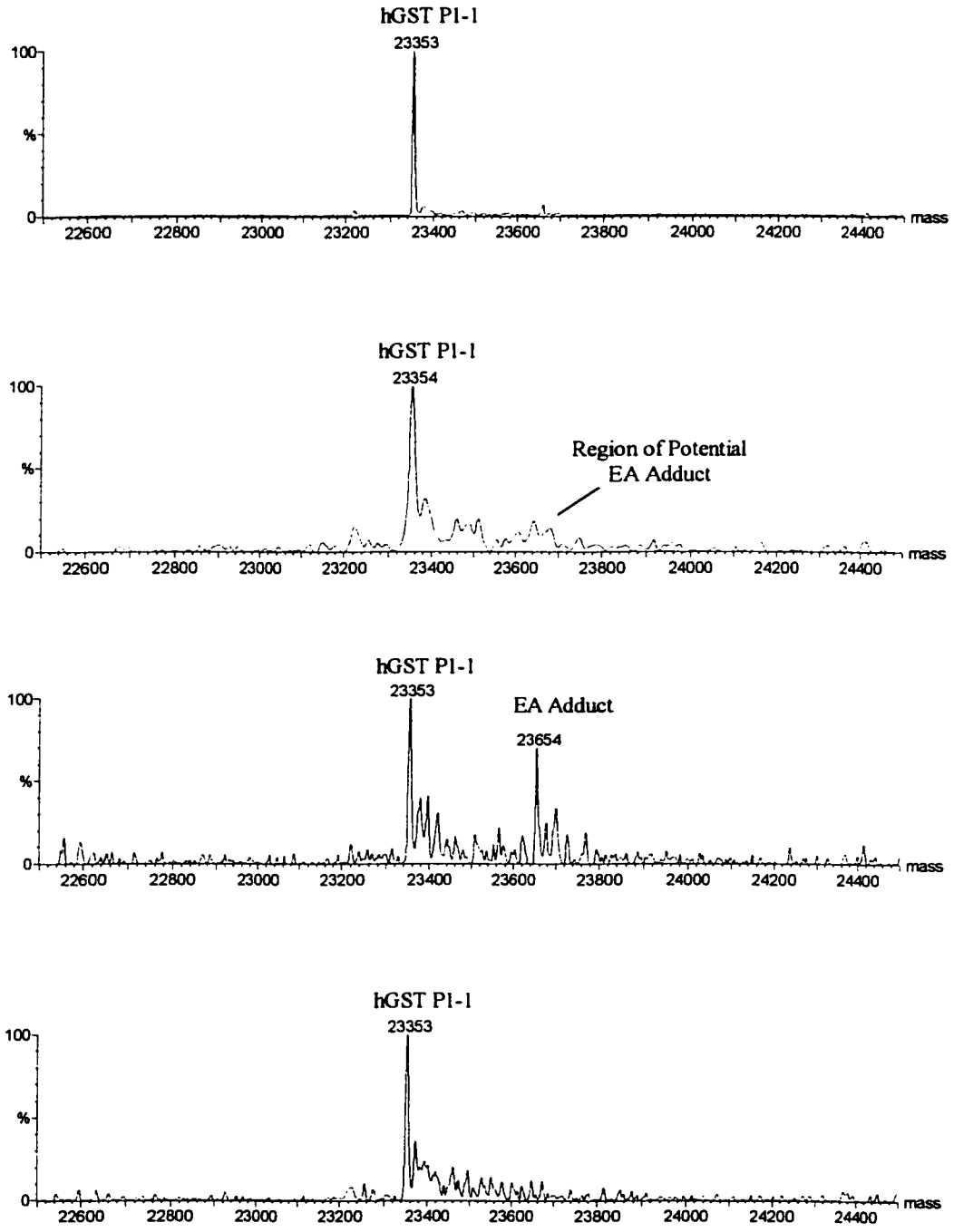

Figure 4.10: Electrospray ionization mass spectra of hGST P1-1 in the absence (first panel) and presence of ESG after 1 hour (second panel) and 24 hours (third panel) of incubation. An overnight incubation with GSH (fourth) panel was also performed. Molecular mass addition of ~301 Da relative to control protein corresponds to EA adduct.

complete loss, followed by full recovery of CDNB conjugating activity after overnight dialysis in buffers containing excess GSH or N-acetyl-cysteine (Ploemen, et al., 1994; van Iersel, et al., 1998). Because the enzymes in the present studies were incubated overnight, it is likely that the liberated EA from ESG and GS-EA was mainly responsible for the loss of GST activities. Moreover, the exchange buffer used in the dialysis did not contain GSH or any reducing agent. Thus, full restoration of activity was not observed. Nonetheless, the partial recovery of catalytic activity in inactivated enzymes suggests that

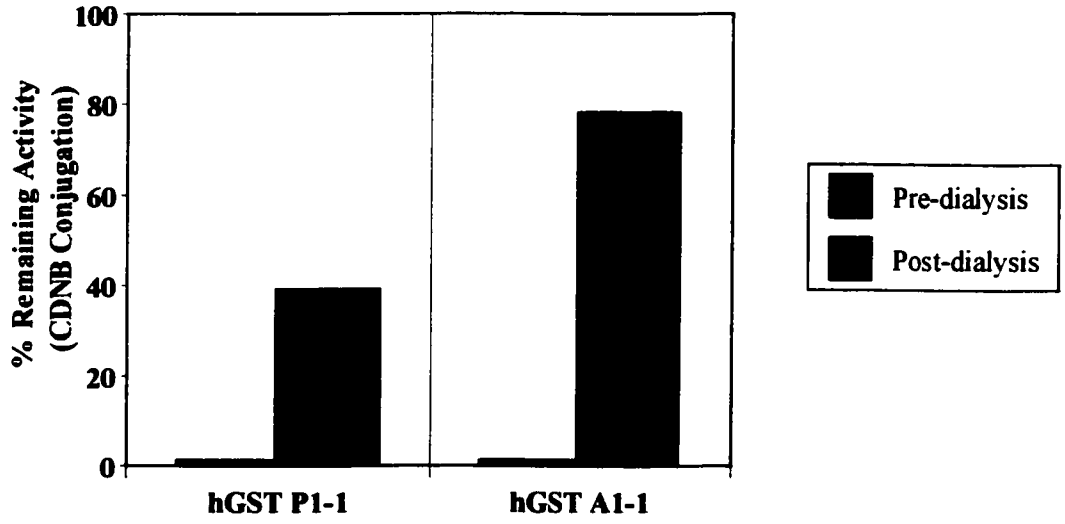

Figure 4.11: Effect of dialysis on the remaining activity of human GSTs. Approximately 5 μM GST was incubated with 100 μM ESG for 24 hours at room temperature. Afterwards, an aliquot of the incubation mixture was tested for activity. The remaining mixture was then dialyzed overnight at 4°C in 500 ml of 50 mM potassium phosphate, pH 7. Controls were treated similarly.

ESG is not a true irreversible inhibitor. Nonetheless, at extensive incubation period, hGST P1-1 remains significantly inhibited, consistent with adduction of Cys-47 by EA, as indicated by the mass data (Figure 4.10) and previous studies.

4.4 Discussion

As described in Chapter 1, GSH conjugation does not always constitute a detoxification pathway for electrophilic compounds (Monks, et al., 1990). In fact, GSH conjugates can exert their toxic effects by the release of reactive species. In this case, the conjugates can serve as transport as well as targeting agents. For this to occur, GSH conjugation must be reversible. To date, there are three classes of compounds that are known to undergo reversible conjugation, namely isocyanates, isothiocyanates, and α,β-unsaturated ketones or aldehydes (van Bladeren, 2000). For the α,β-unsaturated compounds (i.e., Michael-acceptor substrates), the spontaneous and GST-catalyzed conjugations are important biotransformation pathways. Given the acidic nature of the carbon α to the carbonyl group of these Michael acceptors, it seems reasonable that the reverse reaction is facile. Therefore, the GSH conjugates of α,β-unsaturated compounds are also potential substrates for GST in the opposite direction (i.e., retro-Michael reaction), as required by the Haldane relationship in which both forward and reverse reactions are catalyzed by the same enzyme. Although the importance of retro-Michael addition of GSH has been studied with the veterinary drug furazolidone (Vroomen, et al., 1988) and the diuretic drug ethacrynic acid (Ploemen, et al., 1994; van Iersel, et al., 1998), enzyme-catalyzed reverse reaction has been only proven for 4-phenyl-3-buten-2-

one in M-class GSTs (Chen, et al., 1995). Similarly, the dietary constituents of cruciferous vegetables, namely isothiocyanates, undergo nonenzymatic and GST-catalyzed conjugations. The reversibility of conjugate formation has been observed for this class of compounds, and it is mediated by GST (Zheng, et al., 1995; Meyer, et al., 1995).

In the present studies, the hydrolysis of the thiol ester conjugate formed from EA and GSH was characterized in the presence of human GSTs. The thiol esterase studies on rGST A1-1 (Dietze, et al., 1998) suggest that human GSTs might also catalyze such a reverse reaction. In fact, the human isoforms are more efficient than rGST A1-1 in cleaving the thiol ester conjugate, as indicated by apparent k_{cat} values on Table 4.1. Among the isoenzymes tested, hGST P1-1 was the most active toward ESG hydrolysis. As for all of the reverse reactions studied here, the contribution of nonenzymatic hydrolysis to the overall rate of thiol ester cleavage is negligible (i.e., $\leq$ 1% of catalyzed reactions). With the exception of hGST M2-2, the apparent K_M values for ESG in human GSTs are comparable. These K_M values, however, are remarkably lower than known K_Ms for typical substrates of conjugation, such as GSH (150-460 μM), EA (130-210 μM), and CDNB (780-1200 μM) (Nuccetelli, et al., 1998). It is interesting to note that even though the rates of thiol ester hydrolysis in human GSTs (Tables 4.1 and 4.2) are remarkably less efficient than many GSH conjugation reactions, the "net" rate of hydrolysis is significantly more efficient than known GST-catalyzed cleavage of GSH thiocarbamate or retro-Michael reactions (Meyer, et al., 1995; Chen, et al., 1995). This difference is attributed to significant enzyme-mediated reformation of GSH conjugates

involving isothiocyanates and Michael acceptors (Figure 4.12). To determine if hGST P1-1 and hGST A1-1 exhibit substrate specificity, other thiol ester conjugates were characterized (Table 4.2). These conjugates were chosen on the basis of their ability to dramatically reduce the conjugation of CDNB to GSH, as indicated by preliminary studies (data not shown). While the A-class did not show preference for a particular thiol ester, the P-class GST was quite selective in cleaving ESG.

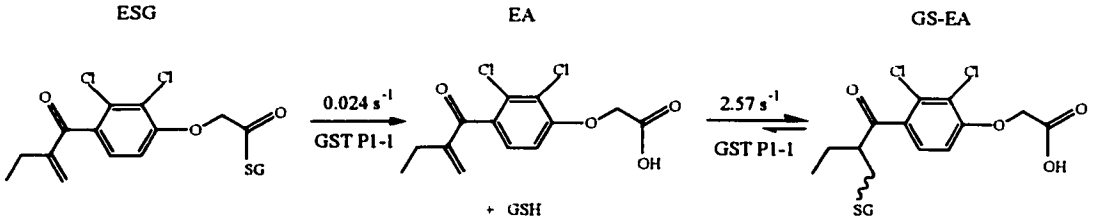

Figure 4.12: Fate of ESG and its hydrolysis by-products in hGST P1-1. The reported k_{cat} for the Michael addition reaction was adapted from Nuccetelli, et al., 1998.

Although k_{cat}/K_M has traditionally been used as an index of specificity, there are a few critical cases where this index may not reflect specificity of substrate and isoenzyme. In a recent paper by Bauer and co-workers, a systematic approach was undertaken to examine all the possible variations of kinetic constants k_{cat}, K_M, and k_{cat}/K_M (Bauer, et al., 2001). These variations were then related to the standard free energy (G^o) of the ES or activated $ES^{\neq}$ complexes, where E is the free enzyme, S is the free substrate, and $S^{\neq}$ is the transition state of the reactant. From this analysis, 13 possible cases were obtained, one of which is a reference (i.e., no variation, Case 1) and the remaining are different

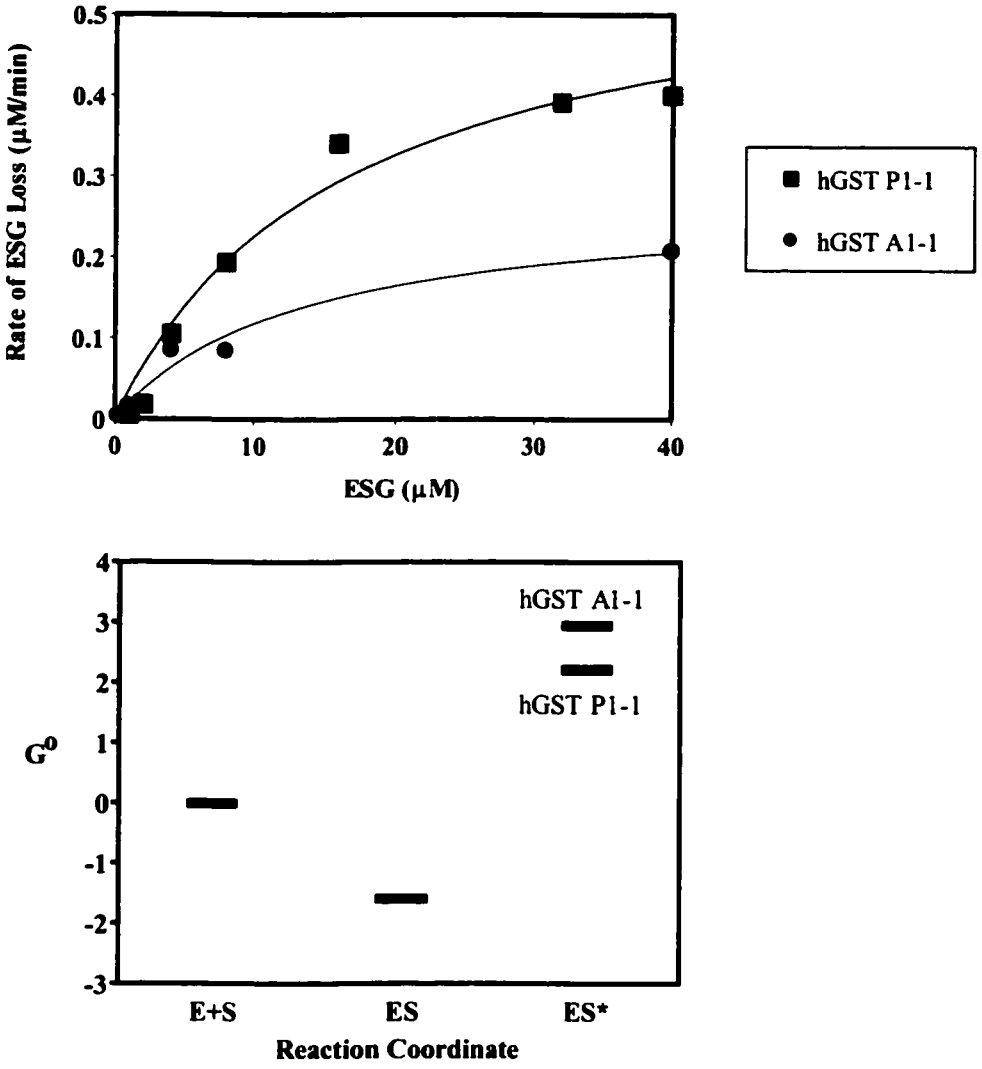

Figure 4.13: Substrate saturation curves (top panel) and free energy diagram (bottom panel) for the hydrolysis of ESG in hGST P1-1 and hGST A1-1. ES and ES* correspond to the Michaelis-Menten complex, GST•ESG, and the transition state of this binary complex, respectively. Comparison of P-class and A-class reflects Case 9 as described in the text.

variations (Table 4.5). In reality, the other twelve cases can be classified into six pairs, since an individual case (for example, Case 4) mirrors another (Case 9).

Table 4.5: Possible Variations of Kinetic Parameters on the Basis of Standard Gibbs Free Energy Levels of Michaelis-Menten Complex (ES) and Transition State (ES*) of the Enzyme Reactions[a]

k_{cat}/K_M	=	=	=	↓	↓	↓	↓	↓	↑	↑	↑	↑	↑
K_M	=	↑	↓	=	↑	↑	↑	↓	=	↑	↓	↓	↓
k_{cat}	=	↑	↓	↓	=	↑	↓	↓	↑	↑	=	↑	↓
Case	1	2	3	4	5	6	7	8	9	10	11	12	13

[a]Adapted from Bauer, et al., 2001.
Key: (=) invariance; (↑) increase; (↓) decrease.

In the following analysis, the systematic approach described above was employed to further gain an insight into thiol ester hydrolysis by GST. The results on hGST P1-1 will be referred to as the first system that is directly being compared to a second system, such as hGST A1-1. While Table 4.1 addresses isoenzyme specificity toward the hydrolysis of ESG, Table 4.2 addresses the substrate specificity of hGST P1-1. With the exception of hGST M2-2, the direct comparisons with hGST A1-1 and C47S P1-1 mutant reflect Case 9 (Tables 4.1 and 4.5), where k_{cat}/K_M is a good indicator of specificity at any experimental condition (Bauer, et al., 2001). In this case, the P-class GST stabilizes the transition state complex (GST•ESG$^{\neq}$). Consequently, the activation energy of k_{cat} is lowered, thereby increasing the rate of reaction as well as k_{cat}/K_M (Figure 4.13). This situation is also applicable when substrate specificity of hGST P1-1 is taken into consideration. Meanwhile, the comparison of thiol esterase activity in P- and M-class GSTs reflects Case 2. This is a situation in which the P-class has evolved to bind ESG weakly (i.e., high K_M) so that much of the enzyme is in the unbound form, so as to

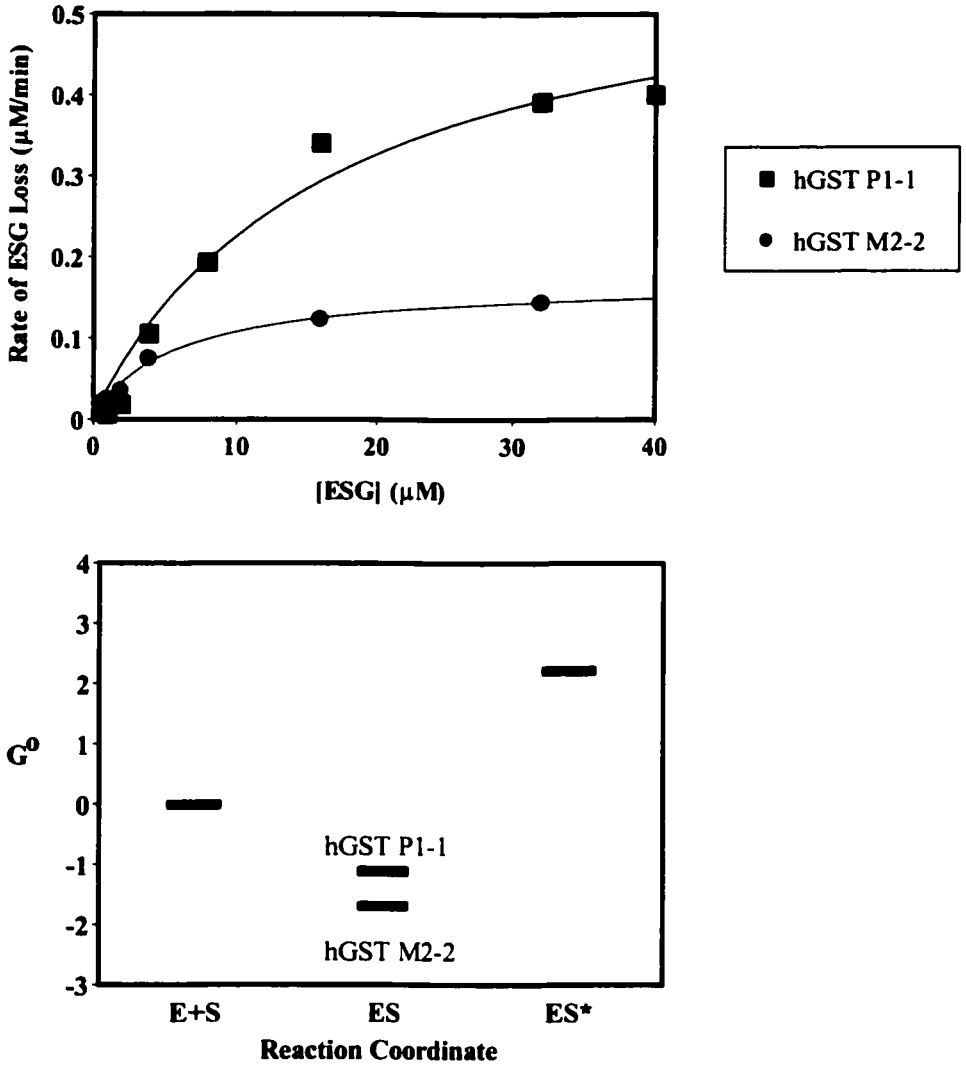

Figure 4.14: Substrate saturation curves (top panel) and free energy diagram (bottom panel) for the hydrolysis of ESG in hGST P1-1 and hGST M2-2. ES and ES* correspond to the Michaelis-Menten complex, GST•ESG, and the transition state of this binary complex, respectively. Comparison of P-class and M-class reflects Case 2 as described in the text.

maximize the rate of reaction (Fersht, 1999). As a result of the slightly higher K_M in P-class GST, the ES complex (GST•ESG) is at higher energy, thereby lowering the activation energy barrier of the transition state GST•ESG‡ (Figure 4.14). In their

systematic analysis of the six possible enzymatic situations, Bauer and co-workers proposed a modification to the commonly accepted definition of enzyme specificity. In this case, the modification requires that "for one enzymatic system to have a greater specificity (velocity) than another in any experimental condition, it is necessary (and sufficient) that the values of both k_{cat}/K_M and k_{cat} are greater in the first system than in the second" (Bauer, et al., 2001). The results of the present studies clearly indicate that thiol ester conjugates are catalytically hydrolyzed by GSTs, however, with slight differences in kinetic parameters. In fact, some combinations of GST and thiol ester result in faster hydrolysis than others.

Although the exact mechanism of thiol ester hydrolysis in human GSTs remains to be determined, the role of catalytic Tyr could not be ignored, as demonstrated in the previous studies (Dietze, et al., 1998). Given the efficiency of P-class GST in ESG hydrolysis (Table 4.1) and the known reactivity of Cys-47 in this isoform, it was thought that this residue might play an even more important role. Obviously, this was not the case since the C47S mutant did not completely abolish the thiol esterase activity. Moreover, the 3-fold decrease in the (turnover) rate of hydrolysis in M-class GST, with Tyr pK_a of ~10.2, suggests the contribution of tyrosinate anion in A- and P-class GSTs. Although a Y7F mutant of P-class was not immediately available for testing, it is reasonable to speculate that the thiol esterase activity in this mutant would be significantly low compared to the wild-type, given the similarity of active site Tyr pK_a in A- and P-class GSTs. Whether the catalytic Tyr of human A-, P-, and M-class GSTs are more critical in hydrolysis activity than in conjugation activity remains to be seen.

The time-dependent studies on hGST P1-1 and hGST A1-1 suggest a direct correlation between the thiol esterase activity and the extent of inhibition. In this case, hGST P1-1 was not only most efficient in hydrolyzing ESG (Table 4.2), but it was also the most inhibited enzyme (Figure 4.6). This was not surprising since the release of EA in hGST P1-1 was expected to eventually modify Cys-47, as shown in previous studies as well as by the mass spectra of the enzyme after 24-hr incubation with ESG (Figure 4.10). This protein modification resulted in >95% decrease in conjugation activity toward CDNB (Figure 4.11). Apparently, this inhibition is reversible, as activity was recovered after overnight dialysis. It is also interesting to note that some of the released EA and GSH subsequently formed GS-EA via Michael addition (Figure 4.5). This reaction was especially pronounced in the hGST P1-1 than its C47S mutant or hGST A1-1. The efficiency of hGST P1-1 toward GS-EA conjugation is largely due to the apparent tight binding affinity of GSH toward this isoform (Table 4.3). This binding affinity is reduced by ~3-fold upon substitution at Cys-47, suggesting the importance of this residue in promoting proper conformation for GSH binding. Whether GS-EA conjugation occurs in the active site or surrounding medium is not known for certain. Because such reaction is generally more efficient than the reverse reaction and the small amounts of released EA and GSH have higher K_Ms than ESG, it is likely that the apparent formation of GS-EA also occurs spontaneously. Furthermore, GS-EA adduct could not be detected from the mass spectra, suggesting that the GSH conjugate is short-lived and inevitably hydrolyzes back to GSH and EA. In the case of P-class GST, the EA is ultimately responsible for the inhibition and modification of this enzyme.

With all of the competing reactions within or near the active site of hGST P1-1, it is not surprising that the inhibition by ESG is mixed noncompetitive. The calculated dissociation constants, as measured by K_I and K_I', indicate that ESG apparently binds better to free GST than to inhibitor-bound enzyme by an order of magnitude (Table 4.4). Similarly, ESG inhibits hGST A1-1 via mixed noncompetitive mechanism. Possibly, the observed mixed inhibiton kinetics in hGSTs are further complicated by the presence of two active sites that do not necessarily have the same affinity for the same substrate. However, no indication of cooperativity was observed from either ESG hydrolysis or CDNB conjugation in the presence of ESG. Stoichiometry binding experiments would have to be performed to determine if ESG exhibits preferential binding to the active sites of GSTs. Although the apparent inhibition parameters are nearly identical in the two isoforms, the hGST P1-1 showed a slightly greater change (~2-fold) in K_M for CDNB than hGST A1-1. Presumably, the pronounced GS-EA formation (Figure 4.5) and stronger affinity of this conjugate in hGST P1-1 (Awasthi, et al., 1993) alter the affinity of CDNB and ultimately the rate at which this substrate is turned over (i.e., V_{max}).

Perhaps, one of the most widely studied residues in hGST P1-1 is Cys-47. Available X-ray crystal structure of this enzyme in complex with S-hexylglutathione (Figure 4.15) indicates that Cys-47 is located on the surface with its thiol group pointed toward the hydrophobic pocket formed by some main chain atoms of Lys-44 and Gln-51 and side chains of Trp-38 and Leu-52 (Lo Bello, et al., 1995). Incidentally, these residues are also involved in the binding of GSH on the opposite side. In the presence of GSH, Cys-47 is rendered less accessible to solvent. As described earlier, the mutation of

Figure 4.15: Ribbon representations of hGST P1-1 in the bound complex (left) and apo-enzyme (right). The S-hexylglutathione in the ligand bound complex is indicated in magenta. Note that the region surrounding Cys-47, in which the thiol group is enclosed in a hydrophobic pocket (represented in green) formed by the main chain and side chain atoms of Lys-44, Gln-51, Trp-38, and Leu-52, is only visible in the presence of ligand. Presumably, Cys-47 is highly exposed to solvent in the absence of ligand (right), resulting in poor electron density.

this residue to serine had no effect in the catalytic activity toward CDNB, but it induces positive cooperativity between the two subunits of the protein (Kong, et al., 1991; Ricci, et al., 1995). Thus, Cys-47 may serve as a molecular switch for different conformations, depending on whether GSH or thiol-containing compounds bind first to the enzyme. It is interesting to speculate that the GSH released from ESG does not bind productively to the active site in the presence of excess thiol ester. As a result, the Cys-47 remains solvent exposed, allowing EA released in the medium to bind to the thiol group. This Michael addition product (i.e., EA adduct, Figure 4.10) was indeed observed via mass spectrometry. Moreover, the lack of observable Michael adduct in the incubation

containing C47S suggests that the Cys-47 of hGST P1-1 is in fact the site of modification by EA. Furthermore, overnight dialysis of modified hGST P1-1 restores the activity of the enzyme, indicating that inhibition by EA is indeed reversible.

The search for *in vivo* inhibitors of GSTs continues, considering that these enzymes contribute significantly to the detoxification of many alkylating agents used in cancer chemotherapy. By inhibiting GST activity, especially in cells known to overexpress this enzyme, the efficacy of these chemotherapeutic agents may be enhanced. Considerable efforts have been expended to this end, and they have resulted in the design of stable analogs of GSH conjugates, mechanism-based inhibitor, and product analogs (Flatgaard, et al., 1993; Ouwerkerk-Mahadevan, et al., 1997; Zheng, et al., 1997; Rosario, et al., 2000). Many of these inhibitors target the P-class GSTs, as they are predominantly overexpressed in several malignancies. In principle, GST-dependent metabolism of drugs that release the desired pharmacologically active agents and therefore increase their duration of action, as well as isoform-specific inhibitors, have become attractive approaches to rational drug design. As the present studies indicate, the toxicological and therapeutic utility of thiol esterase activity will largely depend on whether a particular thiol ester is hydrolyzed by GSTs. But more importantly, the utility of such reverse reaction will depend on isoenzyme specificity. Theoretically, both endogenous and xenobiotic thiol esters of GSH could effectively compete with GSH for active sites in GST, and yet be hydrolyzed at a significantly modest rate *in vivo*. Ideally, such reactions would be most efficient in tissues with low levels of GSH. This is especially relevant to the hydrolysis of ESG by P-class GST, since excess GSH is likely

to reverse the inhibition by the liberated EA. Moreover, thiol esters formed from numerous carboxylic acid-containing compounds will likely contribute to the distribution and steady-state levels of free acid and GSH conjugate.

In summary, the efficiency of the enzymatic hydrolysis of thiol ester is dependent on the combination of GST and thiol ester. Perhaps, the most interesting result of the present studies is the increased hydrolysis of ESG by hGST P1-1 and the subsequent inhibition of the same enzyme by the liberated EA and/or GS-EA formed from hydrolysis by-products. Potentially, such mediated metabolism of thiol ester can be exploited in the design of more potent GSH-based prodrugs. Although the catalytic mechanism of thiol ester hydrolysis was not directly addressed in the present studies, the importance of active site Tyr in P-class could not be ruled out, considering its comparable Tyr pK_a to that of A-class and the apparent non-essential role of Cys-47 in hydrolysis. However, the contribution of Cys-47 in inhibition of P-class GST is clear, as a Michael adduct was not identified in the C47S mutant.

BIBLIOGRAPHY

Adman, E. T., Le Trong, I., Stenkamp, R. E., Nieslanik, B. S., Dietze, E. C., Tai, G., Ibarra, C. & Atkins, W. M. (2001) Localization of the C-terminus of rat glutathione S-transferase A1-1: Crystal structure of mutants W21F and W21F/F220Y. *Proteins: Struct., Funct., Genet* **42**, 192-200.

Allardyce, C. S., McDonagh, P. D., Lian, L. Y., Wolf, C. R. & Roberts, G. C. K. (1999) The role of tyrosine-9 and the C-terminal helix in the catalytic mechanism of alpha-class glutathione S-transferases. *Biochem. J.* **343**, 525-531.

Allardyce, C. S., McDonagh, P. D., Prescott, A., Roberts, G. C. K. & Lian, L. Y. (2000) NMR and kinetic studies of the role of C-terminus region of human GST A1-1: interactions with 1-chloro-2,4-dinitrobenzene and ethacrynic acid. *Clin. Chem. Enzymol. Commun.* **8**, 239-253.

Armstrong, R. N. (1994) Glutathione S-transferases: Structure and mechanism of an archetypical detoxification enzyme. *Adv. Enzymol. Relat. Areas Mol. Biol.* **69**, 1-44.

Atkins, W. M. (1994) Supramolecular self-assembly of *E. coli* glutamine synthetase: effects of pressure and adenylylation state on dodecamer stacking. *Biochemistry* **33**, 14915-14973.

Atkins, W. M., Dietze, E. C. & Ibarra, C. (1997) Pressure-dependent ionization of Tyr-9 in glutathione S-transferases: Contribution of the C-terminal helix to a 'soft' active site. *Prot. Sci.* **6**, 873-881.

Atkins, W. M., Wang, R. W., Bird, A. W., Newton, D. J. & Lu, A. Y. H. (1993) The catalytic mechanism of glutathione S-transferase (GST). Spectroscopic determination of the pK_a of tyr-9 in rat α1-1 GST. *J. Biol. Chem.* **268**, 19188-19191.

Awasthi, S., Srivastava, S. K., Ahmad, F., Ahmad, H. & Ansari, G. A. (1993) Interactions of glutathione S-transferase-pi with ethacrynic acid and its glutathione conjugate. *Biochim. Biophys. Acta.* **1164**, 173-178.

Awasthi, Y. C., Sharma, R. & Singhal, S. S. (1994) Human glutathione S-transferases. *Int. J. Biochem. Cell Biol.* **26**, 295-308.

Babu, Y. S., Sack, J. S., Greenhough, T. J., Bugg, C. E., Means, A. R. & Cook, W. J. (1985) Three-dimensional structure of calmodulin. *Nature* **315**, 37-40.

Baillie, T. A. & Kassahun, K. (1994) Reversibility in glutathione-conjugate formation. *Adv. Pharmacol.* **27**, 163-181.

Baillie, T. A. & Slatter, J. G. (1991) Glutathione: a vehicle for the transport of chemically reactive metabolites in vivo. *Acc. Chem. Res.* **24**, 264-270.

Bauer, C., Osman, A. M., Cercignani, G., Gialluca, N. & Paolini, M. (2001) A unified theory of enzyme kinetics based upon the systematic analysis of the variations of k_{cat}, K_M, and k_{cat}/K_M and the relevant ΔG° values-possible implications in chemotherapy and biotechnology. *Biochem. Pharmacol.* **61**, 1049-1055.

Bennet, W. S. & Steitz, T. A. (1978) Glucose-induced conformational change in yeast hexokinase. *Proc. Natl. Acad. Sci., USA* **75**, 4848-4852.

Bjornestedt, R., Stenberg, G., Widersten, M., Board, P. G., Sinning, I., Jones, T. A. & Mannervik, B. (1995) Functional significance of arginine 15 in the active site of human class alpha glutathione transferase A1-1. *J. Mol. Biol.* **247**, 765-773.

Board, P. G., Baker, R. T., Chelvanayagam, G. & Jermiin, L. S. (1997) Zeta, a novel class of glutathione transferases in a range of species from plants to humans. *Biochem. J.* **328**, 929-935.

Board, P. G., Coggan, M., Chelvanayagam, G., Easteal, S., Jermiin, L. S., Schulte, G. K., Danley, D. E., Hoth, L. R., Griffor, M. C., Kamath, A. V., Rosner, M. H., Chrunyk, B. A., Perregaux, D. E., Gabel, C. A., Geoghegan, K. F. & Pandit, J. (2000) Identification, characterization, and crystal structure of the omega class glutathione transferases. *J. Biol. Chem.* **275**, 24798-24806.

Board, P. G., Coggan, M., Wilce, M. C. J. & Parker, M. W. (1995) Evidence for an essential serine residue in the active site of the theta class glutathione transferases. *Biochem. J.* **331**, 247-250.

Board, P. G. & Mannervik, B. (1991) The contribution of the C-terminal sequence to the catalytic activity of GST2, a human alpha-class glutathione transferase. *Biochem. J.* **275**, 171-174.

Board, P. G. & Webb, G. C. (1987) Isolation of a cDNA clone and localization of human glutathione S-transferase 2 genes to chromosome band Gp12. *Proc. Natl. Acad. Sci. USA* **84**, 2377-2381.

Booth, J., Boyland, E. & Sims, P. (1961) An enzyme from rat liver catalyzing conjugation with glutathione. *Biochem. J.* **79**, 516-524.

Brakenhoff, J. P. G., Commandeur, J. N. M., Kaufer, F. J. J., Van Baar, B. L. M., Luijten, W. C. M. M. & Vermeulen, N. P. E. (1994) Chemical and glutathione conjugation-related degradation of fotemustine: formation and characterization of glutathione conjugate of diethyl(1-isocyanotoethyl)phosphate, a reactive metabolite of fotemustine. *Chem. Res. Toxicol.* **7**, 380-389.

Burley, S. K. & Petsko, G. A. (1985) Aromatic-aromatic interactions: A mechanism of protein structure stabilization. *Science* **229**, 23-28.

Burley, S. K. & Petsko, G. A. (1988) Weakly polar interactions in proteins. *Adv. Protein Chem.* **39**, 125-141.

Caccuri, A. M., Antonini, G., Board, P. G., Parker, M. W., Nicotra, M., Lo Bello, M., Federici, G. & Ricci, G. (1999) Proton release on binding of glutathione to alpha, mu, and delta class glutathione transferases. *Biochem. J.* **344**, 419-425.

Caccuri, A. M., Lo Bello, M., Nuccetelli, M., Nicotra, M., Rossi, P., Antonini, G., Federici, G. & Ricci, G. (1998) Proton release upon glutathione binding to glutathione transferase P1-1: kinetic analysis of a multistep glutathione binding process. *Biochemistry* **37**, 3028-3034.

Calugaru, S. V., Swanson, R. & Olson, S. T. (2001) The pH-dependence of serpin-proteinase complex dissociation reveals a mechanism of complex stabilization involving inactive and active conformational states of the proteinase which are perturbable by calcium. *J. Biol. Chem.* **276**, 32446-32455.

Cameron, A. D., Sinning, I., L'Hermite, G., Olin, B., Board, P. G., Mannervik, B. & Jones, T. A. (1995) Structural analysis of human alpha-class glutathione transferase in the apo-form and in complexes with ethacrynic acid and its glutathione conjugate. *Structure* **3**, 717-727.

Case, D. A. & Karplus, M. (1979) Dynamics of ligand binding to heme proteins. *J. Mol. Biol.* **132**, 343-368.

Chang, M., Bolton, J. L. & Blond, S. Y. (1999) Expression and purification of hexahistidine-tagged human glutathione S-transferase P1-1 in *Escherichia coli*. *Protein Expression Purif.* **17**, 443-448.

Chang, M., Hong, Y., Burgess, J. R., Tu, C.-P. D. & Reddy, C. C. (1987) Isozyme-specificity of rat liver glutathione S-transferases in the formation of PGF_2 and PGE_2 from PGH_2. *Arch. Biochem. Biophys.* **259**, 548-557.

Chang, M., Shin, Y. G., Van Breemen, R. B., Blond, S. Y. & Bolton, J. L. (2001) Structural and functional consequences of inactivation of human glutathione S-transferase P1-1 mediated by the catechol metabolite of equine estrogens, 4-hydroxyequilenin. *Biochemistry* **40**, 4811-4820.

Chao, C. C.-K., Huang, Y.-T., Ma, C. M., Chou, W.-Y. & Lin-chao, S. (1992) Overexpression of glutathione S-transferase and elevation of thiol pools in multidrug-resistant human colon cancer cell line. *Mol. Pharmacol.* **41**, 69-75.

Chasseaud, L. F. (1979) The role of glutathione and glutathione S-transferases in the metabolism of chemical carcinogens and other elecrophilic agents. *Adv. Cancer Res.* **29**, 175-274.

Chen, J. & Armstrong, R. N. (1995) Steroselective catalysis of a retro-Michael reaction by class mu glutathione S-transferase. Consequences for the interval distribution of products in the active site. *Chem. Res. Toxicol.* **8**, 580-585.

Cioni, P. & Strambini, G. B. (1996) Pressure effects on the structure of oligomeric proteins prior to subunit dissociation. *J. Mol. Biol.* **263**, 789-799.

Cole, S. P. C., Downes, H. F., Mirski, S. E. L. & Clements, D. J. (1990) Alterations in glutathione and glutathione-related enzymes in a multidrug-resistant small cell lung cancer cell line. *Mol. Pharmacol.* **37**, 192-197.

Crowl, C. V., Gugajewski, A., Yang, C. S., Reddy, G. R., Hamilton, G. A. & Mastru, A. M. (1996) Inhibition of proliferation and IL-2 production and utilization in lymphocytes by S-oxalylglutathione. *Exp. Cell Res.* **225**, 1501-1507.

Czwerwinski, M., Gibbs, J. P. & Slattery, J. T. (1996) Busulfan conjugation by glutathione S-transferases alpha, mu, and pi. *Drug Metab. Dispos.* **24**, 1015-1019.

Dietze, E. C., Grillo, M. P., Kalhorn, T., Nieslanik, B. S., Jochheim, C. M. & Atkins, W. M. (1998) Thiol ester hydrolysis catalyzed by glutathione S-transferase A1-1. *Biochemistry* **37**, 14948-14957.

Dietze, E. C., Ibarra, C., Dabrowski, M. J., Bird, A. & Atkins, W. M. (1996a) Rational modulation of the catalytic activity of A1-1 glutathione S-transferases: Evidence for incorporation of an on-face hydrogen bond at tyrosine-9. *Biochemistry* **35**, 11938-11944.

Dietze, E. C., Wang, R. W., Lu, A. Y. H. & Atkins, W. M. (1996b) Ligand effects on the fluorescence properties of tyrosine-9 in alpha 1-1 glutathione S-transferase. *Biochemistry* **35**, 6745-6753.

Dirr, H. W. & Wallace, L. A. (1999) Role of the C-terminal helix 9 in the stability and ligandin function of class alpha glutathione transferase A1-1. *Biochemistry* **38**, 15631-15640.

D'Souza, U. M. & Strange, P. G. (1995) pH Dependence of ligand binding to D_2 dopamine receptors. *Biochemistry* **34**, 13635-13641.

Fersht, A. (1999) *Structure and mechanism in protein science*. New York: W.H. Freeman and Company, pp. 103-131, 349-376.

Flatgaard, J. E., Bauer, K. E. & Kauvar, L. M. (1993) Isozyme specificity of novel glutathione S-transferase inhibitors. *Cancer Chemother. Pharmacol.* **33**, 63-70.

Gallivan, J. P. & Dougherty, D. A. (1999) Cation-π interactions in structural biology. *Proc. Natl. Acad. Sci., USA* **96**, 9459-9464.

Garrett, R. H. & Grisham, C. M. (1995) Enzyme Kinetics In *Biochemistry*, pp. 352-385. Orlando: Saunders College Publising.

Gervasio, F. L., Chelli, R., Procacci, P. & Schettino, V. (2002) The nature of intermolecular interactions between aromatic amino acid residues. *Proteins: Struct., Funct., Genet* **48**, 117-125.

Gilbert, L., Elwood, L. J., Merino, M., Masood, S., Barnes, R., Steinberg, S. M., Lazarous, D. F., Pierce, L., Angelo, T., Moscow, J. A., Townsend, A. J. & Cowan, K. H. (1993) A pilot study of pi-class glutathione S-transferase expression in breast cancer: correlation with estrogen receptor expression and prognosis in node-negative breast cancer. *J. Clin. Oncol.* **11**, 49-58.

Graminski, G. F., Kubo, Y. & Armstrong, R. N. (1989) Spectroscopic and kinetic evidence for the thiolate anion of glutathione at the active site of glutathione S-transferase. *Biochemistry* **28**, 3562-3568.

Green, J. A., Robertson, L. J. & Clark, A. H. (1993) Glutathione S-transferase expression in benign and malignant ovarian tumours. *Cancer* **68**, 235-239.

Gustafsson, A., Etahadieh, M., Jemth, P. & Mannervik, B. (1999) The C-terminal region of human glutathione transferase A1-1 affects the rate of glutathione binding and the ionization of the active site Tyr-9. *Biochemistry* **38**, 16268-16275.

Habig, W. H., Pabst, M. J., Fleischner, G., Gatmaitan, Z., Arias, I. M. & Jakoby, W. B. (1974a) The identity of glutathione S-transferase B with ligandin, a major binding protein in liver. *Proc. Natl. Acad. Sci., USA* **71**, 3879-3882.

Habig, W. H., Pabst, M. J. & Jakoby, W. B. (1974b) Glutathione S-transferase. The first enzymatic step in mercapturic acid formation. *J. Biol. Chem.* **249**, 7130-7140.

Harrison, D. J., May, L., Hayes, J. D. & Neal, G. E. (1990) Glutathione S-transferase localization in aflatoxin B1-treated rat livers. *Carcinogenesis* **11**, 927-931.

Hayes, J. D. & Pulford, D. J. (1995) The glutathione S-transferase supergene family: regulation of GST and the contribution of the isoenzymes in cancer chemoprotection. *Crit. Rev. Biochem. Mol. Biol.* **30**, 445-600.

Hayes, J. D. & Wolf, C. R. (1990) Molecular mechanisms of drug resistance. *Biochem. J.* **272**, 281-295.

Herzberg, O. & James, M. N. G. (1985) Structure of the calcium regulatory muscle troponin-C at 2.8 Angstrom resolution. *Nature* **313**, 653-659.

Hightower, K. E., Huang, C., Casey, P. J. & Fierke, C. A. (1998) H-Ras peptide and protein substrates bind protein farnesyltransferase as an ionized thiolate. *Biochemistry* **37**, 15555-15562.

Hofmann, O. & Brittain, T. (1996) Ligand binding kinetics and dissociation of the human embryonic haemoglobins. *Biochem. J.* **315**, 65-70.

Ibarra, C., Nieslanik, B. S. & Atkins, W. M. (2001) Contribution of aromatic-aromatic interactions to the anomalous pKa of tyrosine-9 and the C-terminal dynamics of glutathione S-transferase A1-1. *Biochemistry* **40**, 10614-10624.

Ishikawa, T. (1992) The ATP-dependent glutathione S-conjugate export pump. *Trends Biochem. Sci.* **17**, 463-468.

Jakobsson, P., Mancini, J. A., Riendeau, D. & Ford-Hutchinson, A. W. (1997) Identification and characterization of a novel microsomal enzyme with glutathione-dependent transferase and peroxidase activities. *J. Biol. Chem.* **272**, 22934-22939.

Jakoby, W. B. & Habig, W. H. (1980) *Enzymatic basis of detoxification* (vol. 2). New York: Academic, pp. 63-94.

Jemth, P. & Mannervik, B. (1999) Fast product formation and slow product release are important features in a hysteretic reaction of glutathione transferase T2-2. *Biochemistry* **38**, 9982-9991.

Jeong, S.-S. & Gready, J. E. (1994) Ionization state and pK_a of pterin-analogue ligands bound to dihydrofolate reductase. *Eur. J. Biochem.* **221**, 1055-1062.

Ji, X., von Rosenvinge, E. C., Johnson, W. W., Tomarev, S. I., Piatigorsky, J., Armstrong, R. N. & Gilliland, G. L. (1995) Three-dimensional structure, catalytic properties and evolution of a sigma class glutathione transferase from squid, a progenitor of the lens S-crystallins of cephalopods. *Biochemistry* **34**, 5317-5328.

Ji, X., Zhang, P., Armstrong, R. N. & Gilliland, G. L. (1992) The three-dimensional structure of a glutathione S-transferase from the Mu gene class. Structural analysis of the binary complex of isoenzyme 3-3 and glutathione at 2.2 Angstrom resolution. *Biochemistry* **31**, 10169-10184.

Keen, J. H. & Jakoby, W. B. (1978) Glutathione transferases. Catalysis of nucleophilic reactions of glutathione. *J. Biol. Chem.* **253**, 5654-5657.

Ketterer, B. (1988) Protective role of glutathione and glutathione transferases in mutagenesis and carcinogenesis. *Mut. Res.* **202**, 343-361.

Kirsch, R., Fleischner, G., Kamisaka, K. & Arias, I. M. (1975) Structural and functional studies of ligandin, a major renal organic anion-binding protein. *J. Clin. Invest.* **55**, 1009-1019.

Kolm, R. H., Sroga, G. E. & Mannervik, B. (1992) Participation of phenolic hydroxyl group of Tyr-8 in the catalytic mechanism of human glutathione transferase P1-1. *Biochem. J.* **285**, 537-540.

Kong, K.-H., Inoue, H. & Takahashi, K. (1991) Non-essentiality of cysteine and histidine residues for the activity of human class pi glutathione S-transferase. *Biochem. Biophys. Res. Commun.* **181**, 748-755.

Kong, K.-H., Takasu, K., Inoue, H. & Takahashi, K. (1992) Tyrosine-7 in human class pi glutathione S-transferase is important for lowering the pK_a of the thiol group of glutathione in the enzyme-glutathione complex. *Biochem. Biophys. Res. Commun.* **184**, 194-197.

Kretsinger, R. H. & Nockolds, C. E. (1973) Carp muscle calcium-binding protein. II. Structure determination and general description. *J. Biol. Chem.* **248**, 3313-3326.

Kuzmich, S. & Tew, K. D. (1991) Detoxification mechanisms and tumor cell resistance to anticancer drugs. *Med. Res. Rev.* **11**, 185-217.

Lakowicz, J. R. (1999) *Principles of Fluorescence Spectroscopy*. 2nd edition. New York: Kluwer Academic/Plenum Publishers, pp. 445-481.

Le Trong, I., Stenkamp, R. E., Ibarra, C., Atkins, W. M. & Adman, E. T. (2002) 1.3 Å resolution structure of human glutathione S-transferase with S-hexyl glutathione bound reveals possible new binding site. *Proteins: Struct., Funct., Genet.* (in press)

Lian, L. Y. (1998) NMR structural studies of glutathione S-transferase. *Cell Mol. Life Sci.* **54**, 359-362.

Listowsky, I., Abramovitz, M., Homma, H. & Niitsu, Y. (1988) Intracellular binding and transport of hormones and xenobiotics by glutathione S-transferases. *Drug Metab. Rev.* **19**, 305-318.

Liu, S., Ji, X., Gilliland, G. L., Stevens, W. J. & Armstrong, R. N. (1993) Second-sphere electrostatic effects in the active site of glutathione S-transferase. Observation of an on-face hydrogen bond between the side chain of threonine 13 and the π-cloud of Tyr-6 and its influence on catalysis. *J. Am. Chem. Soc.* **115**, 7910-7911.

Liu, S., Zhang, P., Ji, X., Johnson, W. W., Gilliland, G. L. & Armstrong, R. N. (1992) Contribution of tyrosine 6 to the catalytic mechanism of isoenzyme 3-3 of glutathione S-transferase. *J. Biol. Chem.* **267**, 4296-4299.

Lo Bello, M., Battistoni, A., Mazzetti, A. P., Board, P. G., Muramatsu, M., Federici, G. & Ricci, G. (1995) Site-directed mutagenesis of human glutathione transferase P1-1. *J. Biol. Chem.* **270**, 1249-1253.

Lyon, R. P. & Atkins, W. M. (2002) Kinetic characterization of native and Cys 112-modified glutathione S-transferase A1-1: reassessment of nonsubstrate ligand binding. *Biochemistry* (in press)

Lyttle, M. H., Satyam, A., Hocker, M. D., Bauer, K. E., Caldwell, C. G., Hui, H. C., Morgan, A. S., Mergia, A. & Kauvar, L. M. (1994) Glutathione-S-transferase activates novel alkylating agents. *J. Med. Chem.* **37**, 1501-1507.

Mannervik, B. (1985) The isoenzymes of glutathione transferase. *Adv. Enzymol. Relat. Areas Mol. Biol.* **57**, 357-417.

Mannervik, B., Alin, P., Guthenberg, C., Jensson, H., Tahir, M. K., Warholm, M. & Jornvall, H. (1985) Identification of three classes of cytosolic glutathione transferase common to several mammalian species: Correlation between structural and enzymatic properties. *Proc. Natl. Acad. Sci., USA* **82**, 7202-7206.

Mannervik, B. & Danielson, U. H. (1988) Glutathione transferases - structure and catalytic activity. *CRC Crit. Rev. Biochem.* **23**, 283-337.

McDonagh, P. D., Judah, D. J., Hayes, J. D., Lian, L. Y., Neal, G. E., Wolf, R. & Roberts, G. C. K. (1999) Determinants of specificity for aflatoxin B_1-8,9-epoxide in Alpha-class glutathione S-transferases. *Biochem. J.* **339**, 95-101.

Mecozzi, S., West, A. P. & Dougherty, D. A. (1996) Cation-π interactions in aromatics of biological and medical interest: Electrostatic potential surfaces as a useful qualitative guide. *Proc. Natl. Acad. Sci., USA* **93**, 10566-10571.

Meyer, D. J., Coles, B., Pemble, S. E., Gilmore, K. S., Fraser, G. M. & Ketterer, B. (1991) Theta, a new class of glutathione transferases purified from rat and man. *Biochem. J.* **274**, 409-414.

Meyer, D. J., Crease, D. J. & Ketterer, B. (1995) Forward and reverse catalysis and product sequestration by human glutathione S-transferases in the reaction of glutathione with dietary aralkyl isothiocyanates. *Biochem. J.* **306**, 565-585.

Meyer, D. J. & Thomas, M. (1995) Characterization of rat spleen prostaglandin H D-isomerase as a sigma-class GSH transferase. *Biochem. J.* **311**, 739-742.

Mitchell, A. E., Zheng, J., Hammock, B. D., Lo Bello, M. & Jones, A. D. (1998) Structural and functional consequences of haloenol lactone inactivation of murine and human glutathione S-transferase. *Biochemistry* **37**, 6752-6759.

Mitchell, J. B. O., Nandi, C. L., McDonald, I. K. & Thornton, J. M. (1994) Amino/aromatic interactions in proteins: Is the evidence stacked against hydrogen bonding? *J. Mol. Biol.* **239**, 315-331.

Monks, T. J., Anders, M. W., Dekant, W., Stevens, J. L., Lau, S. S. & Van Bladeren, P. J. (1990) Glutathione conjugate mediated toxicities. *Toxicol. Appl. Pharmacol.* **106**, 1-19.

Moore, J. W. & Pearson, R. G. (1981) *Kinetics and Mechanism*. New York: Wiley, pp. 159-169.

Murzin, A. G., Brenner, S. A., Hubbard, T. & Chothia, C. (1995) SCOP: a structural classification of protein database for the investigation of sequences and structures. *J. Mol. Biol.* **247**, 536-540.

Nicholson, D. W., Ali, A., Vaillancourt, J. P., Calagcay, J. R., Mumford, R. A., Zamboai, R. J. & Ford-Hutchinson, A. W. (1993) Purification to homogeneity and the N-terminal sequence of human leukotriene C4 synthase: A homodimeric glutathione S-transferase composed of 18-kDa subunits. *Proc. Natl. Acad. Sci., USA* **90**, 2015-2019.

Nieslanik, B. S. (2000) *A structure-function analysis of the C-terminus in glutathione S-transferase A1-1*, University of Washington.

Nieslanik, B. S. & Atkins, W. M. (2000) The catalytic Tyr-9 of glutathione S-transferase A1-1 controls the dynamics of the C-terminus. *J. Biol. Chem.* **275**, 17447-17451.

Nieslanik, B. S., Dabrowski, M. J., Lyon, R. P. & Atkins, W. M. (1999) Stopped-flow kinetic analysis of the ligand induces coil-helix transition in glutathione S-transferase A1-1: Evidence for a persistent denatured state. *Biochemistry* **38**, 6971-6980.

Nieslanik, B. S., Ibarra, C. & Atkins, W. M. (2001) The C-terminus of glutathione S-transferase A1-1 is required for entropically-driven ligand binding. *Biochemistry* **40**, 3536-3543.

Nilsson, L. O., Gustafsson, A. & Mannervik, B. (2000) Redesign of substrate-selectivity determining module of glutathione transferase A1-1 installs high catalytic efficiency with toxic alkenal products of lipid peroxidation. *Proc. Natl. Acad. Sci., USA* **97**, 9408-9412.

Nuccetelli, M., Mazzetti, A. P., Rossjohn, J., Parker, M. W., Board, P. G., Caccuri, A. M., Federici, G., Ricci, G. & Lo Bello, M. (1998) Shifting substrate specificity of human glutathione transferases (from class pi to class alpha) by a single point mutation. *Biochem. Biophys. Res. Commun.* **252**, 184-189.

Ouwerkerk-Mahadevan, S., Tirona, R. G., Ripping, R. A., Ploeman, J. H. T., Van Bladeren, P. J., Pang, K. S., Van Boom, J. H. & Mulder, G. J. (1997) Inhibition of glutathione conjugation by glutathione analogues in the perfused rat liver. Effect of esterification on the potency of gamma-L-glutamyl-alpha-(D-2-aminoadipyl)-N-2-heptylamine. *Drug Metab. Dispos.* **25**, 1137-1143.

Parsons, J. F. & Armstrong, R. N. (1996) Proton configuration in the ground state and transition state of a glutathione transferase-catalyzed reaction inferred from the properties of tetradeca(3-flurotyrosyl)glutathione transferase. *J. Am. Chem. Soc.* **118**, 2295-2296.

Pemble, S. E., Wardle, A. F. & Taylor, J. B. (1996) Glutathione S-transferase class Kappa: characterization by the cloning of rat mitochondria GST and identification of human homologue. *Biochem. J.* **319**, 749-754.

Phillips, M. F. & Mantle, T. J. (1993) Inactivation of mouse liver glutathione S-transferases YfYf (Pi class) by ethacrynic acid and 5,5'-dithiobis(2-nitrobenzoic acid). *Biochem. J.* **294**, 57-62.

Pickett, C. B., Telakowski-Hopkins, C. A., Ding, G. J.-F., Argenbright, L. & Lu, A. Y. H. (1984) Rat liver glutathione S-transferase - complete nucleotide sequence of a glutathione S-transferase mRNA and the regulation of the Ya, Yb and Yc mRNAs by 3-methylcholanthrene and phenobarbital. *J. Biol. Chem.* **259**, 5182-5188.

Ploeman, J. H. T., Van Ommen, B., Bagaard, J. J. P. & Van Bladeren, P. J. (1993) Ethacrynic acid and its glutathione conjugate inhibitors of glutathione S-transferases. *Xenobiotica* **23**, 913-923.

Ploemen, J. H. T., Van Schanke, A., Van Ommen, B. & Van Bladeren, P. J. (1994) Reversible conjugation of ethacrynic acid with glutathione and human glutathione S-transferase P1-1. *Cancer Res.* **54**, 915-919.

Prohaska, J. R. & Ganther, H. E. (1977) Glutathione peroxidase activity of glutathione S-transferases purified from rat liver. *Biochem. Biophys. Res. Commun.* **76**, 437-445.

Reinemer, P., Dirr, H. W., Ladenstein, R., Huber, R., Lo Bello, M., Federici, G. & Parker, M. W. (1992) Three-dimensional structure of class pi glutathione S-transferase from human placenta in complex with S-hexylglutathione at 2.8 Angstrom resolution. *J. Mol. Biol.* **227**, 214-226.

Ricci, G., Caccuri, A. M., Lo Bello, M., Pastore, A., Piemonte, F. & Federici, G. (1994) Colorimetric and flurometric assays of glutathione transferase based on 7-chloro-4-nitrobenzo-2-oxa-1,3-diazole. *Anal. Biochem.* **218**, 463-465.

Rosario, L. A., O'Brien, M. L., Henderson, C. J., Wolf, C. R. & Tew, K. D. (2000) Cellular response to a glutathione S-transferase P1-1 activated prodrug. *Mol. Pharmacol.* **58**, 167-174.

Rossjohn, J., McKinstry, W. J., Oakley, A. J., Verger, D., Flanagan, J., Chelvanayagam, G., Tan, K. L., Board, P. G. & Parker, M. W. (1998) Human theta class glutathione transferase: the crystal structure reveals a sulfate-binding pocket within a buried active site. *Structure* **6**, 309-322.

Shore, L. J., Fenselau, C., King, A. R. & Dickinson, R. G. (1995) Characterization and formation of the GSH conjugates of clofibric acid. *Drug Metab. Dispos.* **23**, 119-123.

Sinning, I., Kleywegt, G. J., Cowan, S. W., Reinemer, P., Dirr, H. W., Huber, R., Gilliland, G. L., Armstrong, R. N., Ji, X., Board, P. G., Olin, B., Mannervik, B. & Jones, T. A. (1993) Structure determination and refinement of human alpha class glutathione transferase A1-1, and a comparison with the mu and pi class enzymes. *J. Mol. Biol.* **232**, 192-212.

Stenberg, G., Board, P. G., Carlberg, I. & Mannervik, B. (1991) Effects of directed mutagenesis on conserved arginine residues in human class alpha glutathione transferase. *Biochem. J.* **274**, 549-555.

Tew, K. D. (1994) Glutathione-associated enzymes in anticancer drug resistance. *Cancer Res.* **54**, 4313-4320.

Thorson, J. S., Shin, I., Chapman, E., Stenberg, G., Mannervik, B. & Schultz, P. G. (1998) Analysis of the role of the active site tyrosine in human glutathione transferase A1-1 by unnatural amino acid mutagenesis. *J. Am. Chem. Soc.* **120**, 451-452.

Uotilla, L. & Koivusalom (1996) Expression of formaldehyde dehydrogenase and S-formylglutathione hydrolase activities in different rat tissues In *Enzymology and Molecular Biology of Carbonyl Metabolism*, pp. pp. 365-370. New York: Plenum Press.

Van Bladeren, P. J. (2000) Glutathione conjugation as a bioactivation reaction. *Chem-Bio Int.* **129**, 61-76.

Van Iersel, M. L. P. S., Van Lipzig, M. M. H., Rietjens, I. M. C. M., Vervoort, J. & Van Bladeren, P. J. (1998) GSTP1-1 stereospecifically catalyzes glutathione conjugation of ethacrynic acid. *FEBS Lett.* **441**, 153-157.

Vidugiris, G. J., Markley, J. L. & Royer, C. A. (1995) Evidence for a molten globule-like transition state in protein folding from determination of activation volumes. *Biochemistry* **34**, 4909-4912.

Vidugiris, G. J. & Royer, C. A. (1998) Determination of the volume changes for pressure-induced transitions of apomyoglobin between the native, molten-globule, and unfolded states. *Biophys. J.* **75**, 463-470.

Wang, R. W., Bird, A. W., Newton, D. J., Lu, A. Y. H. & Atkins, W. M. (1993) Fluorescence characterization of Trp 21 in rat glutathione S-transferase 1-1: microconformational changes induced by S-hexyl glutathione. *Prot. Sci.* **2**, 2085-2094.

Wang, R. W., Newton, D. J., Huskey, S. E. W., McKeever, B. M., Pickett, C. B. & Lu, A. Y. H. (1992) Site-directed mutagenesis of glutathione S-transferase YaYa. Important roles of tyrosine-9 and aspartic acid-101 in catalysis. *J. Biol. Chem.* **267**, 19866-19871.

Wang, R. W., Pickett, C. B. & Lu, A. Y. H. (1989) Expression of a cDNA encoding a rat liver glutathione S-transferase Ya subunit in *Escherichia coli*. *Arch. Biochem. Biophys.* **269**, 536-543.

Weber, G. (1986) Phenomenological description of the association of protein subunits subjected to conformational drift. Effects of dilution and of hydrostatic pressure. *Biochemistry* **25**, 3626-3631.

Widersten, M., Bjornestedt, R. & Mannervik, B. (1996) Involvement of the carboxyl groups of glutathione in the catalytic mechanism of human glutathione transferase A1-1. *Biochemistry* **35**, 7731-7742.

Wilce, M. C. J., Board, P. G., Feil, S. C. & Parker, M. W. (1995) Crystal structure of a theta-class glutathione transferase. *EMBO J.* **14**, 2133-2143.

Zhang, Y., Kolm, R. H., Mannervik, B. & Talalay, P. (1995) Reversible conjugation of isothiocyanates with glutathione catalyzed by human glutathione transferases. *Biochem. Biophys. Res. Commun.* **206**, 748-755.

Zhao, T., Singhal, S. S., Piper, J. T., Chang, J., Pradya, U., Clark-Wronski, J., Awasthi, S. & Awasthi, Y. C. (1999) The role of glutathione S-transferase hGSTA1-1 and hGSTA2-2 in protection against oxidative stress. *Arch. Biochem. Biophys.* **367**, 216-224.

Zheng, J., Wurz, G. T., Cadman, T. B., DeGregorio, M. W., Jones, A. D. & Hammock, B. D. (1997) Haloenol lactone: a new synergist of chemotherapy in vitro. *Biochem. Biophys. Res. Commun.* **241**, 13-17.

CURRICULUM VITA

Catherine A. Ibarra

EDUCATION

1996-2002 Ph.D. in Medicinal Chemistry, University of Washington

1990-1994 B.S. in Biology, Seattle University
Magna Cum Laude

RESEARCH EXPERIENCE

1996-2002 Research Assistant, University of Washington, Seattle, WA
Acquired skills in site-directed mutagenesis, protein expression via *E. coli* and baculovirus systems, protein purification, steady-state kinetics via absorption and fluorescence spectroscopy, and stopped-flow kinetics via fluorescence spectroscopy.
Developed capillary HPLC assay to characterize small molecules and peptides.
Developed reverse-phase HPLC to characterize the hydrolysis of thioester conjugates of glutathione.
Analyzed protein samples via LC-ESI mass spectrometry.

1995-1996 Research Technician, University of Washington, Seattle, WA
Assisted with spectroscopic characterization of site-directed mutant proteins.
Performed site-directed mutagenesis on glutathione S-transferase A1-1 and protein purification.

1993 Summer Undergraduate Research Trainee
Assisted with site-directed mutagenesis on glutamine-synthetase.

AWARDS

2001-2002 Hope Barnes Graduate Fellowship
1999-2001 NIH Research Service Award (Pre-doctoral Fellowship)
1991-1994 Hawaii Community Foundation Scholarship
1991-1993 Anne and Frank West Science Scholarship
1990-1994 Seattle University Trustee Scholarship

PUBLICATIONS

Le Trong, I., Stenkamp, R.E., **Ibarra, C.**, Atkins, W.M., and Adman, E.T. (2002) 1.3 Å Resolution structure of human glutathione S-transferase with S-hexyl glutathione bound reveals possible new binding site. *Proteins: Struct., Funct., Genet.* (in press).

Ibarra, C., Nieslanik, B.S., and Atkins, W.M. (2001) Contribution of aromatic-aromatic interactions to the anomalous pKa of Tyr-9 and the C-terminal dynamics of glutathione S-transferase A1-1. *Biochemistry* 40, 10614-10624.

Nieslanik, B.S., **Ibarra, C.**, and Atkins, W.M. (2001) The C-terminus of glutathione S-transferase A1-1 is required for entropically-driven ligand binding. *Biochemistry* 40, 3536-3543.

Adman, E.T., Le, Trong, I., Stenkamp, R.E., Nieslanik, B.S., Dietze, E.C., Tai, G., **Ibarra, C.**, and Atkins, W.M. (2001) Localization of the C-terminus of rat glutathione S-transferase A1-1: Crystal structure of mutants W21F and W21F:F220Y. *Proteins: Struct., Funct., Genet.* 42, 192-200.

Wang, H., Yi, E.C., **Ibarra, C.A.**, and Hackett, M. (2000) A remote flow cell for UV absorbance detection with capillary HPLC based on single fiber optic. *Analyst* 125, 1061-1064.

Lang, D.H., Yeung, C.K., Peter, R.M., **Ibarra, C.**, Gasser, R., Itagaki, K., Philpot, R.M., and Rettie, A.E. (1998) Isoform specificity of trimethylamine N-oxygenation by human flavin-containing monooxygenase (FMO) and P450 enzymes. *Biochem. Pharmacol.* 56, 1005-1012.

Atkins, W.M., Dietze, E.C., and **Ibarra, C.** (1997) Pressure-dependent ionization of Tyr-9 in glutathione S-transferase A1-1: Contribution of the C-terminal helix to a 'soft' active site. *Protein Sci.* 6, 873-881.

Dietze, E.C., **Ibarra, C.**, Dabrowski, M.J., Bird, A.W., and Atkins, W.M. (1996) Rational modulation of the catalytic activity of A1-1 glutathione S-transferase: Evidence for incorporation of an on-face (π•••OH-Ar) hydrogen bond at tyrosine-9. *Biochemistry* 35, 11938-11944, accelerated publication.

Ibarra, C.A. and Atkins, W.M. (2002) The functional significance of the anomalous pK_a of Tyr-9 in glutathione S-transferase: Parallel pathways for product dissociation (submitted to *Protein Science*).